Impedance Spectroscopy for Fault Identification in Underground Power Cables

by

Audrey Danielle Fotso Nzeche

A thesis submitted in partial fulfillment of the requirements for the degree of

Master of Science

in

Engineering Management

Department of Mechanical Engineering

University of Alberta

Abstract

In the ongoing energy transition and renewable energy era, maintaining the integrity and resilience of power distribution networks is paramount. It is necessary to minimize power outages and deliver electricity to consumers safely and reliably. Underground power cable failures are one of the leading causes of power disruption. To meet the increasing demand for electricity and adhere to safety and aesthetic considerations, power distribution lines are frequently installed in extended lengths, often in remote and challenging locations. This poses an issue for inspection and maintenance. Despite the development of diagnostics methods such as domain reflectometry and very low frequency methods, coupling standalone diagnostics methods to develop more efficient and robust fault detection models have not really been explored. This thesis work investigates the feasibility of detecting cable anomalies using a focused impedance spectroscopy approach. Such a focused approach aims to propose an efficient and highly fault-sensitive diagnostic technique for anomalies in power cables.

Amongst several aging and damage mechanisms in underground power cables, utility operators tend to pay more attention to thermal anomalies as they can possibly enhance other damage mechanisms. They also bear higher risks such as fire outbreaks in extreme scenarios. This thesis project presents a multi-physics model for thermal fault identification in underground power cables using cable resistive impedance. Resistive impedance spectroscopy is a potential diagnostic technique which utilizes impedance measuring instruments to measure and record real impedance for fault analysis.

Three damage models were investigated with an emphasis on thermal anomalies. A steady and transient model for the temperature distribution of a healthy cable was first developed in python and MATLAB respectively. The thermal model was then coupled to the resistive portion of impedance to assess its behavior with temperature change. Since cable faults increase cable

temperature during operations, the anomaly detection method relied on observing the temperature-induced alteration in cable resistive impedance as a distinctive fault indicator.

An experimental study was further carried out to validate the developed models for a healthy cable and to extend the hypothesis to faulted cables. For this purpose, single core XLPE insulated cables were subjected to increasing temperatures and their impedance recorded using a vector network analyzer. The results from the extracted resistive impedance showed that, although resistive impedance increased with increasing temperatures, it was highly sensitive and fluctuated with temperature changes. For this reason, it stands a chance of being a thermal anomaly detection, provided there is an existing healthy-cables-impedance baseline derived from historical data in electric utility operating systems. The proposed research work stretches to other damage models including mechanical damage and water trees in underground power cables.

Mechanical damages such as abrasion and bending weakens the cable's protective layers, leaving it susceptible to short circuits. Cable impedance sensitivity to such faults was investigated. The results revealed that, resistive impedance of the line increases in the presence of a notch, but it depends on the depth of the notch. This implies that damages on the outermost layers of the cable may not be perceived as a fault alarm, however, when such damages are left unattended, they tend to gradually escalate, potentially leading to more severe faults over time. According to these findings, resistive impedance spectroscopy may not be a suitable early mechanical anomaly diagnostic method. Resistive impedance of water-trees-induced coaxial cables in the lab showed subtle changes compared to those of thermally and mechanically damaged cables.

The result from this study brings significant potential contribution to the cable health monitoring and fault diagnostic fields. Future work beyond this study includes additional modeling and characterization for simple cable and damage models, and large-scale cable testing of three-phase cables with realistic insulating layers and damage accumulation, and finally field testing and implementation in real-operating power cable networks.

Dedication

To my mother, Mrs. Koguem Ernestine, for all the sacrifices she continuously makes towards my growth and happiness. This shero, has been a constant source of inspiration and motivation. I was reminded of her strength, hard work, humility, and grace throughout my master's program.

To you mum! I love you!

Acknowledgement

I would like to express my deepest gratitude to my supervisor, Dr. Michael Lipsett, for his invaluable patience, encouragement, and feedback.

Contents

List of Tables

List of Figures

Acronyms

AC:	Alternating Current
BIS:	Broadband Impedance Spectroscopy
CC:	Capacitive Coupler
CM:	Condition Monitoring
CWT:	Continuous Wavelet Transform.
DAC:	Damped Alternating Current
DF:	Dissipation Factor
DWT:	Discrete Wavelet Transform
EPR:	Ethylene-propylene Rubber
FFT:	Fast Fourier Transform
FDR:	Frequency Domain Reflectometry
FEM:	Finite Element Method
HIF:	High Impedance Faults
LIF:	Low Impedance Faults
MV:	Medium Voltage
NERC:	North American Electric Reliability Corporation
PSO:	Particle Swarm Optimization
PD:	Partial Discharge
PMU:	Phasor Measurement Unit
PLC:	Power Line Communication
PLM:	Power Line Modem
PPLP:	Polypropylene-laminated Paper
RIS:	Resistive Impedance Spectroscopy
SDGs:	Sustainable Development Goals
TDR:	Time Domain Reflectometry
TWT:	Traveling Wave Methods
XLPE:	Cross-linked polyethylene
UHF:	Ultra-high Frequency
VLF:	Very Low Frequency

Chapter 1 Introduction

Electricity is generated using fossil fuels, nuclear energy or renewable energy sources and transmitted by long power lines at high voltages to distribution substations. It is then converted to lower voltages by power transformers at these substations and sent to customers (both residential and industrial buildings) through transmission and distribution lines. Electrical distribution and transmission systems consist of several components which form an extensive network. The ability of these systems to perform their intended function, which is to deliver electric power to customers without any interruptions in supply voltage, highly depends on overhead and underground power cables. According to [1], distribution systems account for 90% of all customer reliability problems and improving distribution reliability is the key to improving customer reliability.

Maintenance, inspection, and replacement activities are important aspects to improve system reliability. As the demand in electrical energy continues to rise, and as more underground power cables are being installed to deliver electricity to houses and industrial buildings, it is important that energy and electrical organizations put in place excellent maintenance and repair strategies to enhance reliability. In a long-term assessment report released in 2022 by North American Electric Reliability Corporation (NERC) [2], it was predicted that there will be a continuous increase in electricity demand over the next 10 years due to the adoption of electric vehicles and energy transition programs. Besides satisfying the demand, movement towards cleaner grids is another factor that has influenced the decision to build new transmission projects. The report stated that “energy organizations have begun increasing the number of miles of transmission line projects for integrating renewable generation over the next 10 years. Some of which include, approximately 80 km of 230 kV transmission line is currently under construction phase in

Saskatchewan due to load growth and to meet reliability needs; 1,635 miles of transmission line projects are planned in New York, over the 10-year assessment period total. In Ontario, several transmission projects are underway to address bulk system reliability concerns, reinforce connection in the northwest, and connect new loads in the southwest area of the province."

With the growing number of transmission and distribution line projects, meaningful and impactful reliability measures should be taken. On average, cable lifetime is about 40-50 years, and many electric utilities implement an age-based policy as a replacement policy. There is a high probability that a good number of cables report an acceptable score for their performance analysis throughout their lifetime, however, some cables break down before expected time and potentially lead to a power outage. Sudden faults and aging in cables could be due to electrical, thermal, chemical, or mechanical stress. On the other hand, some cables remain in service past their expected lifetime. This can be attributed to a low amount of load on these cables, or the environment in which the cables are located might be favorable and can only become problematic at a more advanced age. In adverse conditions such as extreme temperatures and overloading, cable degradation begins to occur and potentially lead to insulation breakdown.

Furthermore, enhancing the reliability and ensuring continuous operation of these distribution and transmission cables align with the objectives of the Sustainable Development Goal 7 (SDG7) under the United Nations which is to ensure access to affordable, reliable, sustainable, and modern energy for all. Key factors impacting the reliability of distribution and transmission lines include:

- **Weather conditions:** The weather has a significant impact on the probability of failure of distribution and transmission lines. The number of power outages recorded over the years related to climate change and weather events such as storms and hurricanes keep increasing. In December 2022 alone, the powerful arctic storm sweeping across US and Canada, caused an outage that affected about three hundred and eighteen thousand

customers in the provinces of Ontario and Quebec [3] with several vegetation management activities taking place to remedy the situation.

- **Aging infrastructure and equipment failures:** Most of Canada's power grids and facilities were built before 1980 [4] and may no longer be sufficient and reliable to satisfy high electricity demands. Weather events are also a major cause of equipment failures as stated earlier. According to Ausgrid, between 2014 and 2016, 869 power outages were recorded and attributed to component failures. 598 of those outages occurred during adverse weather conditions [5], [6].
- **Installation and maintenance practices:** Proper installation techniques and regular maintenance are critical to long-term reliability of power cables. Using reliability models, [5] demonstrated how preventive maintenance analysis of electric distribution system components can help electric utilities plan and derive strategies for downtime and component faults, especially under certain weather conditions.
- **Load fluctuations and overloading:** Excessive current or voltage surges can lead to conductor overheating and possible insulation damage.

Other factors impacting the reliability of power lines include mechanical damage and excavation, wildlife and rodents, cable quality and environmental factors such as temperature and chemical exposure. For underground power cables, environmental conditions and cable ampacity are two critical factors when discussing underground distribution system reliability. Condition monitoring (CM), optimal inspection and preventive actions are tools which can be used to enhance energy systems reliability.

1.1 Motivation

Proactive measures such as vegetation management programs [7], improved weather forecasting so utilities can plan ahead [8] and decentralized power generations [9] can be tools to better manage weather-related power outages. However, those related to equipment failures, especially for components which cannot be visually inspected such as underground power cables, remain a concern. Several researchers and manufacturers in the field continue to brainstorm ways in which underground power cables can be monitored remotely for prognostic health management purposes. Common diagnostic methods are partial discharge measurement, thermal imaging, time domain reflectometry, dielectric spectroscopy, and data analytics and just recently, AI-based prognostics. Continual monitoring of cables' health condition enables utilities to adopt proper and in-time preventive maintenance strategies and reduces operational risks.

Cable Manufacturers specify their estimated lifetime, and these estimates are intended to provide a reasonable assurance of the cable's performance over a specified time. However, lifetime estimation depends on a range of parameters such as installation conditions, weather conditions, operating environment, cable load, inspection, and maintenance frequency. Though most in-service underground power cables remain in service with little to no repair, some break down before their estimated lifetime. There is a high probability that one cable breakdown, especially primary feeders since they are closer to the substation can affect the entire network, leading to a power outage. Underground power cables failure, amongst other causes of electrical outages, is one of the leading causes of power outages and given that maintenance activities are not easily achievable, it remains a major concern to utility operators. Gradual and continuous cable degradation over time causes under performance of cable systems and potentially cable breakdown. Therefore, it is important that cable faults are detected, monitored, and managed on time. Further, besides detecting cable faults, condition monitoring of cables can help utilities to re-allocate load on the network, with higher loads on more healthy cables.

1.1.1. Impact of power outage

In a survey [10] carried on the number of large power outages between 2000 and 2016 in the US, it was found that severe weather was the number one cause of most historical power outages, followed by electromagnetic events, intentional cyber-physical attacks and equipment failure; slightly followed by fuel supply emergency and Islanding. Depending on the nature of unplanned power outages, they could have severe economic, environmental, and social impact. Power outages disrupt business operations and daily activities. This leads to reduced productivity and revenue losses. According to [11], the cost of downtime on average due to power outages can range from thousands to millions of dollars per hour, depending on the industry and business size. The loss of electricity interrupts medical services, telecommunications, transportation, and disrupts the supply chain. Social costs include high rates of crime [12] , and halt activities in educational institutions. Electricity outages impact on the environment include, the use of backup generators and other emergency power sources used during power outages which contribute to increasing greenhouse gas emissions and air pollutants. In addition, it limits recreational activities and causes social isolation. It can also cause fear and anxiety [13] in individuals and communities, especially when prolonged.

1.1.2. Cable damage models

Common damage models in distribution voltage cables are water trees, voids, inclusions, cable shape deformation and thermal damage. Water trees and thermal degradation being the most problematic of them, there has been continuous research and innovation on these damage models. Water trees are when moisture invades extruded dielectrics such as cross-linked polyethylene (XLPE) or ethylene-propylene rubber (EPR), causing breakdown patterns resembling a tree which reduces the voltage withstanding capability of the cable [1, Ch. 3]. Over the years manufacturers have developed both jacketed cable and tree retardant cable (TR-XLPE) to address this issue. However, the severity of treeing is strongly related to thermal aging since

moisture absorption occurs more rapidly at high temperatures [13]. Thermal activities taking place within and around underground cables, cause gradual deterioration of their electrical, mechanical, and geometry properties, reducing cable lifespan. Furthermore, overheating of cable insulation can potentially lead to insulation breakdown and reduced current-carrying capacity, which goes against the mission of electricity suppliers which is to satisfy demand in a reliable and safe way. In extreme cases, overheating of cables can create fire risks for the public.

1.1.3. Research gap

In this study, two diagnostic techniques – that is, cable temperature distribution and resistive impedance spectroscopy - are integrated to form a multi-physics based diagnostic model. This has been a challenging task as there is a lack of comprehensive studies combining these two techniques to observe and understand cable behavior during faults. In addition, existing physics-based fault simulation models in the literature do not consider all cable layers and the dynamic behavior of temperature and resistive impedance during faults, whose results are closer to real life operating conditions compared to steady-state analysis. Existing impedance spectroscopy for fault identification utilizes the reactive portion of impedance, whose data can be complex to interpret. Focusing on the resistive portion of impedance to observe cable behavior could be a practical and efficient technique to detect anomalies in power lines.

1.2 Thesis statement

To address the challenges associated with thermal degradation of underground power cables, physics-based models emulating cable behavior under thermal stress and resistive impedance variations are derived. An experimental study to analyze changes in electrical and material properties of cable under simulated faults is proposed. Mechanical damage and water trees are two other damage models whose effects on cable will be studied through resistive impedance

behavior. Idealized analogs for all three damage models will be studied rather than actual damage effects.

1.3 Thesis objectives

The main aim of this research work has been to derive accurate comprehensive physics-based models which reflect gradual thermal insulation degradations and changes in resistive impedance of the conductor. This involves monitoring temperature variation and analyzing the heat dissipation process within a cable system. Another key objective is to investigate variations in resistive impedance data with temperature which are then associated with fault types and severity. Despite thermal behavior and impedance spectroscopy being separate fault diagnostics methods, this study seeks to establish correlations between them, resulting in a multi-physics model, enabling more robustness in fault detection in remote power cables. The developed model will be validated by comparing its simulation results with experimental results obtained from laboratory experiments on damaged and undamaged power cables. Observing the influence of mechanical damage such as a notch on cable electrical properties is also one of the objectives of this study. The impact of water trees on cable impedance is also explored. Finally, there are plans to test and implement the results of this study to a real network of underground power cables in a utility company in Edmonton.

1.4 Manuscript organization

In this first chapter, an overview of the electrification grid was briefly discussed, and we elaborated on how paramount ensuring reliability of distribution and transmission lines is. A physics-based model has been proposed in this study as one of the ways to improve reliability. In the next section, an extensive literature review on heat dissipation and impedance spectroscopy on underground power cables is discussed. In chapter 3, a temperature-impedance model is proposed, and a numerical analysis is carried out by simulating the heat dissipation process in a

cable system and observing how temperature changes affect cable resistive impedance. In chapter 4, a laboratory analysis is presented, and its results are discussed. Finally, chapter 5 summarizes the work done, concludes and discusses future work.

Chapter 2 Literature review

Through an extensive exploration of relevant studies on underground power cables, key aspects, the state-of-the-art, and research gap related to temperature monitoring, impedance spectroscopy and an integration of both techniques to develop a model for fault diagnostics in underground power cables are summarized and discussed in this section.

2.1 Underground power cable components

For better understanding of cable systems and some terms used interchangeably throughout the write up, a brief review of cable systems is first tackled. Figure 1 shows a general cable composition, and a summary of the function of each layer is outlined below.

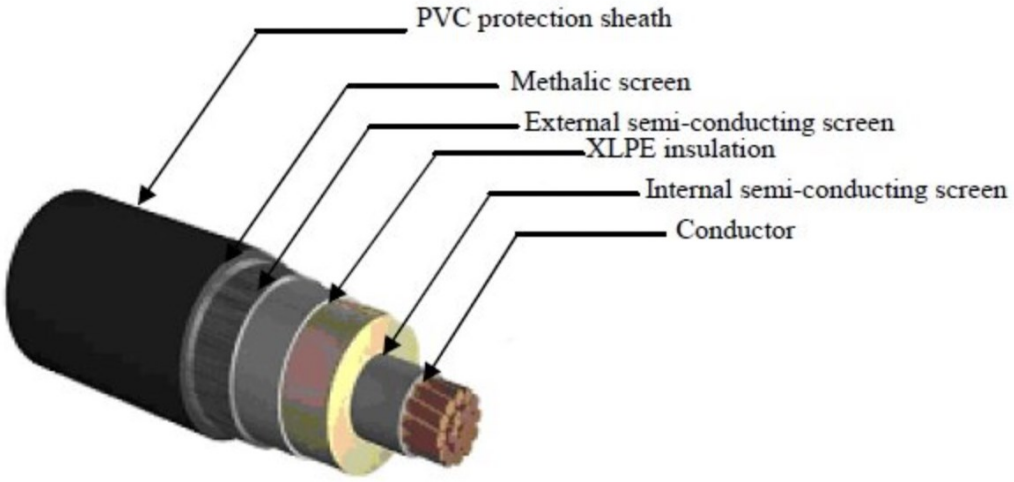

Figure 1 [14]: Components of a primary distribution single-conductor cable

A typical underground cable will have a conductor or core which is the current carrier of the cable, and it is covered by insulation. Some conductors are stranded while others are bonded. Cable insulation is one of the targeted components in this study as well as in most existing literature when discussing cable degradation and failures (not that other cable components are not prone to aging or faults but because cable insulation primarily acts as an electrical insulation, as well as

thermal and mechanical insulator together with other cable layers). Cable insulation prevents the flow of electricity from operating conductors to the ground or adjacent conductors[15], preventing short circuit and leakage. In addition, the insulation layer protects the conductor from bending, abrasion, and other external impacts. It is possible to find operating cables with just insulation and no extra layer. Metallic sheath or concentric neutral wires protect the insulation and carry fault current to the earth; they are always connected to earth at one or at both the extremities of the cable [15]. Additional concentric layers namely, armor, bedding, jacket and external coverings can be found in some cables for supplementary mechanical protection or other functions beyond the scope of this study. Semi-conducting screens are often considered as part of the insulation during analysis. This is because they are very thin and have similar properties to that of the insulation.

2.2 Aging mechanisms

Aging mechanisms that affect cable insulation systems in underground power cables can be classified into mechanical, electrical, thermal and environmental [16], [17]. Figure 2 [16] presents a summary of these mechanisms and their causes and effects.

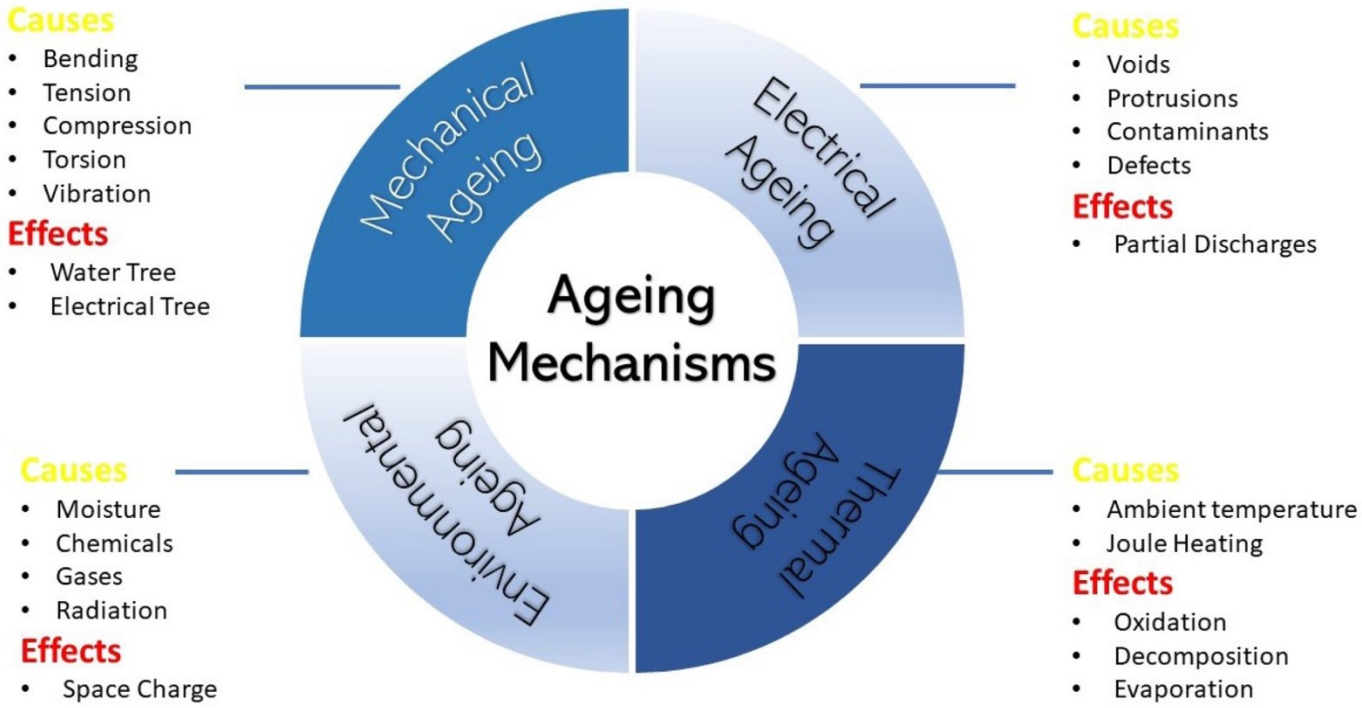

Figure 2 [16]: Aging mechanisms in underground power cables

Each fault has its causes and effects as seen in Figure 2. However, in the long run, these effects are interconnected and create conducive environments for more damage, increasing the rate of cable failure. Some aging mechanisms enhance other faults or lead to different types of faults in cables. For example, continuous temperature variations can cause adhesion losses between cable layers, creating a void which leads to partial discharge [17]. Thermal aging and thermal faults remain a great concern to engineers and researchers. Thermally aged cables tend to enhance the development of water trees and partial discharges (PDs). Even though aging and degradation processes in underground power cables are gradual processes, there is still a need to monitor them.

Condition monitoring of underground power cable systems is a useful maintenance activity to detect localized faults and degradations. Fault detection and localization in underground power cables present unique challenges. Firstly, because these power cables are installed underground or in ducts which are often inaccessible. Secondly, faults such as thermal anomalies and material

decomposition are not often visually perceived, however they affect electrical properties of the line over time. Therefore, remote condition monitoring and conditioned-based maintenance of underground power cable networks are necessary to ensure system reliability.

Condition monitoring diagnostic techniques include time-domain reflectometry (TDR), partial discharge (PD) monitoring, dielectric spectroscopy, insulation resistance testing, sheath testing, thermal imaging, and impedance spectroscopy. Some of these techniques are discussed further in the chapter. The next section in this literature review chapter focuses on the state-of-the-art of impedance spectroscopy as a diagnostic method. The second section discusses heat dissipation across cable layers and the third section tackles potential benefits of integrating these two diagnostic methods to create a robust and efficient multi-physics model for condition monitoring of underground power cables.

2.3 Overview of impedance spectroscopy

Impedance spectroscopy is a diagnosis technique which uses impedance measurement as a function of frequency to gain valuable information about electrical, chemical, and physical properties of a system or material. Electric impedance models have been used since 1969 to analyze dielectric properties for numerous materials [18]. Also known as dielectric spectroscopy, it is used in various fields including electrochemistry in the biomedical field to monitor implanted devices and biological cell suspensions [19] and in fault diagnostics across several industries [20]–[22].

Impedance (Z) is obtained as a ratio of voltage to current in an electric circuit (1). It exhibits resistance to the flow of electrical current just like resistance, but it is a complex resistance as it also reflects the ability of a circuit to store electrical energy [19]. Impedance is a combination of resistance and reactance (2) and is encountered when current flows through a circuit composed of resistors, capacitors, and inductors in alternating current (AC) circuits. In contrast to direct

current (DC) circuits, which are unaffected by the supply of frequency, impedance is an AC characteristic which varies with operating frequency. Its reactance portion is a combination of capacitive and inductive elements which also represent the imaginary part of the complex value (also phase). Resistance represents the real part (also magnitude).

$$Z = {}^{V}/_{I} \qquad \text{in DC circuits} \qquad (1)$$

$$Z = \sqrt{R^2 + (Z_L + Z_C)^2} \quad \text{or} \quad Z = R + j\omega L - {}^{j}/_{\omega C} \qquad \text{in AC circuits} \qquad (2)$$

where Z_L is inductive impedance, Z_C is capacitive impedance, and ω is frequency. R, L, and C are the primary cable parameters—resistance, inductance, and capacitance respectively.

Characteristic impedance (Z_0) and propagation constant (γ) are also two terms used when discussing impedance spectroscopy of a material. While characteristic impedance is a function of the line only, impedance Z is a function of load impedance and frequency. Equations establishing their relationship are elaborated in Chapter 3 under the electrical model section. Variations and behavior of characteristic impedance spectra and temperature profiles during faults, are studied using line parameters in this research work.

Impedance phase and magnitude trends are key factors used by engineers and researchers when carrying out impedance spectroscopy. In circuits with a purely resistive behavior, phase impedance is zero. For a non-purely resistive behavior, the phase differences and values are analyzed to identify anomalies. In healthy cables, the impedance spectrum follows a relatively constant pattern. Impedance varies with applied frequency but the phase angle between voltage and current is relatively stable. Any sudden spikes or deviation from impedance historical data might be an indication of anomalies. Impedance spectroscopy is a powerful technique for detecting such abnormalities, which cannot be captured by visual inspection alone.

2.3.1. Faults characterization using impedance spectroscopy

Thermal localized insulation degradation, cable aging, water trees [20], partial discharges and mechanical damage are defects in underground power cables that can be detected by impedance spectroscopy. Fault detection and characterization is done using the so-called “peak recognition” method. This method involves identifying unique peaks or irregularities within the impedance spectrum that possibly correspond to specific cable conditions and faults.

A detailed assessment of the applicability of impedance spectroscopy in online diagnosis of aging and deterioration of medium voltage (MV) three core cables was recently explored by M. Li *et al* [23]. Peculiar characteristics were observed for the impedance spectroscopies of different cable states and that led the authors to categorize their simulation results into “healthy”, “overall aging”, “large size deterioration” and “small size deterioration”. An overall aging cable was identified by consistent decrease of the value of phase amplitudes and resonance peaks while a large-size local deterioration was determined by varying resonance peaks. Small size deteriorations were determined by the frequency difference between resonance peaks of healthy and unhealthy cables. Further in this classification, amplitude, and phase angles of the first resonance peak was used to locate the position of the defect. Similarly, in an experimental study [24] on short circuit faults in a three-core cable, faults were identified when the number of resonance points in the amplitude spectrum decreased, and the initial phase angle of the phase spectrum deflected more.

2.3.2. Broadband impedance spectroscopy

The Broadband Impedance Spectrometry (BIS) [21] technique developed by the Boeing company to observe the condition of installed aircraft wings and later used by the Nuclear Regulatory Research of the U.S to evaluate electric cables at nuclear power plant utilizes phase and magnitude impedance measurements. Impedance was used to obtain information on wire properties,

including the dielectric properties of the insulation (real and imaginary components of the dielectric function). Electrical properties of damaged and undamaged cables were extracted from impedance data and compared. For a study on thermally degraded cables, this technique revealed that as the amount of degradation increased, the greater the cable's impedance phase shifted away from −90° for low frequency and high frequency ranges. This indicated a more dissipative cable. Significant impedance phase shifts were observed in figure 3 [21] for higher range frequencies and at higher temperature, clearly demonstrating that thermal degradation has an impact on a cable's electrical impedance spectra.

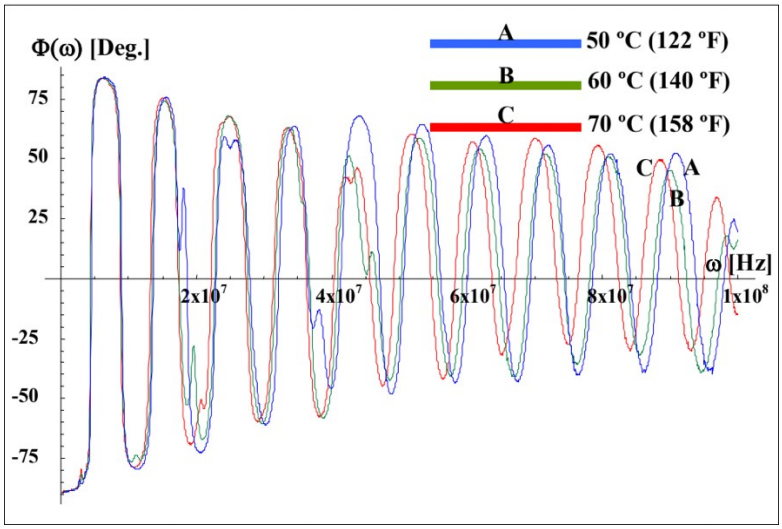

Figure 3 [21]: Impedance phase spectra of cables under varying temperatures

Obtaining impedance characteristics and propagation at high frequency ranges is sometimes problematic [21] due to high noise along the cable. For this study, the authors used an extrapolation method on the results from the low frequency ranges to obtain those of high frequency impedance. The result from this study is very informative. However, analysis made in this research considered steady-state conditions only which is not realistic for real world cable in service, and one can conclude that it is ideal for low frequency ranges.

The BIS technique was verified in [20] by carrying out experimental studies on thermally damaged and water trees induced portions of cables. In both fault scenarios, peaks appeared at locations where gamma rays had been irradiated and at cables with NACL. Sodium chloride was used to induce water trees. Further investigations on the implementation of the BIS technique to precisely locate degraded portions and their severity was done in [22]. The frequency-dependent BIS of a cable sample was transformed to a spatial domain function which showed propagation constant changes along the cable. Changes in propagation constant indicated a bad local insulation condition. Further, a procedure based on particle swarm optimization (PSO) was used to determine complex dielectric permittivity of different degradations and assess insulation condition and to determine fault length [22]. PSO is a computational algorithm inspired by the social behavior of birds and fish. Each particle in the PSO algorithm represented a vector containing values corresponding to the lengths and dielectric permittivity parameters associated with degraded cables. This vector configuration allowed the algorithm to iteratively optimize the goal function, which captured the performance measure related to cable fault analysis. The PSO algorithm, with its population of particles dynamically adjusting their positions in the search space, facilitated the efficient exploration and convergence towards an optimal solution. This showed that impedance spectroscopy cannot only be used to detect a fault but also to locate and assess its severity.

Analytically, impedance at a certain position along a cable of length l, can be measured using the expression in equation (3) [22]:

$$Z_x = \frac{V(x)}{I(x)} = Z_0 \frac{1 + \Gamma_L * e^{2\gamma(x-l)}}{1 - \Gamma_L * e^{2\gamma(x-l)}} \tag{3}$$

where Z_0 is load impedance and Γ_L is the load reflection coefficient given in equation (4),

$$\Gamma_L = \frac{Z_L - Z_c}{Z_L + Z_c} \tag{4}$$

When the reflection coefficient is zero, load impedance is equal to the characteristic impedance, $Z_L = Z_0$. The input impedance of a line Z_{in}, which is the impedance seen by any signal entering the line depends on the load impedance, characteristic impedance, length of the transmission line, and the phase constant of the signals propagating through it. $Z_{in} = Z_0$ when the transmission line length is infinite. In the case where the load terminal becomes short circuited, $Z_L = 0$ and when it becomes open circuited, $Z_L = \infty$.

During experimental analysis of this research work, a 50 Ω load was connected at the end of the cable and an impedance analyzer was used to measure cable impedance. When the load is unreachable, load impedance is measured by method of wavelet-transform-based-time-frequency domain reflectometry [22], [25].

For impedance spectroscopy to be useful and effective, it is recommended to compare fault analysis results to certain historical data of healthy cables and past fault scenarios. This is because impedance also varies slightly with current load, and a load variation should not be mistaken for a fault. With the goal of studying the unpredictable variation in impedance on a line which causes poor communication, Rasool and Co's derived a statistical model of impedance behavior [26]. Using the transmission line matrix, the impedance matrix was obtained, and it was observed that the network impedance varies significantly with varying loads. Both magnitude impedance and phase impedance increased with increasing frequency, but the phase gradually became constant [26]. However, for a test at room temperature and with balanced load, the impedance of conductor was found to oscillate between 0.39 and 2.53 Ω [27]. Successful fault diagnosis in power cables using impedance spectroscopy requires that electric utilities record and save historical data properly. These data can be used to establish impedance baselines for diagnostic purposes.

2.3.3. Impedance measurement techniques

Several researchers have focused on extracting impedance measurements either by models or equipment and used these impedance data to detect, analyze, classify, and quantify damages in

power cables. The common result in these studies is magnitude changes and phase shifts in impedance data which are indicators of cable faults and degradation. A good number of impedance measurement techniques, their limitations and impedance behavior during faults were observed repeatedly in the literature review.

In [28] impedance was measured by applying a single frequency voltage to a cable and the phase shift and amplitude of the resulting signal at that frequency was measured using fast Fourier transform (FFT) analysis. FFT analysis is known to convert signal data obtained as a function of time or space to those represented as a function of frequency and vice versa [20]. Analyzing the relationship between cable system properties and response to periodic voltage or current is difficult in the time domain, hence Fourier transformation is often used [28]. There has been continuous improvement on ways to measure impedance as a function of frequency easily and accurately. Some instruments and techniques include, spectrum analyzers, twin-beam oscilloscopes, transformer ratio arm bridges and automated frequency response analysis [28](chap 3). Although there are continuous improvements, impedance measuring techniques and tools still have limitations in measuring high frequency impedance and in some cases low frequency ranges as well.

As earlier mentioned, obtaining impedance characteristics and propagation function at high frequency ranges is sometimes problematic [21] due to high noise. Existing high frequency impedance measurement techniques cannot be directly linked to the operating power network [29] and in certain cases, the instrument used to measure impedance is heavy and cumbersome [30]. An extrapolation method was used in [21] to obtain impedance measurement for high frequency range during a broadband impedance spectroscopy (BIS) experiment. During the experiment, low frequency impedance was obtained using Hewlett-Packard instrument and recorded by a software but for high frequency ranges, a model was used to extrapolate from low

frequency ranges. Clamp technology [29], [30] which involves a blocking unit, has not proven to be a success as the technology needs to be tested on long and in-service cables.

Recent non-intrusive techniques such as power line communication (PLC) with power line modems (PLMs) which record network parameters seem to be a better option as these PLMs already exist on the grids [31]. PLC uses a carrier-frequency technique to transfer data between terminals. Communication signals are converted from digital to analog in the PLC modem and transmitted through the power line. At the receiving end, the second PLC modem converts the analog signals back into digital form [32]. Distorted signals recorded by PLMs provide information about the physical properties of grid components [33]. PLC have previously been explored for remote metering[34], to determine network topology [35] and just recently, to detect and localize faults [33], [36]. The advantage of this method is that it is cost effective, cables remain in-service, and the estimation is performed continuously [31].

2.3.4. Limitations of impedance spectroscopy

Impedance spectroscopy is a popular diagnostic technique because it requires a simple measurement of electrical impedance, and its results can be analyzed to detect defects, dielectric properties, microscopic processes, composition change [28] and so on. It is a tool for investigating electrical properties of cables and extracting valuable information. However, there are a few limitations to this technique depending on the approach used during the analysis.

Firstly, interpreting impedance results is more accurate when using distributed transmission line models compared to lumped circuit models [28]. Lumped circuit models are suitable for short cable lengths, treating the entire cable as a lumped element. However, for distributed cable systems with longer lengths compared to the wavelength, the cable exhibits distributed effects, leading to variations in its electrical properties along its length. This makes the use of distributed circuit elements necessary for accurate analysis. Another major drawback is the lack of uniqueness in data treatment, as a set of impedance plots can have multiple equivalent circuit

models, making it challenging to determine the most suitable representation [37]. Additionally, the application of AC impedance modeling often requires special measurement equipment and lacks convenient analysis software for handling non-linear and non-static impedance models, further complicating the process [37].

Another limitation lies in the sensitivity of AC impedance, as it can be affected by both internal and external factors during experiments, potentially leading to inaccurate results [37]. The challenge of finding a balance between simplifying the model to relate to real-world situations and maintaining mathematical tractability poses an ongoing obstacle in AC impedance modeling for fault detection in cables [37]. While impedance spectroscopy is an efficient technique for fault diagnostics in underground power cables, these limitations must be carefully considered and addressed to ensure reliable and effective fault detection in cable systems.

2.3.5. Other fault diagnostic techniques

According to [38] common fault diagnostic methods can be categorized into traveling-wave based methods [38], [39], impedance-based methods [40], and artificial intelligence algorithms [41]. Traveling wave methods (TWT) follow the principle that when a fault is encountered, traveling waves are generated and propagate along the transmission line. Analysis of these waves gives valuable information such as cable parameters and fault location. For example, in [42], complex wavelets were combined with continuous wavelet transform (CWT) and impedance phase and magnitude were calculated from the resulting wavelet domain to examine cable conditions. Fault features from voltages are measured and extracted using a discrete wavelet transform (DWT) analysis method to locate high impedance frequency (HIF) faults in [43]. Two well-known reflectometry techniques, time-domain reflectometry (TDR) and frequency-domain reflectometry (FDR) can also be classified as a wave technique. In TDR techniques, when a signal encounters a fault, a portion of the wave is reflected to the source and the other is transmitted forward. The reflected wave characteristics such as amplitude, time for reflection to travel back and

propagation speed provide insights on cable length, cable properties and fault location. The wave characteristics in any of the methods mentioned above are determined by impedance changes along the line. Hence impedance methods are indispensable.

Impedance based fault location models and AI algorithms are the most used methods since they are easy to implement and produce reasonable location estimates [40], [44]. A comparison between the BIS technique and time domain reflectometry done in [45], revealed that BIS is superior to TDR, as clear peaks were observed for degraded portions of the cable specimen, while no such peaks appeared in TDR.

2.4 Power cable thermal management: monitoring and dissipation analysis

Performance of underground transmission and distribution power lines relies mainly on thermal properties of the cable and its surroundings. The maximum current carrying capacity of a cable, referred to as ampacity, depends on the maximum temperature a conductor can withstand [22]. For continuous rating in XLPE – insulated cables, 90 °C is the admissible maximum conductor temperature, with an emergency rating of up to 140 °C [15], [46]–[48] and can go up to 250 °C in short circuit situations [49]. Above these values, overheating and melting can occur. Continuous exposure to extreme temperatures provokes gradual insulation degradation and changes in conductor electrical properties. Over time, this process impacts cable lifespan, causes irreversible changes in material composition, and possibly leads to cable breakdown. It is recommended to de-rate cable ampacity as cables age or degrade.

As current flows in an underground power cable, heat is generated due to cable electrical resistance. This resistive heat is dissipated to the surrounding environment through the process of conduction. The quantity of heat generated depends on conductor electric resistance and current flowing through the conductor, as shown in equation (5).

$$Q = I^2 R_{e\,AC} \quad (5)$$

The higher the current loading, the larger the amount of heat it generates and the higher the cable conductor temperature [50]. For this reason, heat dissipation in cables must be very convenient to avoid overheating. Other factors such as conductor cross-sectional area, buried depth, backfill, soil, insulation resistivity and nearby heat sources also influence temperature rise, ampacity and the process of heat evacuation in underground power cable systems [47]. An experiment on thermal field sensitivities of underground power cables carried out by [51], showed small steady increase in insulation temperature (between 30 °C and 50 °C) as the tested cable was loaded at 300 A and when increased to 600 A, a sudden sharp spike in temperature was observed (to 100 °C) before coming to a steady state. Temperature distribution and temperature profiles of faulty cables provide early warning signs of compromised insulation layers. Accurate Interpretation of these profiles help to detect localized hotspots and overheating along the cable's length.

Technological advancements have made it possible for real-time temperature monitoring and its integration with other parameters such as current, voltage and impedance. Non-intrusive methods for measuring cable temperatures such as fiber-optic distributed temperature sensing (DTS) and infrared thermography provide real-time temperature data along the cable's length, allowing the detection of hotspots and temperature abnormalities. Conductor temperature can also be obtained directly from historical data by determining conductor power losses considering the joule heating through the conductor [52].

2.4.1. Energy balanced equations

Throughout the cable's lifetime, continuous heat movement within and around underground cables gradually causes changes in the cable's physical, chemical, and structural properties. These changes are reflected on cables' electrical properties which when extracted and analyzed can be used for condition monitoring of cables. Electrical losses primarily caused by resistance are

conducted outward through the process of conduction in the form of heat. All cable layers within the cable take part in the process of conduction. Temperature is highest at the core and gradually decreases towards outer layers, forming a temperature gradient. On the outer surface, depending on whether the cables are buried directly in soil or in the duct, the process of convection and radiation occurs. The soil or surrounding medium acts as a heat sink, gaining the heat from within the cable, helping it to cool.

There are also external heat sources to consider when carrying out thermal analysis for a cable system. Some of these heat sources are heating from nearby conductors and mutual heating from other ducts in the vicinity. However, in this paper our focus remains on internal heat sources which are conductor losses, dielectric losses, sheath losses and skin-effect heating. External heat sources are assumed to be zero.

With heat being generated from the conductor, leading to a temperature rise, the energy balanced equation for an operating cable system is given by (6) [53]:

$$Q_{entering} + Q_{generated} = Q_{dissipated} + \Delta Q_{state} \quad \text{(in W/m)} \quad (6)$$

where

- $Q_{entering}$ is rate of heat energy from external sources around the cable,
- ΔQ_{state} is the rate of change of energy stored within the cable,
- $Q_{generated}$ is the rate of heat generated per by the cable (Joule or dielectric losses), and
- $Q_{dissipated}$ is the rate heat transfer from cable system (conduction, convection, radiation)

In this study, $Q_{entering}$ and ΔQ_{state} are considered zero. Equation (6) becomes (7),

$$Q_{generated} = Q_{dissipated} \quad (7)$$

2.4.2. Underground power cable temperature factors

In the absence of faults and under ideal environmental conditions underground power cables operate in a relatively constant thermal equilibrium state. That is, the amount of heat generated due to electrical losses is balanced by the heat dissipated to the surrounding environment through conduction, convection, and radiation (7). Temperature distribution of healthy cables exhibit uniformity along the cables' length and in its radial direction when uniform material properties are assumed. In chapter 3, a finite element analysis for heat conduction in the cable system was solved. The temperature distribution across all cable layers was obtained using a non-faulty cable model. For a steady state analysis, the highest temperature was observed at the conductor and decreased towards ambient. For a transient analysis, as temperature changed with current source load and time, the same trends were observed but with no spikes on the plot.

Although temperature may vary slightly due to load changes and external factors, variations observed within certain limits are acceptable. Monitoring of normal temperature patterns provides a baseline against which deviations caused by faults can be detected. Heat stresses in power cables can cause hotspots abnormalities in the cable's insulation. This causes rapid temperature rise, provoking unacceptable heat dissipation rates and leading to distorted and asymmetrical temperature profiles. Higher peak temperatures signify the presence of faults, reduced value in electric conductivity and more power losses [54].

Environmental factors such as soil thermal properties and moisture also affect the rate at which heat is absorbed by soil. Heat dissipation processes around buried power cables in different bedding materials in a real scale and operating conditions was investigated in [55] and [50] . The results showed that performance of underground power cables strongly depends on the thermal conductivity of the surrounding bedding material and moisture content. Proper choices of materials surrounding the cable help with effective heat dissipation.

Studies on the temperature rise of 33-kV XLPE underground cable [47], showed that larger conductor cross-sectional areas have lower resistance, leading to reduced heat generation. Higher failures rates of MV underground power cables were observed when ambient temperatures peaked, as well as due to an increase in soil thermal resistivity due to no rainfall [49]. Other factors that influence temperature distribution include burial depth, insulation thickness, cable arrangement, cable material properties and proximity to other heat sources.

2.4.3. Thermal aging impact on cable insulation

Electrical insulation is the primary function of cable insulation. It also protects the cable from external objects. While cable insulation is not primarily intended to provide thermal insulation, its thermal conductivity is considered during cable design as it plays an important role in dissipating heat generated during operations. The cable's insulation electrical resistance approaches infinity for a non-faulty insulation but becomes finite for a damaged insulator since it begins to act as a conductor. As insulation degrades and weakens due to thermal activities which causes changes in insulation material composition, its ability to act as a perfect electrical insulator also reduces.

Other key properties that characterize insulating polymers like XLPE are dissipation factor (DF), relative permittivity (ε) or dielectric constant, volume resistivity, dielectric strength, mechanical strength, chemical resistance, and moisture resistance.

1.) **Dissipation factor (DF),** also known as **tan delta (tan δ)** is a measure of dielectric loss. In contrast to conductors, insulators have no free charge and when an electric field is applied, these bound charges rotate to align with the applied electric field. However, at higher frequencies, the inability of insulators to completely reverse the direction of their dipoles when a sinusoidal electric field changes direction is termed dielectric loss. This loss is dissipated in the form of heat. Dielectric loss factor has different behaviors above

and below melting temperature of XLPE insulation [56]. Higher losses at temperatures above melting point are due to the oxidation process which accelerates the concentration of carbonyl groups. According to Anders [15], dielectric losses in low and medium voltage cables are negligible since they have a low tan delta value.

2.) **Dielectric strength or breakdown voltage** is the ability of the insulation to prevent the flow of current at high voltage stresses. It is measured as the maximum voltage required to cause a dielectric breakdown.

3.) **The dielectric constant,** also known as **relative permittivity,** ε_r is the ability of an insulation material to be polarized in an electric field [57]. It's a complex value and the ratio of its imaginary part $\varepsilon_r^{''}$ and real part ε_r' results in **dielectric loss**. Dielectric constant may also be defined as the ratio between the material permittivity to vacuum permittivity.

A healthy cable insulation has very small dielectric losses and a low dielectric constant. Compared to ethylene propylene rubber (EPR), water-tree retardant XLPE (WTR-XLPEs), kraft and polypropylene-laminated paper (PPLP) cables, cross-linked polyethylene (XLPE) cables have the lowest dielectric constant (2.3) and tan delta value (0.0001) [46], which explains their wide use in the industry. They also have low temperature flexibility; they are **moisture** and **chemical resistant** and have a low cost. However, these benefits were more popular from 1963 when XLPE was just invented and later in 1972, problems associated with water trees and contaminants were identified. Section 2.5 discusses water trees and partial discharges.

Observing trends in historical data of dielectric losses in cable networks is another condition monitoring technique for cable health management. Changes in tan delta are proportional to complex physical processes that occur due to factors such as temperature, moisture, operating conditions, voltage, ageing etc. The value of the dielectric losses increases with continual increase in insulation temperature [15].

4.) Over time, thermal aging causes insulation conductivity to increase and consequently decreases **volume resistivity** of insulation material [56]. Volume resistivity can be defined as the electrical resistance of the insulation or the resistance to leakage of electric current.

2.4.4. Prolonged high-temperature cycles: impact on cable electrical properties

An increase in temperature leads to a detrimental impact on the impedance of the cable and leads to cascading failures. Electrical impedance tends to increase with rising temperatures in the conductor. This is often due to changes in electrical properties such as increased resistivity or altered conductivity, which can result in an elevated impedance. Rising temperatures in turn alters the molecular structure and composition of the insulation. Changes in material composition of the insulation affect conductor impedance. When impedance undergoes alterations, it triggers an escalation in dissipation losses, resulting in the generation of more heat. This heat, in turn, accelerates transformations in material properties and potentially impacts the geometry of the insulation. The cumulative effect of these factors contributes to a cascading failure within the system as presented in Figure (4).

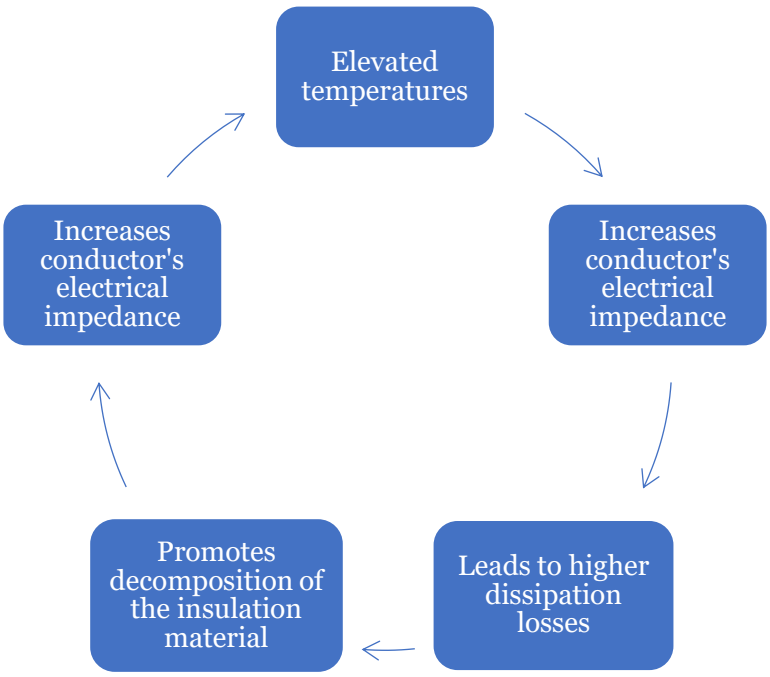

Figure 4: The cyclic effect of continual high temperatures on conductor impedance

Elevated temperatures in operating power cables are often due to unusually high current loads which results in higher Joule losses. In such cases, immediate hotspots could be formed. However, this physics of failure also applies to thermal aging of the cable over time.

In addition to Joule losses, there is an increase in dielectric losses within the insulation. At elevated temperatures, we have a high dissipation factor or $tan\ \delta$ value. $tan\ \delta$ can be given as the ratio between resistive current and capacitive current:

$$\tan \delta = \frac{I_R}{I_C} \tag{8}$$

Large amounts of resistive current results to a high $tan\ \delta$ value and according to equation (20), section 3.3.2 in chapter 3, dielectric losses in the form of heat will be higher. High dielectric losses lead to increased heat generation within the cable, coupled to conductor Joule losses, this excess heat can potentially accelerate molecular breakdown of insulation material. Distortion in the structural and chemical compositions of the insulation also affects its electrical properties;

insulation volume resistivity decreases in thermally damaged cable. A reduced insulation resistance enhances higher heat dissipation rates and weakens the insulation's thermal, electrical and geometry properties. This result has a gradual cyclic effect which goes on throughout the cable's lifetime until complete breakdown occurrence. Further, high dielectric losses in cables create conducive conditions for other damaged models such as partial discharges (PDs) and water trees. Figure 5 summarizes the cyclic effect of continual high temperatures on cable insulation.

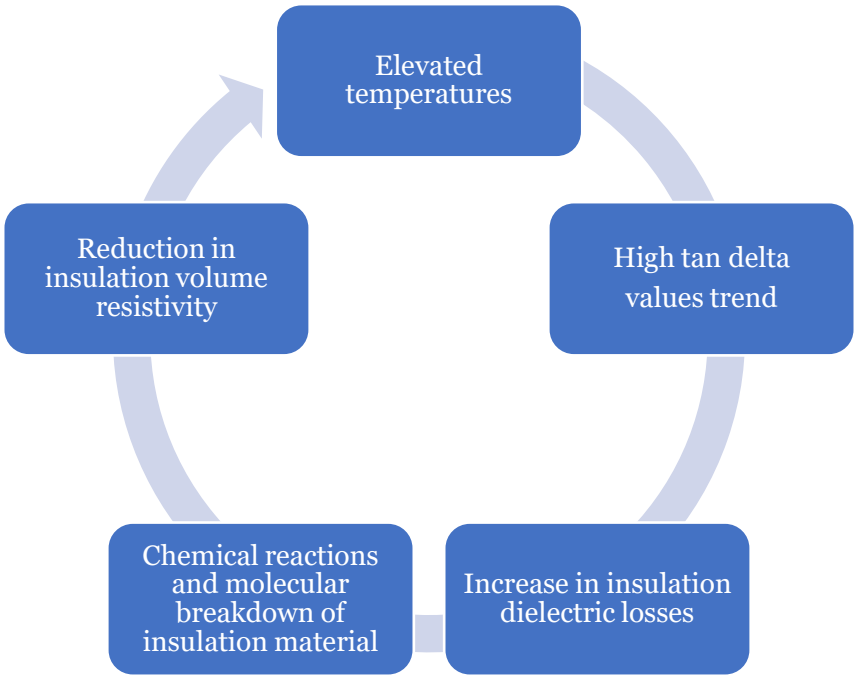

Figure 5: Cyclic impact of prolonged high temperatures on insulation electrical properties

An experimental study on the effect of thermal aging [56] on XLPE insulation, revealed an increase in dielectric losses factor ($tan\ \delta$) with aging time, consequently, increased heat generated within the insulation and faster material deterioration. $tan\ \delta$ was measured using an impedance measurement bridge with an applied voltage of 1 V at 80 °C, 100 °C, 120 °C, and 140 °C, over a period of 5000 hours. Even though $tan\ \delta$ generally increased with aging time, it behaved differently at different temperatures. It can be seen from Figure 6 [56] that temperatures around XLPE specific operating temperatures, which is 90 °C, had fluctuating and decreasing $tan\ \delta$ values

and at higher temperatures above melting point, $tan\ \delta$ increased exponentially. This is due to the concentration of carbonyl groups due to the oxidation process at elevated temperatures [56].

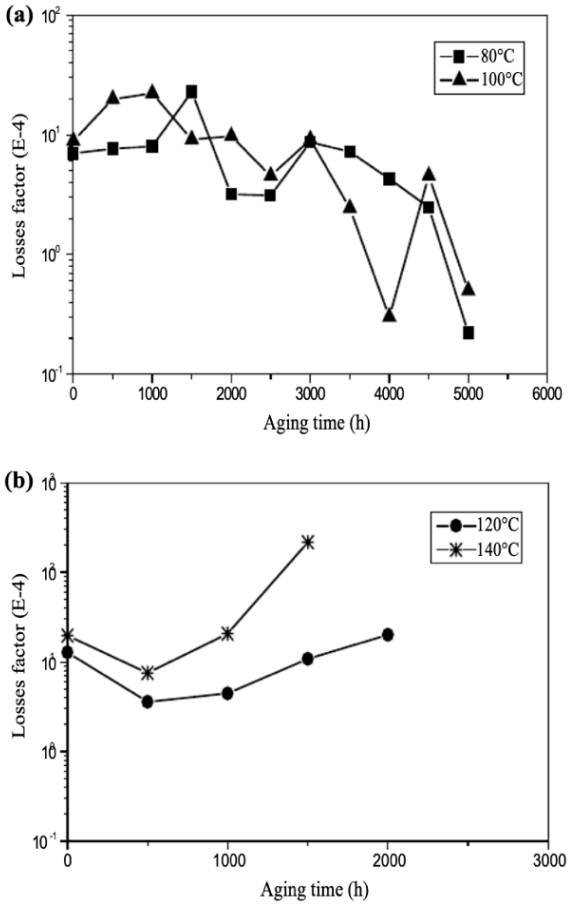

Figure 6 [56]: Cyclic impact of prolonged high temperatures on insulation electrical properties

According to the authors, the existence of peaks in figure 6(a) were attributed to the relaxation phenomena—which is the movement of XLPE molecular chains—leading to more dielectric losses.

Dielectric dissipation factor serves as a straightforward diagnostic technique, where an AC voltage signal is applied to the cable under test across various frequencies. Using a signal analyzer, the dielectric phase angle is measured and recorded at each frequency increment, and this data is then used to calculate the dielectric loss or power factor [21]. Nevertheless, the limitation of this method lies in the requirement to de-energize cables for instrument connection, which is not ideal

for monitoring or diagnosing cables remotely during their operation. This constraint highlights the need for alternative diagnostic approaches that enable real-time assessment without interrupting the cable's operational status.

2.5 Other damage models

2.5.1. Partial discharges (PDs):

Aging of cable insulation often results in partial discharges before it reaches an advanced stage or breakdown point, hence the presence of PDs is an early indication of dielectric failure but not instantaneous breakdown. PDs are localized electrical discharges that originate from defects in the insulation of power cables. If they are not properly addressed, deterioration will occur, usually forming water trees, which are further accelerated by continuous overheating. However, not all PDs are a major concern but should be monitored. For example, [58] mentioned that Internal PDs in cable joints or terminations require immediate attention while periodic monitoring is required for surface PDs. Corona discharges which take place away from the solid insulation also have a different maintenance approach from electrical treeing which is caused due to continuous impact of discharges, forming discharge channels. PDs are stochastic in nature, several factors may account for them, and they tend to exhibit different properties at different aging stages [58].

Conditions necessary for voids in cable insulation to discharge are: they must be large enough; they must not be filled completely with a liquid and if filled with gas, the gas should be at a low pressure [59]. As voltage builds up across a void, the gas in the void will ionize and discharge at a peak voltage commonly referred to as voltage inception. This discharge redistributes electrical charge within the dielectric [21] and this redistribution of charges can alter local electrical properties, including impedance.

PD testing involves applying relatively high-test voltage and measuring these small current pulses from the redistribution of charges. This diagnostic technique provides valuable information about

insulation conditions but there are controversies about whether testing of cables should be done offline or online. Online PD diagnostic methods include high-frequency current transformers (HFCT), ultra-high frequency (UHF), acoustic emission (AE) methods, ultraviolet (UV) imagers, capacitive coupler (CC) sensors, and magnetic coupler (MC) [16]. According to literature, some researchers point out that offline PD tests are more reliable due to the absence of noise compared to online PD tests [60]. However, online tests mimic real operating conditions; considering environmental conditions and the electrical and thermal insulation conditions. Offline diagnostic tests include very low frequency (VLF) voltage, AC voltage test and damped AC voltage (DAC) [16]. Even though the issue of noise is avoided in offline testing, offline PD tests can easily create more PDs in the cable [46].

Thermal degradation-induced partial discharges are PDs resulting from existing voids from the manufacturing stage and thermally caused small cavities. Not only are they enhanced by heat, but when discharging, they also dissipate energy in the form of heat, sound, light, chemical reaction and electric current [16]. In summary, PD detection and monitoring is a predictive test essential to ensure reliability and a good first step for condition monitoring of any damage model in power cables.

2.5.2. Water trees

Moisture ingress in the insulation coupled with existing imperfections generate high electrical stress points, resulting in the growth of water tress [46]. Water trees weaken the insulation and cause premature cable failure. The metallic sheath layer prevents water trees, however in high voltage cables, in the presence of moisture, the electrical stress increases and possibly initiates electrical trees, which rapidly grow and lead to cable failure [46].

A dynamic growth model of water trees as a function of time for insulation tracking degradation was recently studied in [61]. Compared to steady state studies [62], the authors used changing water tree dielectric permittivity, water trees radial growth and length and its angular expansion

to account for the dynamic shape changes of water tree which can help track the progress of insulation degradation. Elevated temperatures accelerate water trees formation. When temperature increases, water trees tend to grow longer and more complex and the water molecules in these trees migrate easily forming more water trees.

Water treed regions have a higher dielectric permittivity compared to healthy regions [63]. This is because water molecules have a higher dielectric or relative permittivity than insulation material. As result of this, we begin to have localized variations in permittivity within the insulation and a weakening insulation. Recalling from section 2.4.3 that the ratio of imaginary permittivity $\varepsilon_r^{''}$ to its real part ε_r' gives the dielectric loss, brings us back to the cyclic effect explained in 2.4.4. Increase in $\varepsilon_r^{''}$ results in higher dielectric losses, which manifest as more heat within the insulation layer.

2.6 Chemical decomposition in thermally aging XLPE insulation

Deterioration in dielectric behavior of cables can be attributed to both chemical and physical changes. Quantum chemical calculations and experiments on polyethylene insulation carried out in [64] gives an insight on how temperature affects molecular composition of insulation material leading to thermal fragmentation and oxidative degradation. Figure 7 [64] summarizes physical and chemical defects that take place in a thermally aging polyethylene insulation material.

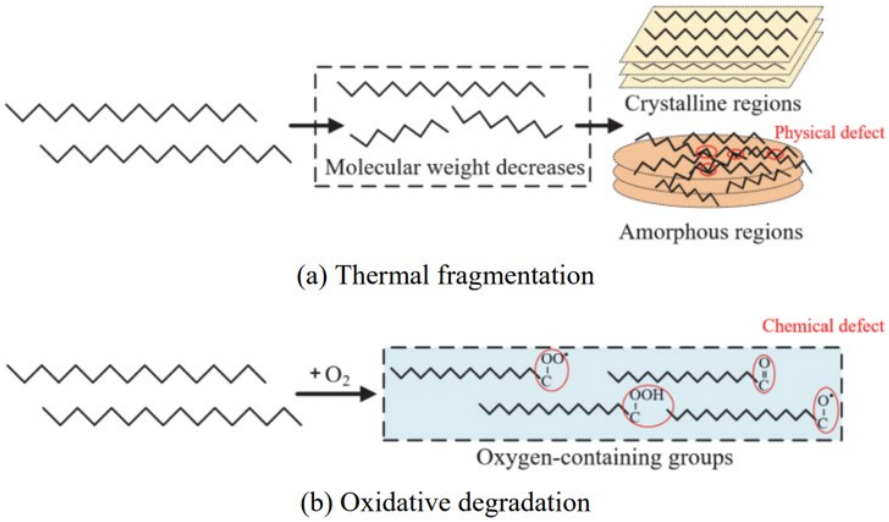

Figure 7 [58]: Chemical decomposition of XLPE insulation

As XLPE thermally aged, there was a decrease in molecular weight due to thermal fragmentation which reduced XLPE crystallinity. Crystallinity reduction was due to strong mobility of these smaller molecular fragments. More amorphous regions were then created, reducing crosslinking with aging time. Inter-chain bond breaking was responsible for physical defects such as shrinkage [56] observed on thermally aging insulations. The increase in the number of cross-linking points made the arrangement of molecules more orderly and the network structure more stable. On the other hand, a decrease in the cross-linking points resulted in unstable and weak network structure and deeper trap depth which eventually formed shallow physical traps in the material.

Further, a Fourier transform infrared spectrometer analysis revealed that as the chemical bonds fractured, new C-O bonds were formed due to thermo-oxidation. This changes the molecular composition of the polymers. In summary, the chemical defect caused by thermo-oxidative degradation is the main reason for observed deeper traps and the decrease in the insulation performance of the material.

Similarly, from the results of an experimental analysis [11] on flame retardant XLPE cables, which are mostly used in nuclear power plants, cross linking and oxidative decomposition was observed

and resulted in the classification of insulation material decomposition into three stages. In the first stage, there was a decrease in the imaginary part of complex permittivity $\varepsilon_r^{''}$ because of cross-linking in the material. The material became harder when cross-linked and this impeded the movement of charge carriers and the orientation of polar groups (loses its softness), indicating that insulation property is improved [65].

In the second stage, oxidation degradation became dominant, and the imaginary part of permittivity $\varepsilon_r^{''}$ increased instead. In the last stage, the two parts of complex permittivity increased with increasing temperatures. This indicated a worsened condition of the insulation property. This three-stage insulation degradation classification is confirmed in [56] wherein consequences of thermal aging on electrical properties of XLPE insulation are explored. The experimental study carried out in this paper showed that induced heat at temperatures of 120 °C and 140 °C showed sharp increases in the dielectric constant towards the end of the aging time whereas the relative permittivity was relatively constant at temperatures of 80 °C and 100 °C. In parallel, dielectric losses factor decreased due to increase in crystallinity at the beginning of aging and later increased exponentially due to increased mobility of charge carriers. In the case of lower temperatures such as 80 °C and 100 °C, a less consistent result with several peaks was obtained. According to the author, these peaks were due to movement of molecular chains and more dissipation losses in the insulation material.

Consequences of thermal degradation are changes in color, reduced thickness and decrease in diameter of samples, weight losses and decrease in crosslinking degree [56]. An AC impedance analysis made on aged samples showed that they have lower impedance compared to new ones with unbroken crystalline structure [66].

2.7 Dynamic vs steady state analysis

In [67], the authors emphasized on the use of temperature distribution rather than temperature when designing high performance cable systems; the best way to calculate instantaneous temperature is through transient analysis, not steady state. It was demonstrated in this study, that at steady state, thermal resistances are higher compared to transient state analysis of the same cable. Results in a phase diagram, showing temperature versus power using time as a parameter is more informative compared to graphs with either temperature or power as a function of time [55], [54]. In [54], a dynamic thermal analysis study was compared to that of a steady state analysis using changing electric power losses as the input signal into the system. Benefits of doing a dynamic analysis is that one can determine instantaneous cable temperatures which are not predicted in the case of a steady state analysis. The only way to achieve steady state condition for power loss is using its mean value (power loss from DC current) and not its variable part. Most publications addressing underground power cables focus on steady-state analysis, assuming constant joule losses and, consequently, consistent cable temperatures over time. However, in practical scenarios, joule losses exhibit variations continuously. As a result, a dynamic analysis becomes essential to gain a comprehensive understanding of the issue.

Recently, impedance-temperature profiles in distribution lines were analyzed in real time through phasor measurement units (PMUs) [27]. PMUs provide voltage and current phase and angle and frequency oscillations at different points. Phasor impedance was recorded for an unbalanced load scenario and for an increasing temperature scenario. The fluctuating behavior of impedance was more noticeable when temperatures were increased. The impedance–temperature relationship demonstrated that temperature negatively influences impedance.

2.8 Advancements in numerical modeling for cable fault diagnostics

Numerical and analytical approaches are used in power cable studies to calculate current carrying capacity and optimal operating temperatures. As previously mentioned, there is a strong link between cable ampacity and temperature distribution. In the past, engineers mostly used analytical approaches to solve heat transfer problems in power cables since this approach is less complicated and has the advantage of computing current ratings in closed form equations [15, p. 31] compared to numerical approaches. Determining the characteristic impedance of a cable with defects proves challenging when employing analytical methods [68]. Analytical methods have a limited application scope since they are only applied for simple geometries and in homogeneous ambient conditions [69]. However, with computer technology advancements, numerical approaches have become popular [14, p. 296] as it is a more flexible and accurate approach [53], [70] . It is possible to incorporate more realistic boundary conditions in numerical solutions. An analytical and numerical approach is used in chapter 3 to determine temperature distribution of an underground power cable and a comparison is made.

Numerical models and solutions have so far been developed for thermal and impedance faults diagnostics as well to study load cycling, temperature, and moisture content of surrounding medium in underground power cables. Simulations of these models allow researchers and engineers to virtually replicate cable physics before and after faults. The finite element method (FEM) is the most popular numerical technique used to solve heat transfer partial differential equations and other physical reactions in power cables [71]. Experimental analyses of power cables or cable networks are often used to verify and validate developed FEM heat models or the other way round [68], [72], [73].

Characteristic impedance of faulted cables were calculated in [68] using the FEM to analyze low impedance faults (LIF) caused by aging and high impedance faults (HIF) caused by damages in shielded cables. The characteristic impedance of those caused by damage was found to increase as the severity of these faults increased. The larger the damage angle, the more characteristic impedance increased. That of aging cables decreased as aging increased. LIFs pose higher threats to the distribution network compared to HIFs. The time reversal time-frequency domain reflectometry (TRT FDR) was further used to locate and evaluate the severity of the faults.

A FEM was used in [74] to develop a model to prove that appropriate backfill and spatial geometry are useful for reducing conductor temperature. Another numerical approach which is often used is the finite difference method (FDM). Faults in shields of coaxial cables were determined by simulating cross-sectional characteristic impedance using FDM [75]. FDM is also commonly used to solve electromagnetic transmission line problems [76]. In [77], the Finite Difference Method was used to analyze thermal resistance between an underground power cable and the ground surface. This assessment included modifying geometrical configurations and adjusting the thermal properties of both the mother soil and the backfill. A combination of volume-element method for thermal analysis and finite-difference time domain technique was used in [78] for a transient analysis of gas-insulated transmission lines. Three main steps considered in a numerical solution for an underground power cable are: discretization of region and boundary conditions, computation of cable losses and selection of time step. A case study is developed in chapter 3 following these steps.

2.8.1. Coupling impedance analysis and thermal distribution in a multi-physics model

The term “Multi-physics” refers to a field of study that involves different simultaneously occurring physical fields [71]. Multi-physics models are based on coupled equations encompassing parameters of various physical fields under study, providing more accuracy in calculations. An

electro-thermal model for a transient state and steady state analysis of temperature and impedance is proposed. Correlating temperature distribution and impedance changes provides a holistic understanding of fault's impact on the cable's behavior. Advantages of developing such multi-physics model for fault diagnostics are:

- It enables a multi-dimensional analysis of cable health. As earlier seen, temperature monitoring can show insulation degradation and localized hotspots, while analysis on an impedance spectrum can reveal insulation breakdown, conductor damage and other abnormalities with the cable's primary line parameters (R, L, G, C). Combining both techniques allows engineers to capture more faults, providing a more precise assessment of the cable's condition.
- Depending on equipment and techniques deployed, integrated models can reduce maintenance costs, downtime, and even human labor. An accurate thermal-impedance model will avoid diagnosing temperature faults separately from impedance related faults. In addition, richer datasets obtained from such models can assist in making optimized asset management decisions.
- Temperature monitoring models can detect faults in a power network but not their exact location. Integrating this diagnostic method with an electrical impedance model and reflectometry diagnostics can aid in locating faults and their severity.

Multi-physics models for fault diagnostics in underground power enhance reliability of power distribution and transmission networks. An electromagnetic thermal coupling model, considering temperature gradient within cables due to air trapped between the wires forming the stranded cables was developed by [79]. This mathematical model examined the combined effects of heat conduction considering variations of electric resistivity with temperature [79]. A coupling parameter, k was used to measure the interaction between the electrical and thermal fields. The

numerical analysis results showed that temperature profiles are strongly influenced by the skin parameter, which depends mainly on frequency of the alternating current.

Current density distribution and temperature variation were simultaneously simulated in COMSOL Multi-physics to analyze changing geometrical and physical parameters of armor wires during short circuits in optical ground wire cables in [80]. A FEM-based Multi-physics approach was used with the commercial ANSYS software suite to model temperature distribution in cable systems [71], in which it was seen that heat exchange rate are significantly affected by uneven current distribution caused by proximity and skin effects, their spatial configuration and environmental boundary conditions [71]. Results from the computed temperature profiles revealed that for trefoil geometry when the cables are set apart, favorable heat exchange conditions were achieved. However due to space limitations, sometimes the use of congested geometry is necessary [71].

Extensive studies have been carried out on Multi-physics analysis of coupled electromagnetic and thermal phenomena of underground power cables. However, a coupled analysis correlating electrical resistive impedance and resistive heat to analyze cable abnormalities and insulation degradation has not really been explored to the best of my knowledge.

2.8.2. Equivalent thermal circuits

For the thermal analysis of a cable with four layers (including core, insulation, sheath, and jacket), Figure 8 represents a schematic of Foster-equivalent RC thermal network. One can further model an additional layer which represents soil surrounding the cable or additional cable layers.

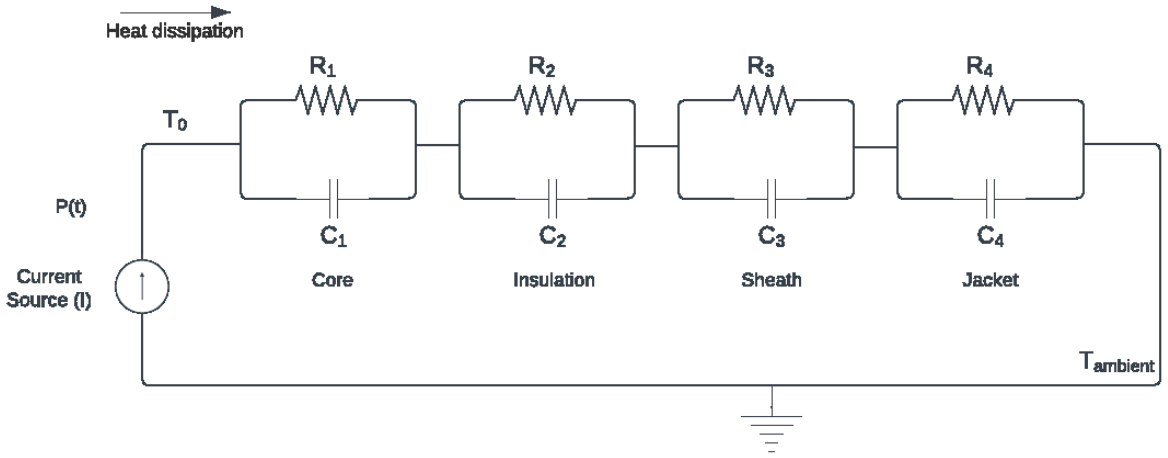

Figure 8: Underground cable system Foster-equivalent thermal circuit

Each layer has thermal and corresponding electrical parameters. An electro-thermal analogy is shown in Table 1.

Table 1: An electro-thermal analogy

Electrical Model	**Thermal Model**
Potential difference(V)	Temperature difference(K)
Electrical resistance (ohms)	Thermal resistance(K/W)
Electrical current(I)	Power (heat flow) (W)
Electrical Capacitance(F)	Thermal Capacitance (J/K)

A current source (I) applied to the cable is directly proportional to the instantaneous power P(t) and inversely proportional to voltage. Using a nodal analysis approach, the voltage difference (ΔV) at each node is equivalent in value to the temperature increase from the ambient temperature (ΔT), which is indicated by ground potential. For thermal processes, nodes (through variables) represent heat flux denoted by T, and loops (across variables) represent temperature change denoted by ΔT. For electrical activities, nodes represent current through denoted by current I, and loops represent voltage difference denoted by ΔV.

Foster and Cauer thermal network models are often used for thermal characterization in devices and systems and are modeled in terms of their electrical parameters. However, Foster network circuits are considered less effective as they are suitable for systems where heat storage is significant and heat transfer is relatively slow. On the other hand, the Cauer thermal model extends the modeling capability by accounting for thermal inertia (due to heat capacity and thermal resistance of various layers). It captures fast heat transfers, considers physical parameters [64] and cable geometry. Generally, it provides a better physical reality of the cable system. In addition, more block layers can be added for simulation in a Cauer network. However, the mathematical representation of a Cauer network can be complex to obtain.

A better way to model a cable system will be by using a Cauer circuit since thermal resistance and capacitance can be obtained from the cable geometry and material properties. The maximum temperature rise per unit of applied power represents transient thermal impedance or transient thermal response given by equation (9) [72]:

$$Z_{th}(t) = \frac{T_{core} - T_{\infty}}{P} \tag{9}$$

Where Z_{th} is thermal impedance and t is pulse duration, T_{core} is temperature of the conductor and T_{∞} is ambient temperature.

An equivalent Cauer network is derived from the foster network (Figure 8) and represented in Figure 9.

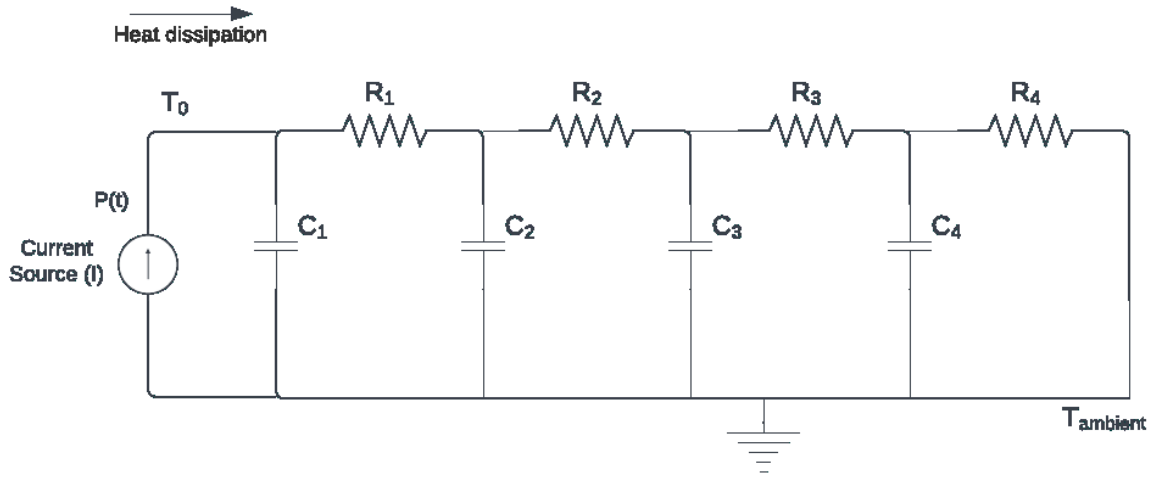

Figure 9: Underground power cable system - Cauer thermal circuit

In summary, fault diagnostic techniques like impedance spectroscopy, temperature monitoring, partial discharge tests, and dissipation loss factor are valuable for monitoring cable health and detecting faults. Despite their effectiveness, these methods have limitations, as discussed in this chapter, including the need to de-energize cables during testing and the unreliable and cumbersome nature of some diagnostic tools. Also, impedance spectroscopy with both phase and magnitude measurements presents data interpretation complexities. In the upcoming chapter, this approach will be streamlined by focusing solely on the resistive component of impedance for fault identification. This simplified method will be integrated with a temperature model, creating a comprehensive temperature-impedance model for detecting thermal anomalies in underground power cables.

Chapter 3 Multi-physics modeling and simulation

In the present work, thermal and electrical phenomena in power cables are coupled using mathematical models. Temperature distribution in the cable system represents the thermal field, and the resistive portion of impedance represents the electrical field. Figure 10 illustrates a process flow chart of the coupled model under study. The electrical and thermal models are related by the Joule effect [71].

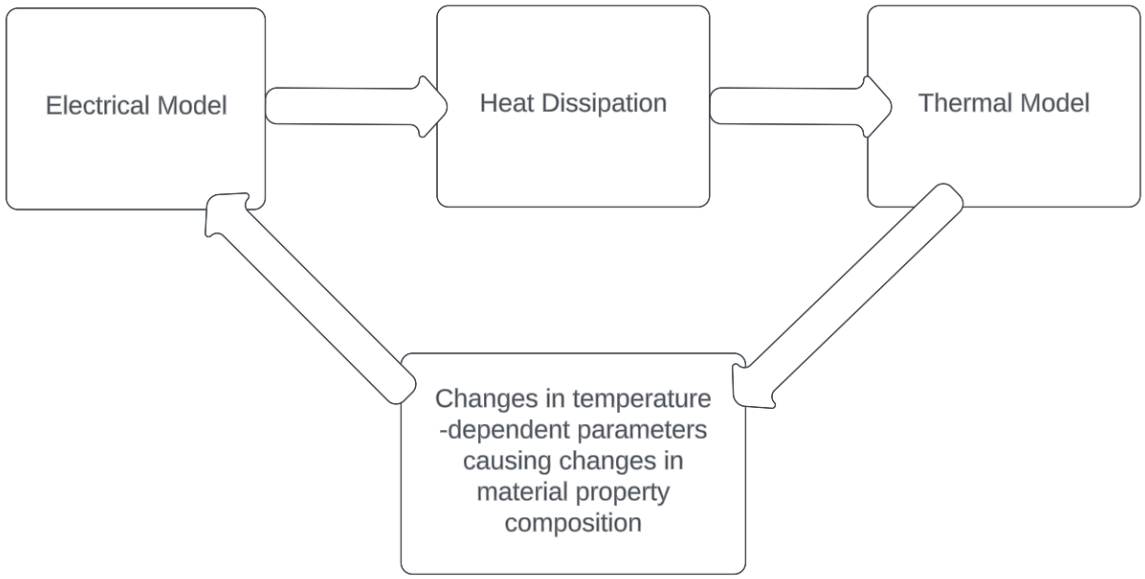

Figure 10: Process flow chart of electro-thermal processes in a cable system

The model and simulation work are limited to the thermal and electrical relationship. However, it is noteworthy that future endeavors will involve the simulation of a geometry damage model, investigating the intricate interaction between the thermal model and material composition of the insulation.

Conductor electrical impedance in an energized cable causes resistive power loss which is released in the form of heat. Combining and simulating the output power loss of the electric circuit portion of the cable with its temperature distribution model across cable layers to obtain a robust and efficient fault diagnostic model is the focus in this chapter. Transient and steady state analyses were both explored, however only the results from that of the steady state analysis are further used in chapter 4 for experimental verifications. The transient heat conduction equations for each layer were solved through the implementation of a FEM approach, utilizing the 'pdpe' function in MATLAB. This methodology was employed to conduct a comprehensive study of transient states within the system. The electrical and thermal coupled cell model was created in the educational simulation environment MATLAB/Simulink (version 23B) by transforming the differential and energy balancing equations into block codes. An analytical approach was used for the steady state and its solution was evaluated in a python code.

A brief overview of fundamental theories behind temperature distribution and impedance analysis have been discussed in the literature review section. In the next subsections, the process of developing a Multi-physics model and assumptions made will be discussed, followed by simulations of the developed model and discussion of results. The chapter will end by listing some challenges and model limitations.

3.1 Numerical analysis and simulations

Temperature distribution was obtained for a 10 KV single conductor XLPE underground power cable. Conductor cross sectional area is 300 mm^2. Its features and parameters are the same as

those used in Anders 1997 – cable model no. 1 [15, p. 363]. Conductor, insulation, copper concentric wires and jacket are the four layers considered. Conductor shield and insulation screen are considered part of the insulation and the numerical data attributed to the copper concentric wires was used as data for copper sheath. Figure 11 is a schematic representation of the cable under study and Table 2 and Table 3 are the cable's geometric properties and material properties respectively.

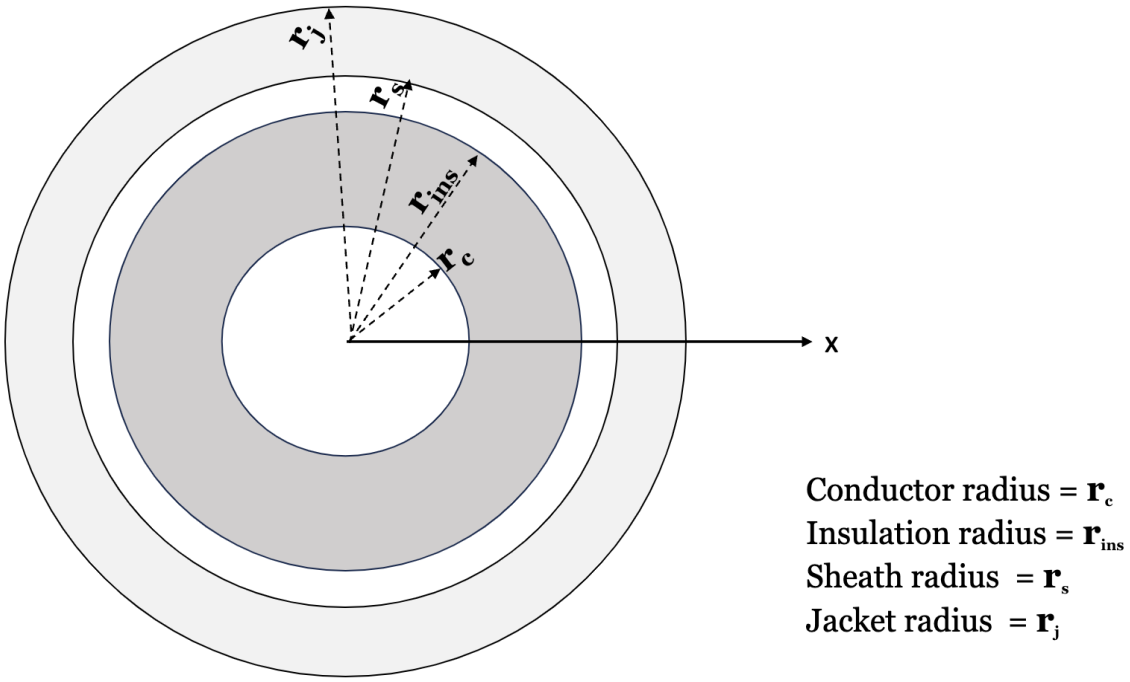

Figure 11: Cross-sectional schematic illustration of heat dissipation in a power cable

Table 2: A 10 KV single conductor underground cable geometry

Cable layer	**Diameter (mm)**	**Thickness (mm)**
Copper Conductor	20.50	0.90
XLPE insulation	30.10	3.4 0
Sheath/screen	31.40	0.70
PVC Jacket	35.80	2.20

Table 3: Cable layers and thermal properties

Cable layer	**Thermal conductivity, k (W/°C .m)**	**Specific heat capacity, c (J/Kg. °C)** [15, p. 198][60]	**Density (kg/m³)**
Copper conductor	400	385	8700
XLPE Insulation	0.286	1739.13	1380
Copper sheath	400	385	8700
PVC jacket	0.10	965.91	1760

The following assumptions were considered:

1) Cable length was assumed to be much larger than its cross-sectional dimensions, and analysis was done in the radial direction. This allowed for the consideration of the cable as a one-dimensional structure.

2) Conductor losses were the main source of heat, and the influence of dielectric and metallic sheath losses were ignored.

3) The cable was assumed to be surrounded by air or in a duct, therefore, a heat convection boundary was applied but radiation was ignored.

4) Cable layers were assumed to be homogeneous and isotropic; they have uniform material properties with thermal conductivities as shown in Table 3.

5) Deformations are thermal only. No forces due to gravity were included.

3.2 Electrical models

DC and AC electrical models are presented in this section. A DC model simulation and experimental analysis was chosen to further explore the thesis hypothesis and establish a

relationship between the electrical and thermal model. This is because amongst several impedance models, Equations 9 and 12 are the most appropriate to capture changes in resistive impedance with varying temperatures. However, section 3.1.2 briefly discusses an AC model.

3.2.1. Electrical model – AC

The transmission line theory [73] suggests that, in the context of high frequency power, a cable system can be viewed as a distributed system with a frequency-dependent resistance, R; inductance, L; conductance, G; and capacitance, C; all per-unit-length [21]. Characteristic impedance Z_o and propagation function are dependent on these four primary line PUL parameters and can be obtained by equations (10) and (11):

$$\gamma = \alpha + j\beta = \sqrt{(R + j\omega L)(G + j\omega C)} \tag{10}$$

where γ represents the propagation constant whose real and imaginary parts, α and β are the attenuation constant (in Np/m) and phase constant (in rad/m); β is $2\pi/\lambda$ and λ is the wavelength of the propagating wave; and ω is the angular frequency.

If the transmission line is ideal, there is no attenuation to the signal amplitudes and the propagation constant turns out to be purely imaginary, with no real power loss along the transmission line. Realistically, operating cables experience some level of attenuation and power losses.

Aging and damage can potentially cause characteristic impedance to vary away from the existing impedance baseline. Characteristic impedance of the line Z_0 can be obtained using equation (11).

$$Z_0 = \sqrt{\frac{R + j\omega L}{G + j\omega C}} \tag{11}$$

Continuous degradation of the insulation causes changes in material property including insulation permittivity, ε . This in turn affects insulation impedance since permittivity has direct

impact on per unit length capacitance (G) and conductance (C) which in turn causes variations in propagation function, γ and characteristic impedance Z_0 [21]. Resulting to magnitude variations and phase shifts in impedance. Given by (12) [21]:

$$G + j\omega C = j\omega\mathcal{E}\frac{2\pi}{ln(r_s/r_c)} \tag{12}$$

Complex permittivity can be obtained by using Cole-Cole functions:

$$\mathcal{E} = \frac{A\mathcal{E}_0}{1 + B(j\omega)^p} \tag{13}$$

$\mathcal{E}_0$ is the permittivity of vacuum, A and B being fitting constants, p is a parameter in the range 0-1.

3.2.2. Electrical model – DC

Contrary to the AC electrical model which considers resistive and reactive impedance, only the resistive portion of impedance is accounted for in a DC circuit. DC electrical resistance $R_{e\,DC}$, value of the conductor per unit length, can be obtained as:

$$R_{e\,DC} = R_{e\,ref}\,[1 + \alpha_{ref}(T_c - T_{ref})] \tag{14}$$

where $R_{e\,ref}$ and α_{ref} are the electrical resistance of the conductor and temperature coefficient at reference temperature T_{ref}.

The reference temperature of the cable under study is 20 °C and T_c is the conductor's limit operating temperature. $R_{e\,ref}$ is often obtained as:

$$R_{e\,ref} = \frac{\rho_{20}\,L}{A_c} \tag{15}$$

where ρ_{20} is specific electrical resistivity of copper conductor at 20°C, in Ω·m.

For the cable under study, $R_{e\,ref}$ = 5.75e-05 Ω and α_{ref} = 3.93e-03. A length L of 1m was considered.

3.3 Power losses in cables

In this section, electrical energy losses in the form of heat are calculated. These losses are used to compute temperature rise in power cables. Conductor losses due to electrical resistance, circulating current losses caused by the metal sheath, and dielectric losses can be calculated according to IEC-60287 standard.

3.3.1. Conductor losses

Heat generation Q, within a power cable is primarily due to conductor electrical resistance. This is termed Joule heating effect and is sometimes labeled conductor losses. It can be obtained using equation (16):

$$\Delta Q = I^2 R_{e\,AC} \quad \text{(W/m)} \qquad (16)$$

where I is the electrical current passing through the cable (in Amperes), and $R_{e\,AC}$ is the AC electrical resistance of the cable's conductor per unit length (in Ohms).

$R_{e\,AC}$ is a function of DC electrical resistance ($R_{e\,DC}$) and the skin and proximity coefficients denoted as y_s and y_p respectively, given by (17) [44]:

$$R_{e\,AC} = R_{e\,DC}\,(1 + y_s + y_p) \qquad (17)$$

Skin effect is a tendency for AC to flow mostly near the outer surface of an electrical conductor, creating a false increase in conductor cross sectional, resulting in an increase in conductor resistance. Proximity effect is the influence of the magnetic fields of neighboring cables, causing current redistribution within the cables in that vicinity. The skin effect and proximity effect in this case study are considered zero for the direct current case.

As a certain amount current flows through the conductor, volumetric heat flux $q_v(T_c)$, generated within the conductor is given as:

$$q_v(T_c) = \frac{\Delta Q}{A_c} = \frac{I^2 R_{e\,AC}}{A_c} \quad \text{(in W/m}^3\text{)} \quad (18)$$

For the steady state DC simulation, $R_{e\,AC}$ in (18) was replaced by $R_{e\,DC}$. A_c is the conductor cross-sectional area.

For the cable under study, initial DC electrical resistance at initial temperature of 20 °C for conductor and sheath were 0.0601 and 0.0781 Ω/km respectively [15].

Equation (19) couples the thermal and electrical model.

$$Q = I^2\left(\left(R_{e\,ref}\left[1 + \alpha_{ref}\left(T - T_{ref}\right)\right]\right)\right) \quad (19)$$

3.3.2. Dielectric losses

Dielectric losses of the insulation layer of the cable per unit length, which was defined in Chapter 2, Section 2.7.3 and can be calculated according to (20).

$$Q = \omega C {U_0}^2 tan\delta \quad \text{(W/m)} \quad (20)$$

Dielectric losses are highly voltage dependent. In [15], it was suggested that they should only be accounted for in high-voltage cables. A verification of this was done by doing an analytical calculation using the 10 KV XLPE cable model no. 1 in [15].

- ω is 2πf and f is 50Hz — 314.16 m
- C is the capacitance of the insulation — 4.23e^{-7} F/m
- U_0 is the voltage that the cable insulation layer bears — 127 KV

- $tan\delta$ is the insulation loss factor 0.004

Dielectric loss = 0.00854 W/m

This value confirms Anders' suggestion. For higher voltages such as a 400 KV cable dielectric loss will have a range between 4.6 and 6.53 W/m [15, p. 112]. Therefore, the temperature rise caused by dielectric losses was neglected in this study.

3.3.3. Metallic sheath losses

A certain amount of circulating current loss and eddy current loss is generated in the metal sheath when the cable is connected to alternating current. Eddy current is assumed to be zero and circulating current loss is obtained by using the ratio of the loss of the metal sheath to the loss of the cable conductor (proportional factor P).

$$P = \frac{R_s}{R}\frac{1}{1+\left(\frac{R_s}{X}\right)^2} \quad \text{(W/m)} \quad (21)$$

where X is the reactance of the metal sheath per unit length given by $X = 2w10^{-7}\ln\left(\frac{2s}{d_s}\right)$, d_s is the diameter of the metal sheath, and R_s is the resistance per unit length at the working temperature of the sheath. This can be obtained by the following equation:

$$R_s = \frac{s_s}{A_s}[1+\alpha_s(T(x,y)\eta) - T_{ref})] \quad \text{(W/m)} \quad (22)$$

where s_s is the conductivity of the metal sheath, α_s is the temperature coefficient of resistance, A_s is the cross-sectional area of the metal sheath, and η is the ratio of the temperature of the metal sheath to the temperature of the conductor.

Metallic sheath losses were considered zero in this study as our focus will be on using DC.

3.4 Thermal model – steady state

A steady state, one dimensional heat conduction equation was solved analytically to determine temperature distribution within an XLPE insulated and solidly bonded conductor cable. The cable heat conduction solution follows a similar study as that in [74]. The rate of heat transfer through each layer of the cable system is expressed as:

$$\frac{\partial^2 T}{\partial r^2} + \frac{1}{r_c}\frac{\partial T}{\partial r} = -q_v \qquad \text{Conductor} \qquad (23)$$

$$\frac{\partial^2 T}{\partial r^2} + \frac{1}{r_{ins}}\frac{\partial T}{\partial r} = 0 \qquad \text{Insulation} \qquad (24)$$

$$\frac{\partial^2 T}{\partial r^2} + \frac{1}{r_{sh}}\frac{\partial T}{\partial r} = 0 \qquad \text{Sheath} \qquad (25)$$

$$\frac{\partial^2 T}{\partial r^2} + \frac{1}{r_j}\frac{\partial T}{\partial r} = 0 \qquad \text{Jacket} \qquad (26)$$

3.4.1. Interface and boundary conditions

A perfect thermal contact is assumed between the layers, and temperature at the interface boundaries are continuous, given by:

$$T_i(r_i) = T_{i+1}(r_i) \qquad for\ i = 1 \dots n \qquad (27)$$

where i is cable layer.

Heat flux passing through various layers are continuous as well:

$$\kappa_i \frac{\partial T_i(\varkappa, t)}{\partial \varkappa}\Big|_{\varkappa_i} = k_{i+1} \frac{\partial T_{i+1}(\varkappa, t)}{\partial \varkappa}\Big|_{\varkappa_i} \qquad for\ i = 1 \dots n \qquad (28)$$

Equations (27) and (28) for layer boundaries are expanded below:

$$k_c \frac{\partial^2 T_c}{\partial r} = 0$$ Heat flux at center of conductor (29)

$$T_c(r_c) = T_{ins}(r_c)$$ Temperature boundary conductor/insulation (30)

$$k_c \frac{\partial^2 T_c}{\partial r} = k_{ins} \frac{\partial^2 T_{ins}}{\partial r}$$ Heat flux conductor/insulation (31)

$$T_{ins}(r_{ins}) = T_{sh}(r_{ins})$$ Temperature boundary insulation/sheath (32)

$$k_{ins} \frac{\partial^2 T_{ins}}{\partial r} = k_{sh} \frac{\partial^2 T_{sh}}{\partial r}$$ Heat flux insulation/sheath (33)

$$T_{sh}(r_{sh}) = T_j(r_{sh})$$ Temperature boundary sheath/jacket (34)

$$k_{sh} \frac{\partial^2 T_{sh}}{\partial r} = k_j \frac{\partial^2 T_j}{\partial r}$$ Heat flux sheath/jacket (35)

Heat Convection boundary was applied at the jacket's external surface.

$$k_j \frac{\partial^2 T_j}{\partial r} = -h(T_j - T_\infty)$$ Jacket/air (36)

Heat transfer coefficient, h_{conv} was set to 10 W/m$^{2.}$ K.

3.4.2. Temperature distribution analytical solution

A general form of equations (23) - (26) can be expressed as follows:

$$T_c = A\ ln\ r_c - \frac{q_v {r_c}^2}{4k_c} + B \quad (37)$$

$$T_{ins} = C\ ln\ r_{ins} + D \quad (38)$$

$$T_{sh} = E\ ln\ r_{sh} + F \quad (39)$$

$$T_j = G\ ln\ r_j + H \quad (40)$$

Where A, B, C, D, E, F, G and H are constants that are determined from boundary and interface conditions (29)-(36). Volumetric heat flux obtained in using Equation 19 becomes the input of the thermal model and A-H are solved as follows:

$$A = 0 \tag{41}$$

$$B = \frac{q_v}{4k_c} {r_c}^2 + C \ln r_c + D \tag{42}$$

$$C = -\frac{q_v}{2k_{ins}} {r_c}^2 \tag{43}$$

$$D = E \ln r_{ins} - C \ln r_{ins} + F \tag{44}$$

$$E = -\frac{q_v}{2k_{sh}} {r_c}^2 \tag{45}$$

$$F = -E \ln r_{sh} + G \ln r_{sh} + H \tag{46}$$

$$G = -\frac{q_v}{2k_j} {r_c}^2 \tag{47}$$

$$H = T_\infty - \frac{k_j}{h}\frac{G}{r_j} - G \ln \ln r_j \tag{48}$$

Equations (41)-(48) were used to obtain a comprehensive temperature distribution across the cable. For the convenience of readers interested in replicating or exploring the details of this analysis, the Python code used has been provided in Appendix A.

3.4.3. Results and discussion

Figure 12 presents the results of the computed analytical equations. A steady state temperature distribution of the cable with respect to its radial axis was obtained.

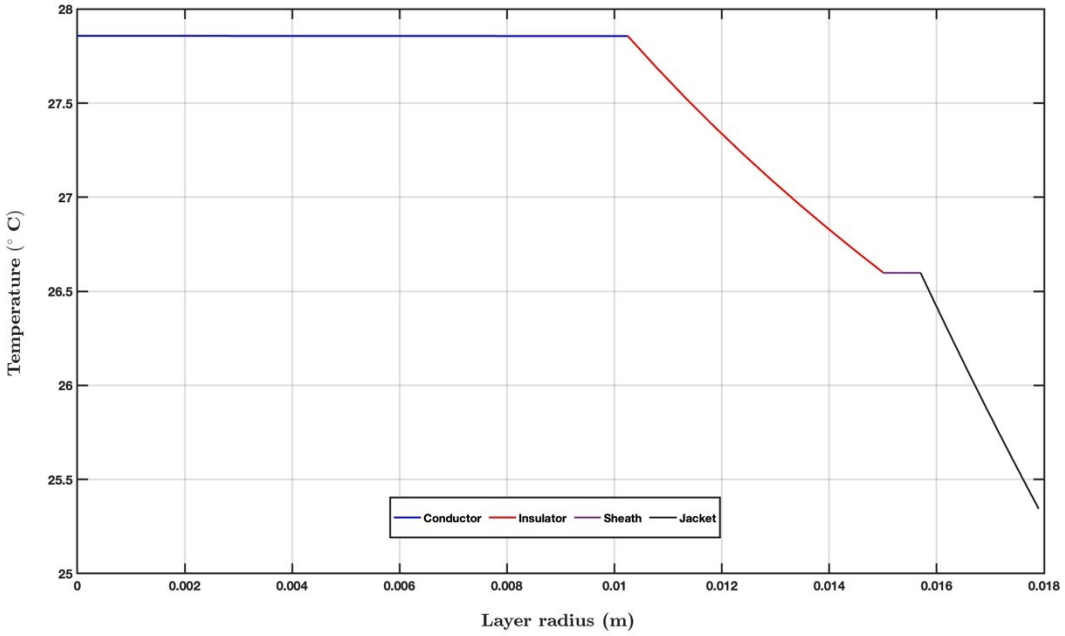

Figure 12: Heat conduction and radial temperature distribution in a power cable. Volumetric heat flux generated by applying a 10A caused conductor temperature (T_c) to rise to 27.8 °C. This establishes a temperature gradient with ambient temperature (T_∞) causing heat to dissipate towards ambient

Load current was 10 A and heat source from the electrical model causes a volumetric heat flux into the conductor, leading to a temperature rise of 7.8 °C, at thermal equilibrium. Heat generated is highest at the conductor as expected. A constant and linear temperature distribution within the conductor is observed. This could be attributed to the fact that, at thermal equilibrium, heat is being generated and distributed uniformly along the radius and length of the conductor whose thermal properties were assumed to be homogeneous. A temperature gradient is established between the conductor and ambient, forcing heat conduction towards the ambient through cable insulation, sheath, and jacket. The amount of heat entering each layer and their thermal conductivities are the reason behind a non-linear trend.

The cable exhibits a declining and non-linear temperature distribution, consistent with findings in [81]. Specifically, the cable conductor and metallic sheath maintain constant temperatures of

27.8 °C and 26.6 °C, respectively, while the XLPE insulation and PVC jacket experience a linear decrease. Engineered for efficient heat dispersion, insulation materials like XLPE prevent cable overheating. The Copper sheath carries little to no heat generation itself as assumed in the computation of model, its temperature distribution is akin to the conductor. The PVC jacket, like the insulation, has a low thermal conductivity, restricting heat transfer and inducing a negative temperature gradient. This simplified model aids in conceptualizing the distinctive functions of various components within the cable structure, providing a solid foundation for comprehending thermal anomalies in power cables.

Elevated dissipation rates contribute to increased cable temperatures. An increase in temperature impacts cable impedance. Monitoring temperature-induced changes in impedance serves as a potential diagnostic method for faults in power cables. A linear relationship is observed when the temperature difference from the thermal model was plotted against resistive impedance from the electrical model, as illustrated in Figure 13.

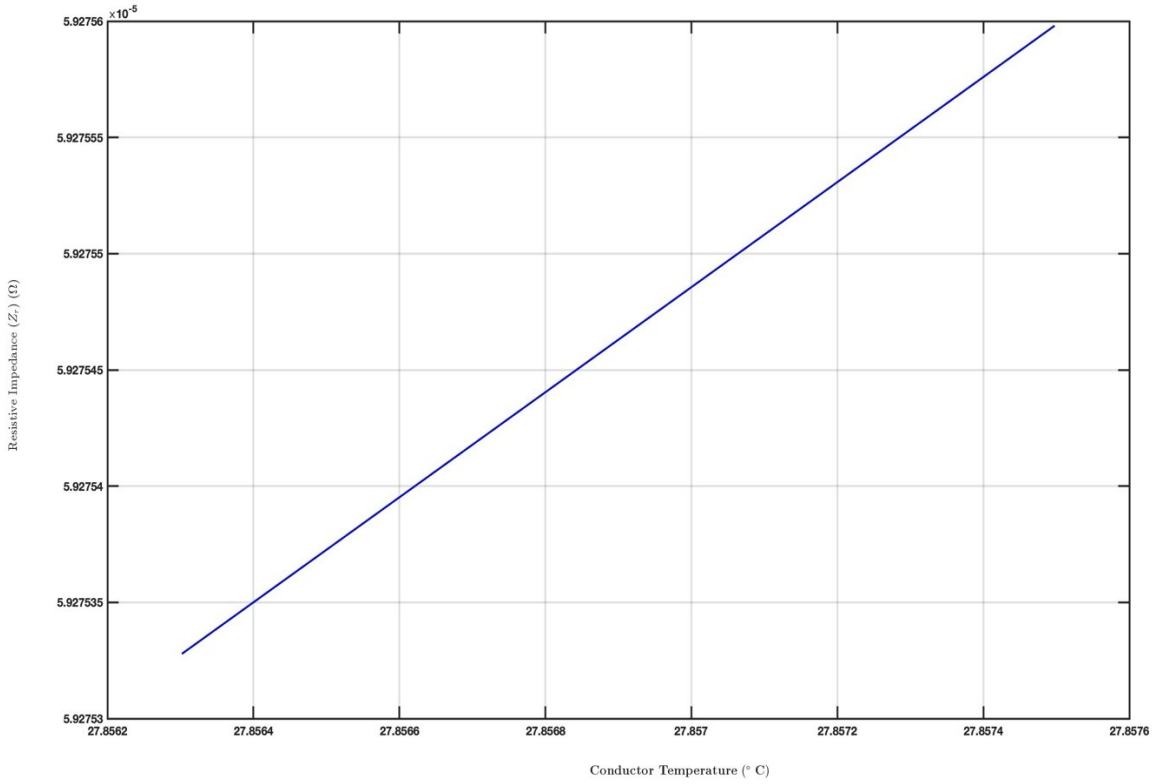

Figure 13: Temperature effect on resistive impedance of the conductor

However, it is important to note that, upon closer scrutiny, the changes in resistive impedance appear to be of minute magnitude in comparison to the dynamic shifts in temperature. This observation implies that electrical impedance of the conductor material does not readily undergo significant changes with temperature over time. This proposition is reasonable, ensuring that our diagnostic approach avoids generating false alarms. In typical operational conditions for healthy cables, slight variations in impedance and temperature are expected throughout the day. However, in the presence of a thermal fault, elevated temperatures cause an increase in cable impedance compared to the existing impedance baseline.

3.5 Thermal model – transient state

For a transient state study, heat transfer analysis was carried on a single power cable using the PDE solver in MATLAB (see Appendix B). The cable's heat conduction analysis follows a similar layer modeling for semiconductors used in [75]. Cable parameters and assumptions in section 3.1 were maintained.

1.) Heat conduction PDEs solution

The rate of change of temperature within a cable layer is equal to propagation of heat flux due to thermal conduction plus the heat generated per unit volume in that layer, given by:

$$\nabla(\kappa_i * \nabla T_i(\varkappa, t)\,) + Q_i \;=\; \rho_i c_i \frac{\partial T_i(\varkappa, t)}{\partial t} \qquad for\ i \;=\; 1 \dots n \qquad (49)$$

where i denotes the layer, κ is thermal conductivity, Q_i is heat generated due to electrical current passing through the conductor, $\rho_i\ and\ c_i$ are the mass density and specific heat capacity of the i^{th} layer respectively, x is the spatial coordinate along the cable's radius and T is temperature.

Considering thermal conductivity, mass density and specific heat capacity of each layer as constants, equation (49) becomes (50). It is often sufficient to model the cable system as one-dimensional since the width of each cable layer is much larger than its thickness [75].

$$\alpha_i \frac{\partial^2 T_i(\varkappa, t)}{\partial \varkappa^2} + \frac{Q_i(\varkappa, t)}{\rho_i c_i} = \frac{\partial T_i(\varkappa, t)}{\partial t} \qquad for\ i \;= 1 \dots n \qquad (50)$$

where α_i is the thermal diffusivity of the i^{th} cable layer, given as $\alpha_i \;= \kappa_i / \rho_i c_i$.

A global heat conduction partial differential equation (PDE) for a healthy cable with respect to time and radial distance was solved using the PDE toolbox in MATLAB. 1-D cylindrical coordinates and cartesian coordinates were both used. The PDE solution for the conductor used

cylindrical coordinates and the 3 other layers used cartesian coordinates. This is because heat conduction of the insulation layer was computed horizontally along the radius, from the outer radius of the conductor to the external radius of the insulation. Same was done for the sheath and jacket.

Rewriting equation (50) into a compatible format for the PDE solver gives:

$$\rho_i c_i \frac{\partial T_i(\varkappa, t)}{\partial t} = k \frac{\partial^2 T_i(\varkappa, t)}{\partial \varkappa^2} + Q_i(\varkappa, t) \qquad for\ i = 1 \dots n \qquad (51)$$

The code equation will be:

$$\rho_i c_i \left(x, t, T, \frac{\partial T}{\partial x}\right) \frac{\partial T_i}{\partial t} = k * x^0 * \frac{\partial}{\partial x}(x^0 \frac{\partial T_i}{\partial x}) + Q_i(\varkappa, t, T, \frac{\partial T}{\partial x}) \qquad for\ i = 1 \dots n \qquad (52)$$

For the cylindrical coordinates, rate of change of temperature within a cable layer is given by:

$$\frac{1}{r_i}\frac{\partial}{\partial r}\left(\frac{r_i}{\rho_i}\frac{\partial T_i(r,t)}{\partial r}\right) + Q_i = c_i \frac{\partial T_i(r,t)}{\partial t} \qquad for\ i = 1 \dots n \qquad (53)$$

Rewriting in equation 53 into a compatible format for the PDE solver:

$$\rho_i c_i \frac{\partial T_i(r,t)}{\partial t} = \frac{1}{r_i}\frac{\partial}{\partial r}\left(r_i \frac{\partial T_i(r,t)}{\partial r}\right) + \rho_i Q_i \qquad for\ i = 1 \dots n \qquad (54)$$

The code equation is:

$$\rho_i c_i\ (r, t, T, \frac{\partial T}{\partial r})\ \frac{\partial T_i}{\partial t} = {r_i}^{-1} \frac{\partial}{\partial r}\left({r_i}^1 \frac{\partial T_i(r,t)}{\partial r}\right) + \rho_i Q_i(r, t, T, \frac{\partial T}{\partial r}) \qquad for\ i = 1 \dots n \qquad (55)$$

2.) Boundary conditions

A perfect thermal contact was assumed between the layers, and temperature at the interface boundaries are continuous, given by

$$T_i(\varkappa_i, t) = T_{i+1}(\varkappa_i, t) \qquad for\ i = 1 \dots n \tag{56}$$

Heat fluxes passing through various layers are continuous as well:

$$\kappa_i \frac{\partial T_i(\varkappa, t)}{\partial \varkappa} \Big|_{\varkappa_i} = k_{i+1} \frac{\partial T_{i+1}(\varkappa, t)}{\partial \varkappa} \Big|_{\varkappa_i} \qquad for\ i = 1 \dots n \tag{57}$$

After the first-time step, temperature and heat flux at each layer boundary begin to change as temperature increases. The left boundary condition of the insulator becomes the heat output from the conductor and the left boundary of the sheath is the heat output from the insulation and so on. To obtain a complete solution of the temperature distribution of the cable system, the following temperature boundary and heat flux boundaries were adopted:

a.) Dirichlet boundary conditions: These boundary conditions specify the temperature values of the solution at boundary. An ambient temperature of 20 °C is applied to the external PVC jacket layer.

$$T(x, t = 0) = T_\infty = 20\ ^\circ\text{C} \tag{58}$$

b.) Neumann boundary conditions: Heat flux Boundary conditions were adopted at the center of the conductor and the outer surface of the jacket.

- **Heat flux boundary at conductor:** Heat flux at center of jacket was,

$$\kappa_c \frac{\partial T_1(\varkappa, t)}{\partial \varkappa} \Big|_{\varkappa = c} = q(t) = 0\ \ W/m^2 \tag{59}$$

- **Convection heat flux boundary at jacket's outer surface:** Thermal convection is applied at the outer surface of the jacket and the air surrounding the cable. The heat transfer coefficient h_{conv} was set to 10 W/m$^{2.}$ K

$$\frac{\partial T_4(\varkappa, t)}{\partial \varkappa} \Big|_{\varkappa = j+1} = -\left(\frac{h_{conv}\left(T_j - T_\infty\right)}{\kappa_j} \right) \tag{60}$$

T_j depends on the sheath and ambient temperatures and it is generated as the code is being simulated over time.

If cable is directly buried in backfill or ground, the same equation applies, only then will the backfill be considered as an additional layer of the cable system and it represents the outermost layer. Backfill conductivity will be used in this case. For a conductive heat dissipation process in a cable system, $h_{conv} \neq 0 \; and \; h_{conv} \neq \infty$ because when $h_{conv} = 0$ there is no heat flux passing through the jacket to the ambient- it acts as a perfect insulator. Further, if $h_{conv} = \infty$, the temperature at the jacket interface is equal to that of the ambient, ($T_j = T_\infty$). To avoid overheating of cables, continuous heat dissipation is paramount. Laboratory cable testing was carried out at room temperature with natural convection having the convection heat transfer coefficient h_{conv} in the range, 5-25 W/m²K. For higher heat dissipation rates, liquid or forced air-cooling can be considered.

In this study, thermal radiation is considered negligible due to the minimal ΔT at the jacket surface; nonetheless, it can be determined using equation 61 [15]. For a cable buried in soil, thermal radiation between T_{soil} and T_∞ can be obtained by:

$$Q = \varepsilon\sigma A\left(T_{soil}^4 - T_\infty^4\right) \tag{61}$$

where ε is emissivity, σ is the Stephan Boltzmann constant and A is the effective radiation area per meter length.

3.) Initial conditions

Initial electrical resistance at 20 °C for conductor and copper screen wires were 0.0601 and 0.0781 Ω/km respectively [15]. The ambient soil temperature was 20 °C and thermal soil resistivity is 1.0 K.m/W. However, the analysis in this study did not consider the soil. All four layers were assumed to have an initial temperature of 20 °C, both left and right boundary conditions.

4.) Discretization

a) Length discretization

The external diameter outer layer of the cable, which is that of the jacket, was 35.80 mm. This gave a cable radius of 17.9 mm. Discretization into smaller mesh units was done from the middle of the conductor to this external radius; precisely 25 smaller units in total were randomly chosen. Selecting small spatial steps allows for the assumption that the central point of any node has the mean temperature of the discrete element where it is placed [76].

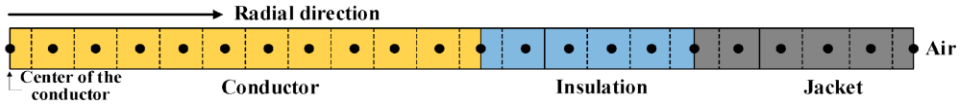

Figure 14 [76]: Cable discretization along the radial axis excluding the metallic sheath

Discretization along the total radial distance was further discretized to create layer nodes by finding the difference between layer radii. For example, at the insulation, discretization of layer nodes was done from the outer radius of the conductor to the outer radius of the insulation. Same analogy was used for the sheath and jacket.

b) Time discretization

The simulation was done for a total of 3600 seconds, with an 18 second time step. The time step was chosen such that the rates of change of heat flux and temperature within that duration were not expected to change significantly. This assumption allows for a more stable and accurate solution. If the time step was too large, rapid changes may occur, leading to inaccuracies in the solution. On the other hand, if the time step was too small, the computation may become unnecessarily complex and time-consuming.

3.5.1. Results and discussion

Alternating current with a frequency of 50 Hz was applied to the cable. The cable was loaded with its maximum operating current, 629 A. The temperature distribution of the cable is shown in Figure 15. It can be seen from the figure that the temperature distribution within each layer is relatively uniform. The maximum temperature is located at the center of the cable conductor. At 3581 s, maximum temperature of the cable conductor was approximately 55.7 °C. Heat generated in the conductor dissipates across various layers and levels off towards ambient in the sheath and jacket.

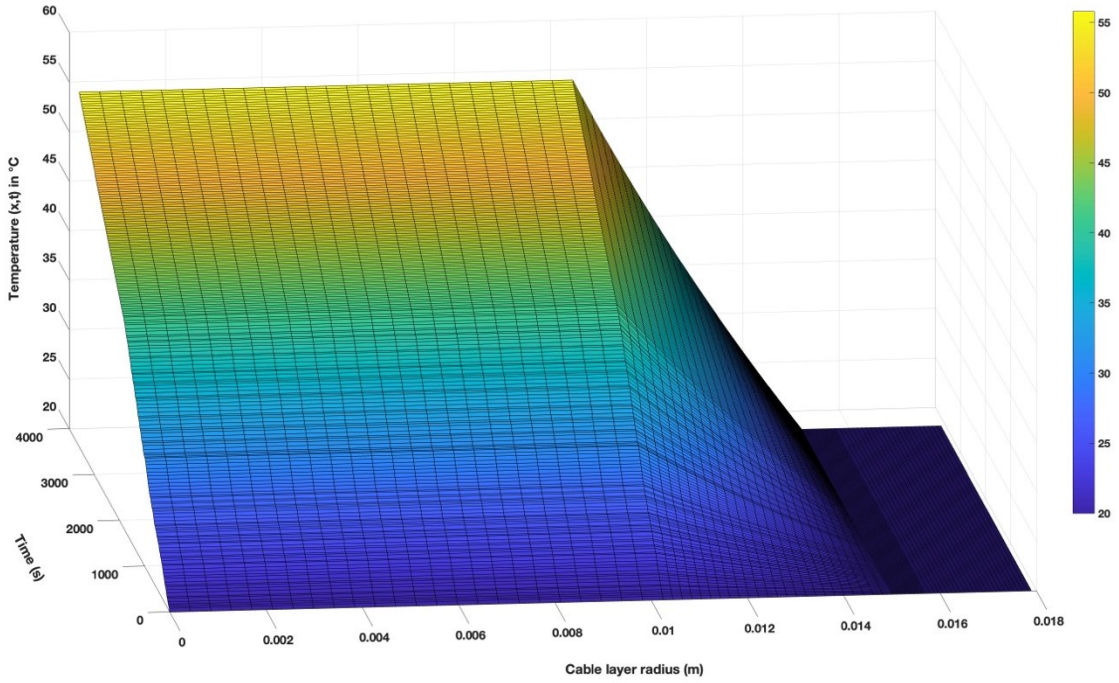

Figure 15: 1-D temperature distribution of an XLPE power cable – transient state

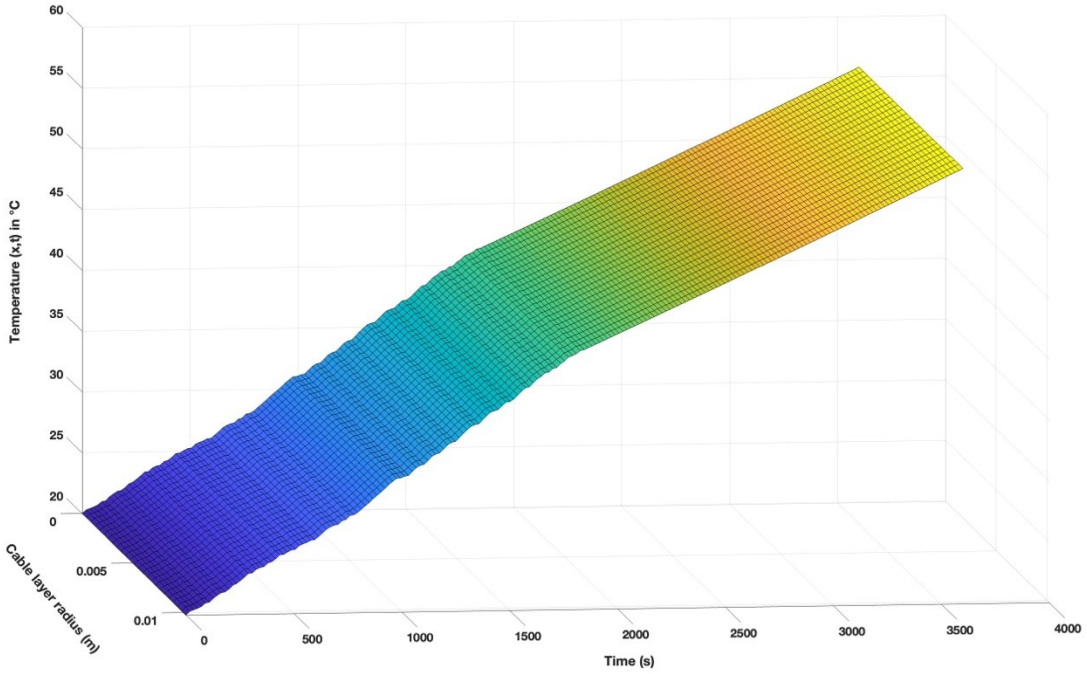

Figure 16: Temperature rise in cable conductor as a function of time

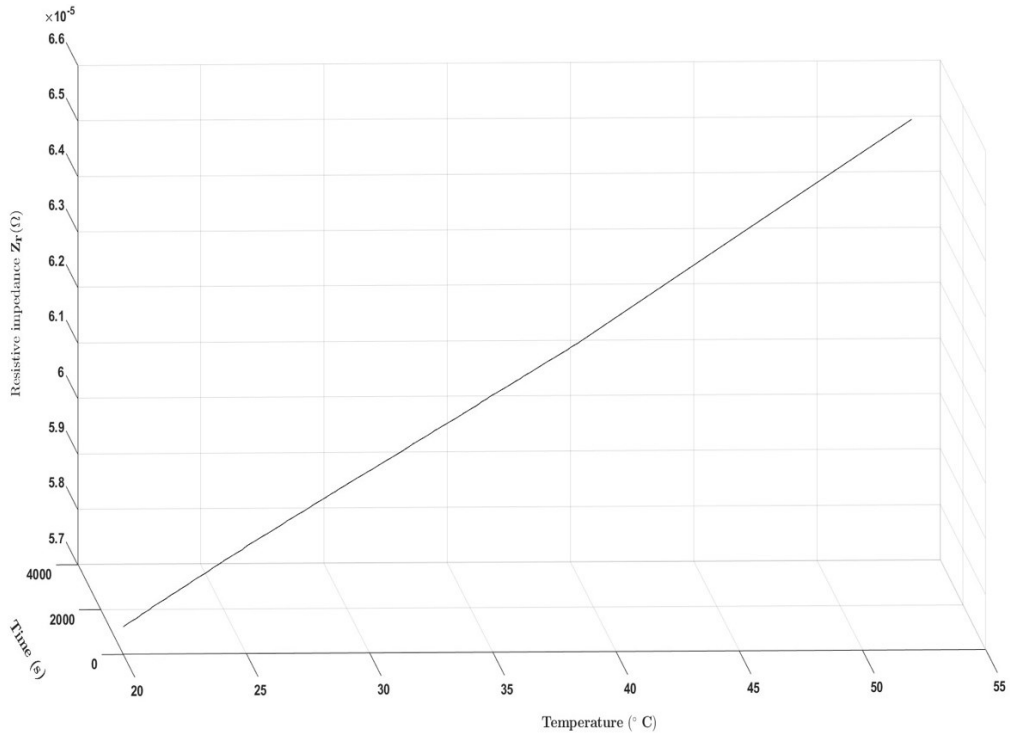

Figure 17: Effect of temperature on resistive impedance of the conductor-transient state

The process of heat generation and dissipation in power cables follows similar patterns during both transient and steady states. A one-hour simulation reveals a temperature increase of approximately 35.8 °C within the conductor (see Figure 16). Consistent with the findings of the steady-state study, a linear relationship between temperature and resistive impedance is observed (see Figure 17). The subtle variations in impedance relative to temperature changes clearly illustrate that the electrical impedance of the conductor material undergoes minimal changes with temperature over time. Consequently, significant deviations in impedance may strongly indicate the presence of a fault along the line.

Even though similar trends are observed in both transient and steady state studies, the transient results will be beneficial to determine instantaneous temperatures during fault diagnostics [54] in real operation settings.

3.6 Mechanical damage simulations

Mechanical damages affect the insulation, which may indirectly influence the cable's electrical and thermal performance. Some impacts include electrical insulation breakdown, reduced dielectric strength, changes in conductor impedance, signal distortion, and increased risk of electrical fires. The severity of their impact depends on the degree and depth of damage, as well as the type of insulation material. It may also affect the cable's ability to dissipate heat properly, potentially leading to overheating.

To observe the impact of mechanical damage on cable impedance, a mechanical damage was simulated by varying conductor cross-sectional area, emulating a torsion damage. The cable's breaking point was not taken into consideration for this computation. For each case, the mechanical damage is incorporated into the resistive impedance model (equations 14, 16, and 18) and the temperature distribution model of the transient analysis is updated. Model assumptions in section 3.1 are the same except that in this case, deformations are both thermal and structural.

The results of simulations after an hour can be seen in Figure 18 and are summarized in table (4). The cases were classified into healthy, less damaged, and severely damaged.

Table 4: Mechanical damage simulations and impedance changes

	Area x 10^{-4} m^2	Impedance x 10^{-5} Ω	Temperature °C
Healthy	3.46	6.85	55.66
Less damaged	2.46	7.29	74.52
Severely damaged	1.46	8.39	120.91

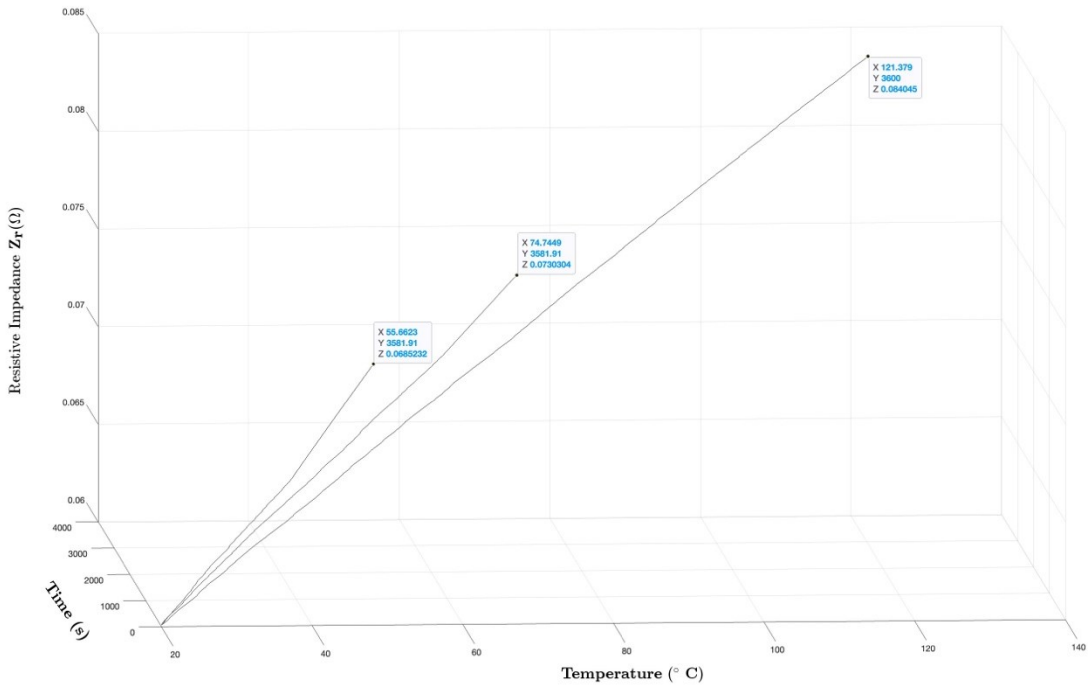

Figure 18: Effect of mechanical damage on resistive impedance of the conductor-transient state

Resistive impedance increased with increasing damage severity. Mechanical damages in power cables increase cable impedance which results in higher power losses when current flows through the conductor. Consequently, higher heat dissipation rates enhance decomposition of insulation material. This further causes an increase in resistive impedance. The accretion of this process impacts cable performance, accelerates cable aging, and potentially leads to insulation breakdown.

3.7 Model limitations

- For simplification purposes, soil surrounding underground power cables was not considered in the computations. This may not fully capture the complexity of real operating underground power cables as the rate of heat dissipation also depends on properties of the soil. The soil layer was not a necessity for this study but could be modeled as an additional layer following the same principles.
- The linear relationship between temperature and resistivity (equation 14, section 3.2.2), holds true for the practical temperature range between -40 and 125 °C [15]. Beyond this temperature range, the linearity assumption may no longer accurately represent the behavior of the material. Therefore, extrapolating the electrical model beyond these limits may lead to inaccurate predictions, as the linear relationship might not hold in extreme temperature conditions.
- The accuracy of the model is contingent on the validity of the assumptions made. While the model may demonstrate accuracy within the conditions used for validation, its ability to generalize to diverse scenarios remains a consideration.
- The model developed is suitable for a laboratory scale verification. Its scalability and transferability across different cable networks remain a consideration.

Chapter 4 Experimental design

The design and execution of a well-crafted laboratory experiment are fundamental to the advancement of the thesis work. An experimental framework which not only supports the ongoing research but also validates the temperature impedance model developed in chapter 3 is proposed. This chapter serves as a comprehensive guide to the structure and rationale of our experimental approach, providing readers with a roadmap to understand the methodology, the variables selected, anticipated outcomes and its implications in the broader context of our research objectives.

This chapter begins with experimental objectives and outlining the experimental variables under consideration. Next, a comprehensive list of all materials and equipment used, followed by safety and ethical considerations and laboratory setup. Subsequently, specific methodologies implemented are discussed; detailing the procedures, measurements, and controls instituted to ensure the integrity and reliability of results. The chapter ends by discussing some challenges encountered during lab work.

4.1 Objectives of experiments

The goal of this experimental analysis was to detect anomalies in underground power cables, which most often are not visually accessible, using resistive impedance spectroscopy. Laboratory analysis involved the use of idealized analogs representing these anomalies and various cable operating conditions.

The main damages considered in the thesis work were thermal anomalies and degradation caused by continuous high operating temperatures. Temperature related experiments were done in two folds; the first was a DC test to verify the rate of heat dissipation in a single conductor and the second test was to investigate the effect of continuous elevated temperatures on cable resistive

impedance. The aim was to validate the integration of temperature distribution and resistive impedance models as one robust Multi-physics model for fault diagnostics in underground power cables. Mechanical damage and water trees are two other damages whose effects on cable impedance were experimentally studied in an idealized manner. For all three damage models, anomaly detection was done through impedance measurement at either end of the cable. Changes in electrical resistive impedance in response to faulted cables was evaluated for all induced faults. Hypotheses are deduced for each damage scenario. That of temperature stress was derived from simulation results in chapter 3 and hypothesis for mechanical damage and water trees were derived from an accumulation of studies from existing literature.

1.) Hypothesis on high-temperature impact on cable resistive impedance

When current flows through a conductor, electrical losses due to electrical resistance are released in the form of resistive heat. This resistive heat dissipates towards ambient through cable layers which on its way provoke microscopic processes in the conductor and insulation material. The accretion of this process causes changes in electrical, thermal, and geometric properties. Cable temperature increases impedance which further generates more heat within the cable, resulting in a measurable variation in impedance. Furthermore, this has a cyclic effect as discussed in section 2.4.4, where changes in insulation material properties leads to variations in insulation volume resistivity, weakening the insulation. This process goes on until the original perfect insulator with infinite resistance begins to conduct and possibly leads to a breakdown.

2.) Hypothesis on notch impact on cable resistive impedance

The presence of a notch in an underground power cable will cause a significant alteration in cable impedance. It is expected that the notch, acting as a discontinuity in the cable structure, will introduce additional resistance, capacitance, or inductance, leading to a detectable change in impedance compared to a cable without any mechanical fault. Notches are introduced into a

healthy cable at different depths and cable impedance for each case was recorded using a nano vector network analyzer.

3.) Hypothesis on water trees impact on cable resistive impedance

The growth of water trees within the insulation of the underground power cable will result in an increase in cable impedance. Water trees, as a form of dielectric degradation, can alter the electrical properties of the cable insulation, causing changes in impedance. The hypothesis is grounded in the assumption that the presence of water trees will introduce irregularities in the insulation material, affecting the cable's overall impedance.

4.2 Experimental variables and parameters

a.) Controllable variables and uncontrollable variables

From the theoretical and simulated model, key factors which can affect the outcome of the experiments are listed in Table 5. These factors are divided into controllable and uncontrollable variables. Controllable variables are those that can be manipulated or controlled during the experiment, while uncontrollable variables are those that cannot be directly controlled but may still impact the results. Changing any of these variables during the experiment will cause a change in the response variables of the system.

Table 5: Controllable and uncontrollable variables for an experimental study on the impact of faults on cable impedance

Controllable variables	Uncontrollable variables
Operating conditions: The amount voltage V and current I, was controlled during the experiments.	**Environmental conditions:** Temperature and humidity of the lab room may have varied despite attempts to control them.
Cable geometry: Different cable samples were prepared with their geometry parameters recorded.	**Noise in the cable line**: This will apply in real operating conditions; however, testing was done offline, in the absence of noise.
Cable electrical properties: Electrical properties of healthy samples were recorded before each test.	**Manufacturing defects** in cable samples are uncontrollable, especially those which cannot be perceived by the human eye.
Boundary conditions were controlled by applying specific values at the boundaries of the cable. Cables were suspended in air and heat convection boundary was applied in these experiments.	
Induced heat: The amount of heat induced to create thermally damaged samples was controlled using current supply and an external heat supply.	
Notch size: The size of the notch was controlled to assess its impact on impedance.	
Moisture content induced in the cable was controlled and varied.	

b.) Manipulated and response variables.

In this experimental study, temperature, notch size and moisture content were selected to investigate cable's response to fault conditions.

1.) Cable temperature and consequently temperature distribution were varied by subjecting the samples to incremental power supply. A 30V / 10 A DC power supply was utilized to control current and voltage. By monitoring temperature distribution along the cable's

length and across its layers we gained insights into the cable's thermal behavior, identifying areas of increased thermal stress and potential hotspots due to varying electrical loads or fault events. A thermal Camera was used to capture temperature of the layers and along the cable length.

2.) Notch size: Fault geometry was introduced into the cable at different depths. This created a forced mechanical damage model, allowing us to observe the cable's response to such mechanical faults. A sharp knife was used to create these notches.

3.) Moisture content: The extent of water treeing in the cable sample was done by controlling and varying the moisture content and NaCl.

Electrical resistive impedance was the response variable. It was observed and measured to assess the effect of manipulated variables for all three tests. Impedance spectra were measured and recorded using a Nano Vector Network Analyzer (NanoVNA), from this data, resistive impedance was extracted and analyzed.

4.3 Materials and equipment

Depending on the damage model being tested, different materials and equipment were used. Table 6 presents a list of these materials and equipment.

Table 6: Materials and equipment used for a laboratory analysis of damage models in underground power cable

Materials, equipment, and variables	Measuring instruments	Units
Cable geometry		
Sample length	Measuring tape, wire cutter	Centimeters (cm)
Diameter	A digital vernier caliper	Millimeters (mm)
All round materials and equipment		
Power supply	A 30V/10A DC power supply	Amperes(A)
Resistive impedance	NanoVNA	Ohms ((Ω)
Time	Stopwatch	Seconds (s)
Ambient temperature (Lab room)	Room climate control system	Degree Celsius (°C)
Manufacturing defects on healthy samples	Visual inspection	-
Temperature stress experiment		
Cable temperature	FLIR Camera-model E60	Degree Celsius (°C)
External heat source	Heater	Degree Celsius (°C)
Mechanical damage experiment		
Notch size	Sharp knife and measuring tape	Centimeters (cm)
Water trees experiment		
NaCl, water	-	-

4.3.1. Safety and ethical considerations

Experiments were planned with safety as a paramount concern. Work entailing any safety risk was planned and executed under no-working-alone guidelines. No ethical concerns were raised, as the author was the sole experimenter, and no human subjects were involved.

- **Environmental conditions:** Before conducting each test, meticulous attention was given to ensuring specific environmental conditions, with any deviations being documented. The ambient room temperature was maintained at 20 °C, and atmospheric pressure was 1 atmosphere (101.325 ± 3.3 kPa).

- **Required tolerances:** Tolerances for temperature data were set at +/- 1 °C, and for impedance, +/- 0.5 Ω. All measurements were recorded to two decimal places.
- **Calibration of measurement tools:** The FLIR camera and impedance analyzers were successfully calibrated prior to each test. To ensure accurate temperature measurements, the FLIR camera was calibrated by setting the camera emissivity ε to 0.95. Atmospheric temperature and reflected temperature were set to 20°C. The NanoVNA used was a one-path-2-port portable VNA and it was calibrated using the "SOL" (Short, Open and load) method.
- **Current control:** The power supply employed was carefully controlled and fuse-protected to ensure a stable and safe current supply during experiments.
- **Heat management:** Cables were subjected to elevated temperatures using an external heater. The test support frame was designed to withstand these high temperatures, and precautions were taken to keep heated cables away from other objects. Flammable materials were removed from the experimental area.
- **Sharp tools for notching:** Creation of notches was conducted with precision and care to ensure safety by not getting in the line of fire of any sharp-edged tool.

4.4 Laboratory setup

The cables under examination were positioned horizontally, suspended in air using two clamps. On both ends of the exposed conductor, a power supply was securely clamped and connected. The supporting clamps were thermally insulated with rubber to minimize heat conduction when in contact with the cable. The entire setup was positioned in one corner of the laboratory, away from direct sunlight to prevent extra heat influences. The room temperature, regulated by the room climate control system, was consistently maintained at 20 °C throughout the experiment, along with a pressure of 1 atmosphere. This minimized external factors that could potentially impact the

accuracy and reliability of the experimental measurements. The setup and equipment listed in section 4.3 can be seen in Figure 19.

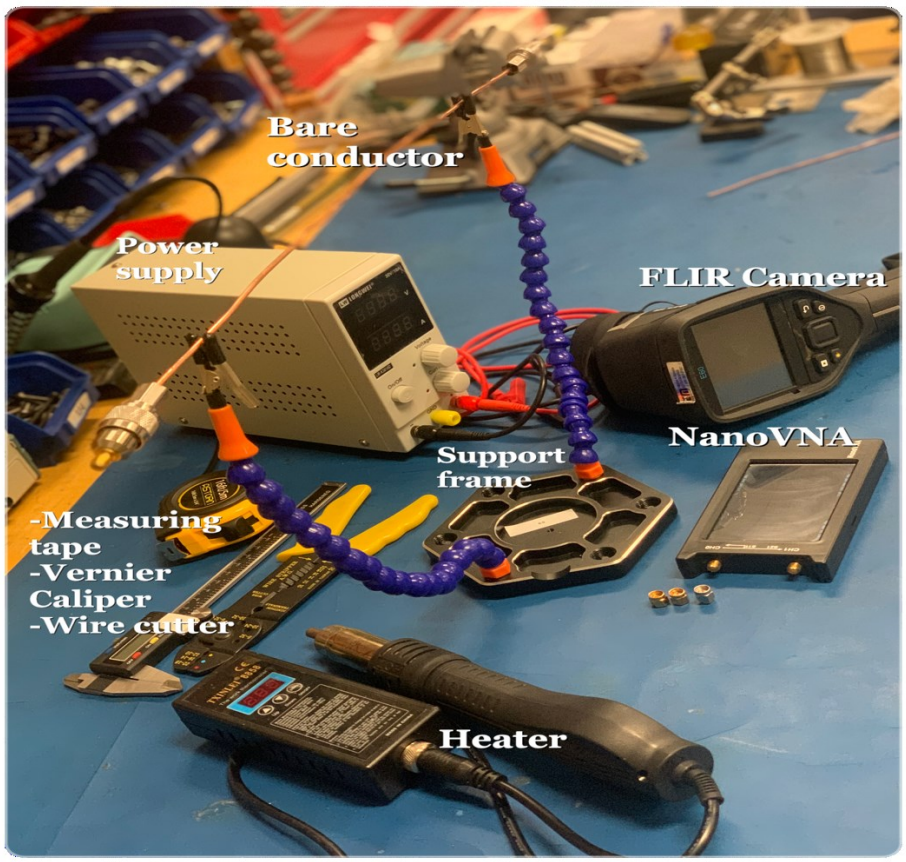

Figure 19: A laboratory setup for a resistive impedance spectroscopy of power cables

4.5 Experimental procedures

4.5.1. Temperature distribution

Cables tested featured low voltage, 35 cm single electrical conductors with solid copper core, surrounded by XLPE insulation. This was the main cable type used for most of the tests, but to simulate faults as well as for comparison purposes, other cable types were used, and their characteristics will be mentioned where applicable. The cross-sectional area of this cable was 3.31

mm^2, with diameters of 2.05 mm and 3.80 mm for the conductor and insulation respectively. The choice of such cables was driven by the available power supply in the laboratory. The cables' specific characteristics ensured that the ensuing tests provided valuable and substantial insights into the thermal and electrical responses under the prescribed conditions. Table 7 summarizes the cable's geometric and thermal properties.

Table 7: Summary of geometric and thermal properties of cable under test

Layers	**Geometry properties**		**Thermal properties**	
	Property	**Value**	**Property**	**Value**
copper conductor	d_c	2.05 mm	Thermal conductivity, k	400 W/m. K
XLPE insulation	d_{ins}	3.80 mm	Thermal conductivity, k	0.28 W/m. K
	Cross-sectional area	3.32 mm^2	Electrical resistance	4.83e-04 Ω/m
	Length	35 cm	Temperature coefficient, α_ref	3.93e-03

Procedure

A measuring tape was used to cut out 0.35 m from the cable bulk. Using a digital caliper, cable diameter was measured. 1 cm of insulation was carefully cut out from both ends of the 0.35 m cable sample to allow contact between the conductor and power supply wires. A DC 30 V/10 A power supply was used to simulate heat flux generated in power cables during their operation. The cable was continuously subjected to a current load between 1-10A. This approach allowed for a comprehensive understanding of the specimen's response to varying current and heat intensities, providing valuable insights into its impedance dynamics under different temperature

conditions. Current loading was allowed to reach steady and after every 10 mins, a FLIR thermal camera was used to measure temperature along the cable's length. Maneuvering the FLIR Camera to obtain direct temperature distribution across cable layers for such small cables is not an easy task. However, the rainbow contrast settings on the FLIR Camera provided insights of the hottest layer which was the conductor, and the external layer of the cable was seen to be the coldest as seen in Figure 20, validating the temperature distribution model developed in chapter 3.

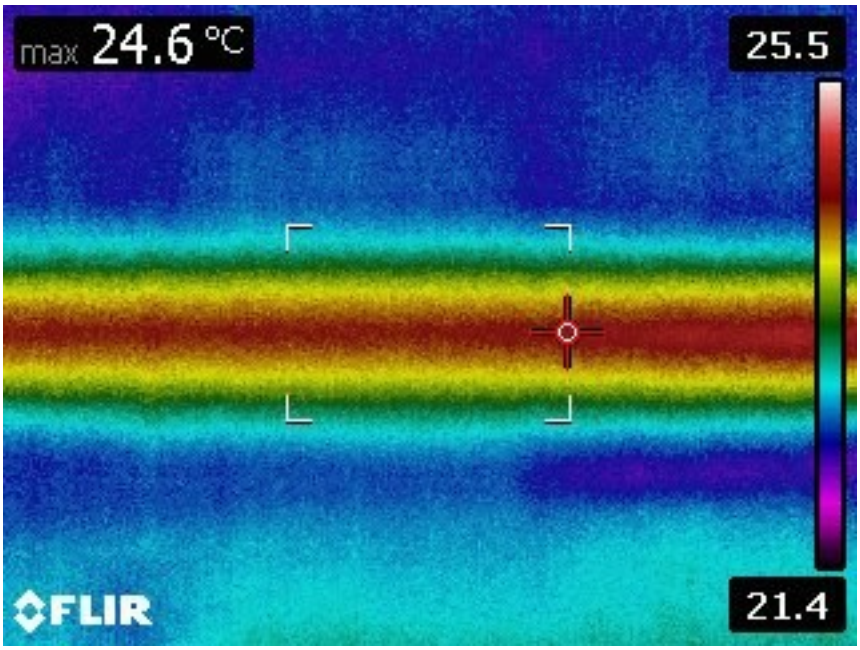

Figure 20: A sample radial temperature distribution in a power cable

The maximum temperature of 24.6 °C was obtained for a current load of 8.5 A over a period of 10 minutes. To ensure accurate temperature readings, measurement points were positioned away from the support frame, at the center of the cable. This allowed for the exclusion of any potential influence from the support frame on the temperature measurements.

Equations (18) and (19) in chapter 3 showed that the volumetric heat generated within the cable is a function of current supply, electrical resistance, and conductor area. Figure 21 presents current loading I as a function of ΔT.

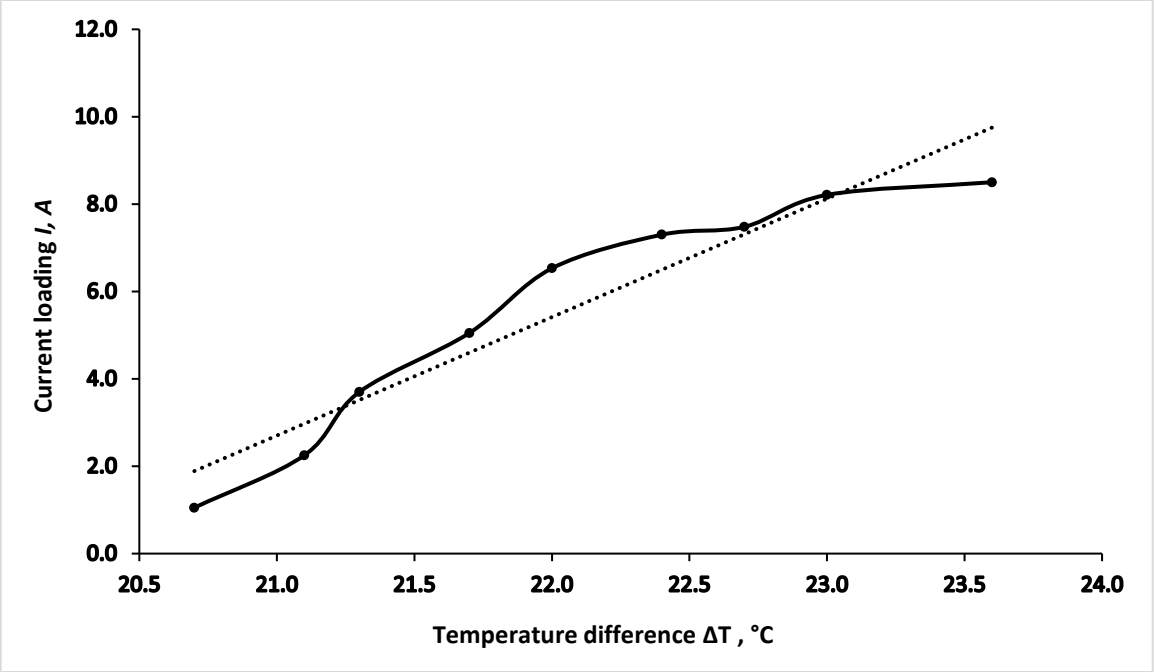

Figure 21: Current load as a function of cable temperature difference with ambient (T - T∞)

Current load I and corresponding temperature difference with ambient were used in the calculation of heat losses ΔQ. By considering the geometric and electrical properties of the sample and utilizing the resulting ΔQ values, volumetric heat flux was determined using Equation (18). This computation is summarized in Table 8 and presented in Figure 22.

Table 8: Computation of volumetric heat flux for an XLPE cable

Current, I (A)	**Temperature, Tc (°C)**	**Resistance, $R_{e\,DC}$ (Ω/m) x 10^{-4}**	**Volumetric heat flux, q_v (KW/m³)**
1.05	20.7	4.84	0.46
2.25	21.1	4.85	2.11
3.70	21.3	4.85	5.72
5.05	21.7	4.86	10.67
6.53	22.0	4.87	17.86
7.30	22.4	4.88	22.36
7.48	22.7	4.88	23.50
8.21	23.0	4.89	28.35
8.50	23.6	4.90	30.46

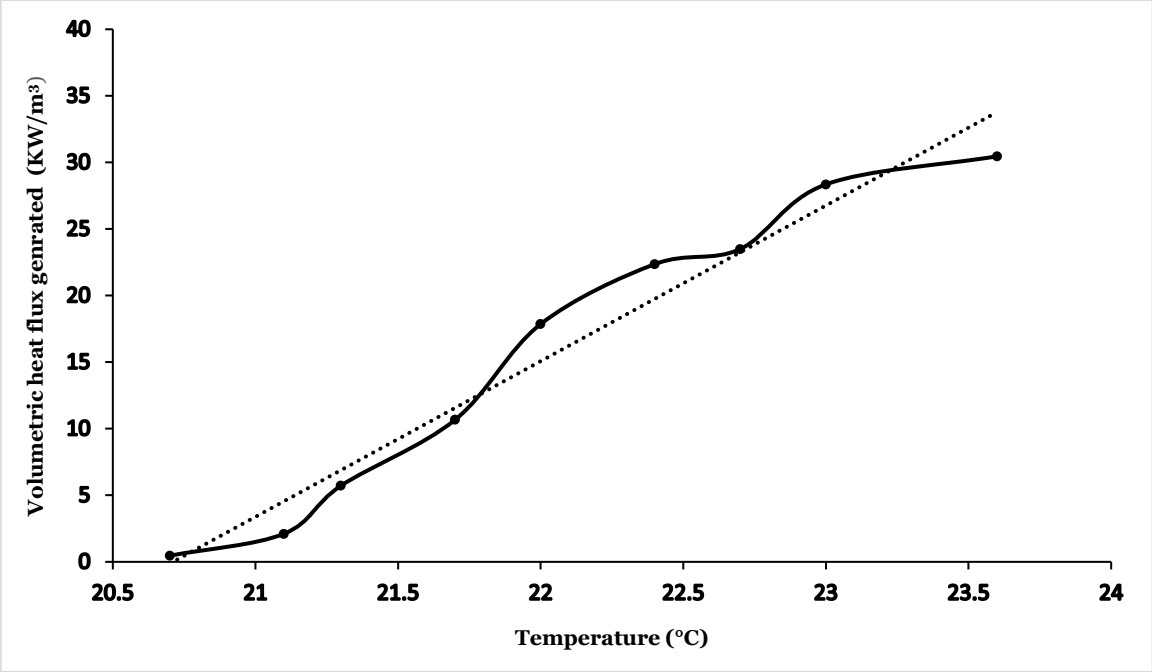

Figure 22: Volumetric heat flux generated for current load 1-10 A

In the Re_{DC} calculations, the external temperature of the cable recorded during the experiment was taken into consideration instead of the temperatures of the conductor. Typically, conductor temperature is utilized, but due to the limited size of the sample under test, obtaining the direct conductor temperature was not feasible. It is important to note that these results did not impact the conclusion drawn, which asserted that higher current loading led to a greater temperature difference between the cables and their surroundings, resulting in increased heat dissipated.

The precision of cable temperature results was possibly impacted by errors beyond control. This resulted in slight deviations from expected outcomes. One notable factor that influenced the results is the precision of the time at which data was acquired. Additionally, the presence of other sources of heat within the experimental environment could have contributed to distorted findings.

4.5.2. Temperature – impedance experiment

The Nano Vector Network Analyzer (NanoVNA) measures complex impedance as a function of frequency and plots them on a smith chart. The VNA utilized in this study uses subminiature version A (SMA) connectors, hence modified coaxial cables were considered for the resistive impedance study to reduce the effect of impedance changes at the connection to the cable. A 50 cm coaxial cable with a diameter of about 1 cm was used. The unmodified cable featured a solid inner copper conductor, a dielectric, tinned copper braided sheath and a PVC jacket. The cable was terminated with a 50 Ω load throughout the experiment. The coax cable was stripped off all other layers leaving only the conductor attached to its connecting ports. An external heater was used to simulate heat flux generated in power cables during operation. A temperature of 400 °C was applied to the conductor for a period of 10 minutes. Impedance was measured after 5 and 10 minutes of the cooling process. These time intervals were most appropriate for two reasons: first for the safety of the VNA—connecting a very hot coax to the VNA's ports could destroy the VNA and secondly, it's a reasonable interval to mimic low voltage current operating temperatures. Impedance measurements were conducted over a frequency range of 50 KHz to 150 MHz. Resistive impedance of the healthy coax was recorded to be 75.8 Ω at room temperature. The room temperature for this experiment was 21°C. At the 6th test trial, a hotspot scenario was emulated at the middle of the conductor. The conductor was continuously heated for 10 minutes along its length and for another 10 minutes just at the center of the conductor. The same cooling intervals and impedance recording time were applied to this scenario.

Typically, transmission lines are terminated in their characteristic impedance, avoiding attenuation. The current-voltage relationship along the transmission results in a constant impedance until an anomaly, open or short circuit is encountered along the line where a different impedance is perceived, and a signal is reflected to the input. Figure 23 reveals the results

obtained for a resistive impedance-temperature analysis and an emulated hotspot in a cable conductor.

Analysis and data interpretation

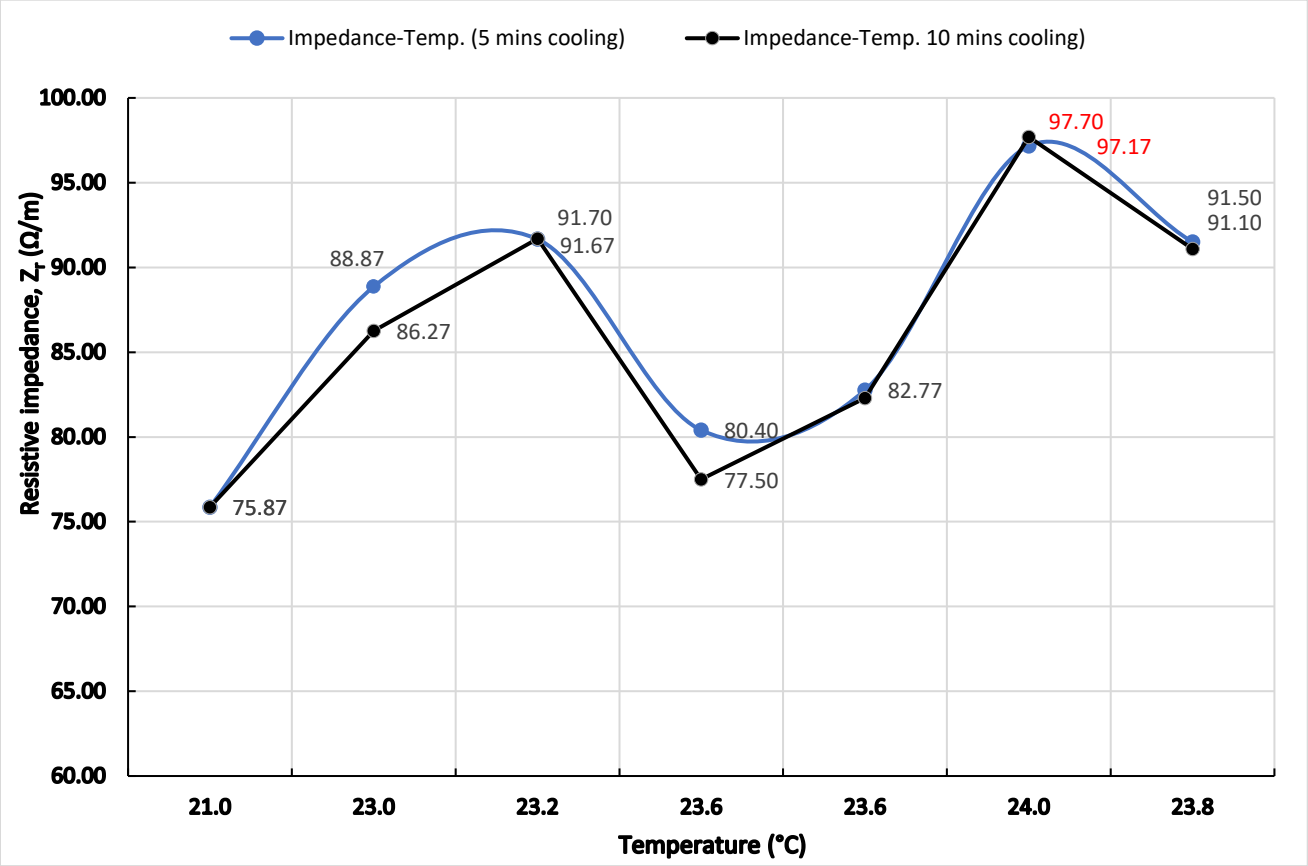

Figure 23: Experimental results of resistive impedance-temperature analysis in a coax cable with sheath removed

Repeated cycles of heating and cooling, with impedance measurements at corresponding temperatures, revealed fluctuating and gradual increase in resistive impedance Z_r with temperature rise. The impedance fluctuated between 75.8 and 91.6 Ω for a healthy range after cooling the coax cable at intervals of 5 and 10 minutes. Impedance was measured at different cooling intervals. The reasons behind this are: first to obtain average impedance and secondly to gain a closer insight into impedance behavior at different temperatures. The recorded resistive

impedance values exhibit an interesting trend, indicating that after a 5-minute cooling interval, the measured resistive impedance is higher than those recorded after a 10-minute interval. This phenomenon can be attributed to the ongoing movement of material electrons at the 5-minute mark, suggesting a delayed stabilization compared to the 10-minute interval, where temperatures have nearly reached room temperature.

For the healthy coax emulated scenario, impedance fluctuated between 75.87 and 91.60 Ω. Whereas a simulated hotspot at the conductor center yielded an average resistive impedance of 97.40 Ω. From these results, assuming constant current loading on power distribution networks and a resistive impedance baseline for fault detection, resistive impedance spectroscopy is a potential thermal anomaly detection.

4.5.3. Mechanical damage – impedance experiment

To demonstrate impedance behavior of a cable that is physically damaged; where such damages could be abrasion, bending, tension or compression, a coaxial cable with the same geometries as those used in section 4.5.2 was used. The cable was terminated with a 50 Ω load, and an input impedance Z_{in} of 50.2 Ω was recorded from NanoVNA. Using equation (62) its characteristic impedance was obtained to be 50.09Ω.

$$Z_0 = \sqrt{Z_{in} * Z_L} \tag{62}$$

Circuitry could be accounted for this minute mismatch between the impedance of the line and the load impedance. All impedance measurement for this test was done at 7.5475 MHz. This was the frequency at which the curve first crossed the prime axis of the smith chart, which is the axis for the purely resistive component of impedance.

About 5cm of the jacket was cut off around the center of the coax cable as shown in Figure 23.1. Its impedance was measured to be 50.2 Ω also. The coax cable under test had an inner conductor

and outer sheath, separated by a dielectric. When the outer sheath was peeled off (23.2), a 0.4 Ω increase in impedance was observed. Further, taking off 5 cm in length of the dielectric at this same spot revealed a 1 Ω increase in impedance. A deep notch was created into the wire using a wire cutter, and impedance increased from 51.6 Ω to 52.1 Ω. Finally, the cable was open circuited and capacitive reactance was 126 pF (purely reactive) with infinity resistance.

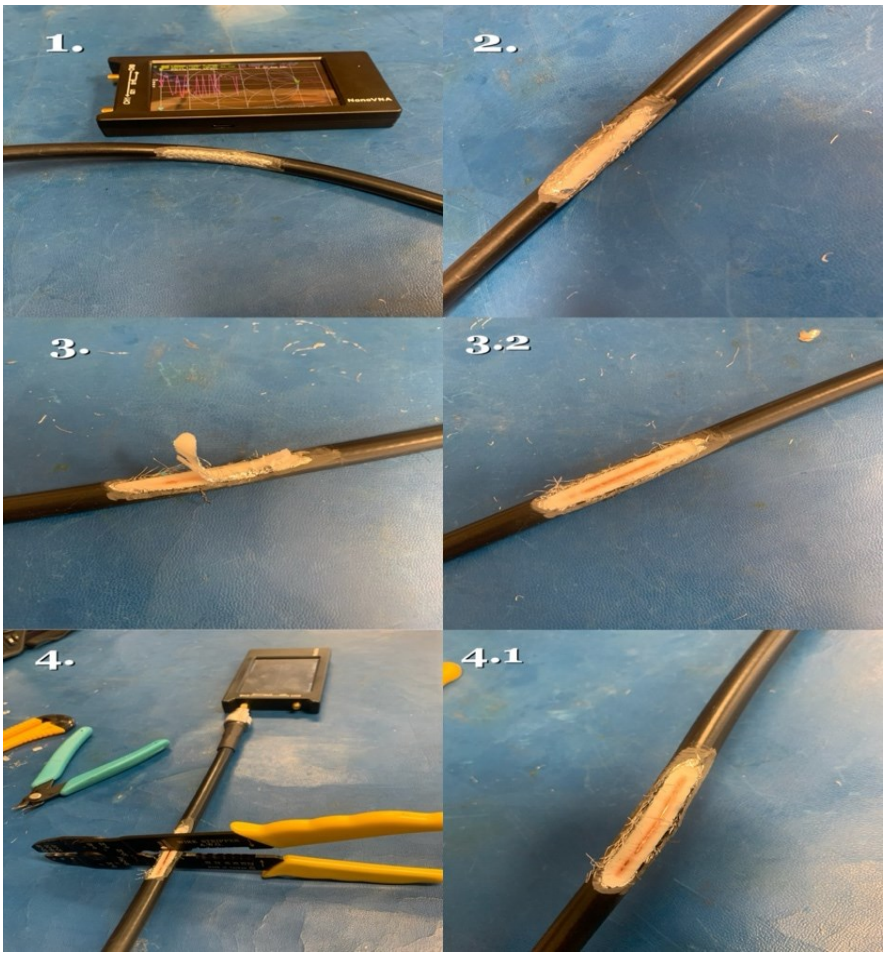

Figure 24: Mechanical damage for resistive impedance testing

Analysis and data interpretation

Figure 25 showcases resistive impedance sensitivity in response to a notch in a cable.

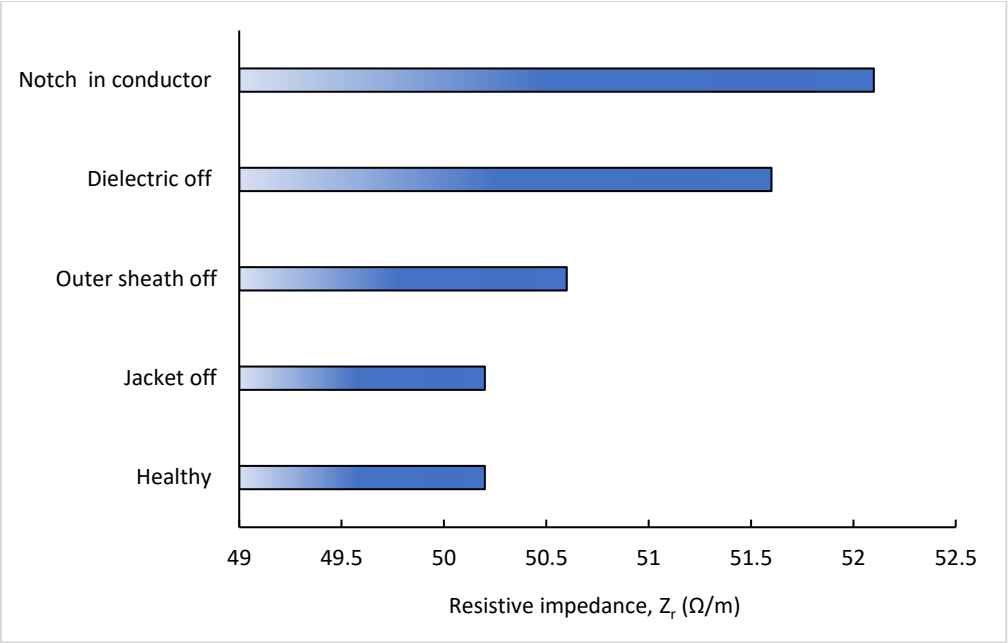

Figure 25: Impedance sensitivity for a mechanically damaged cable

The conducted impedance measurements at 7.5475 MHz provide valuable insights into the detection of mechanical faults in distribution and transmission lines. The identified impedance changes, such as the 0.4 Ω increase when the sheath was peeled off and the 1 Ω increase when 5 cm of the dielectric was removed, showcase the sensitivity of impedance measurements to cable damage. The intentional creation of a deep notch into the conductor resulted in a 0.5 Ω increase in impedance. These findings suggest that impedance measurements, particularly at the specified frequency, can be a reliable method for detecting and assessing cable mechanical damage. Also, these findings align with the observations in a referenced paper [68] where it was noted that characteristic impedance of damaged cables increased as the severity of these faults increased. The consistent trend observed in both studies emphasizes the significance of impedance changes as an indicator of mechanical damage and their severity in cables.

The observed correlation between the depth of the notch and the intensity of impedance change further emphasizes the diagnostic potential of impedance analysis in identifying and characterizing mechanical faults in coaxial cables used in underground electrical infrastructure.

4.5.4. Water trees – impedance experiment

Conditions that promote the formation of water trees in operating cables were created in a controlled laboratory environment. Water trees are commonly associated with high-voltage power cables. The cable sample used to simulate this damage was a low voltage coaxial cable with a healthy impedance of 50.1 Ω. About 0.2 cm of circular notches were created into the cable, making sure notches reach the insulation layer (see Figure 26). Small pieces of a sponge were soaked in a NaCl/water solution in the ratio of 15 g of NaCl to 0.25 l of pure water (a modified ratio from [20]) and the wet sponges were firmly tied on each notch. Using the NanoVNA, a new impedance was recorded to be 50.6Ω.

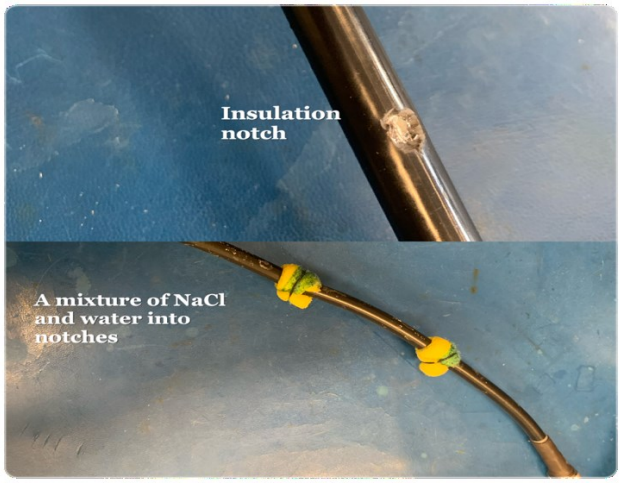

Figure 26: Creating conditions for water trees formation in power cables

Analysis and data interpretation

Despite using a low-voltage coaxial cable, the intentional creation of circular notches in the insulation, coupled with the introduction of a NaCl and water mixture-soaked sponge, led to a

measurable increase in impedance from the healthy baseline value of 50.1 Ω to 50.6 Ω as recorded by the NanoVNA. This finding suggests that the impedance measurement using the NanoVNA is sensitive to the simulated water tree damage, providing a potential method for detecting such faults in underground distribution and transmission lines. The laboratory setup offers insights into how impedance changes can serve as indicators of water tree formation, contributing to the development of diagnostic techniques for identifying cable damage in real-world scenarios.

4.6 Challenges and mitigation strategies

- **Power supply:** The utilization of a 30 V / 10 A power supply was a deliberate safety measure, recognizing the inherent risks associated with working at high voltage and current levels for both equipment and personnel. While this choice contributed to adhering to all safety protocols and guidelines, and a thorough risk assessment was conducted prior to initiating experiments, it is important to acknowledge that it introduced limitations in faithfully replicating real-world conditions for high-power transmission lines. This safety-conscious approach emphasized a commitment to maintaining the well-being of both equipment and personnel throughout the experimental procedures.
- **Cable size limit:** Collecting cable layers' temperature distribution data from small-sized cables proved challenging. The decision to use small-sized cables to represent distribution and transmission lines was driven by the need to capture measurable changes. This choice was made considering the extended timeframes—potentially years—required for underground power cables to experience significant impedance shifts due to thermal aging and water trees. In contrast, the use of small-sized cables allowed for the detection of more immediate changes, such as those resulting from hotspots or deep mechanical damages.

- **Temperature measurement accuracy:** Obtaining accurate temperature measurements, especially in scenarios with rapid temperature changes, was challenging. Temperature readings over short time intervals were averaged to enhance accuracy.
- **Impedance measurement precision:** Obtaining precise impedance measurements at specific time intervals was challenging, primarily because impedance is intricately linked to temperature. Moreover, the rate of cooling also constituted a significant factor in this measurement process.
- **Time-dependent effects:** The experimental timeframes may not entirely capture time-dependent effects in power cables. While minute impedance changes were recorded during the experiments of water trees and mechanical damage, these changes, under real operating conditions, could be perceived as normal variations. For a more comprehensive evaluation of results, it is crucial to consider potential long-term implications and observations.

In summary, despite the acknowledged challenges and limitations, the experimental results contribute valuable insights into the complex interplay of factors influencing power cable impedance behavior. The findings not only validate the sensitivity of impedance measurements in detecting thermal, mechanical damage and water trees but also highlight the potential for these measurements to serve as a reliable diagnostic tool in assessing the health of underground electrical infrastructure. Discussion of results for each test provides a detailed exploration of the observed phenomena, reinforcing the significance of the experimental outcomes.

Chapter 5 Conclusion

The focus of this study was to investigate the feasibility of resistive impedance spectroscopy (RIS) as an anomaly detection method in inaccessible power cables. Unlike conventional approaches analyzing both magnitude and phase of impedance spectra or impedance as whole, this study focused on resistive impedance spectroscopy, offering potential insights into cable anomalies. The goal was not only to reduce complexity associated with interpretation of magnitude and phase information, but also to explore practical implications for cable health monitoring. This focused approach contributed to the innovation of anomaly detection methods within impedance spectroscopy, with the hypothesis that resistive impedance spectroscopy may enhance sensitivity to specific anomalies, advocating for a tailored approach based on the nature of the electrical properties under investigation.

Three damaged models were investigated including thermal anomalies, mechanical damage, and water trees. Thermal anomalies were paid particularly attention to, as it is a major concern to electric utilities. A thermal model represented by temperature distribution was coupled with an electrical model represented by the resistive portion of impedance. Cable temperature was found to increase linearly with increasing current load. Continuous volumetric heat flux generated within the conductor was the heat source into the cable system and a hotspot was simulated using an external heater. Experimentally, resistive impedance was observed to have high sensitivity to cable temperature. A 23.8% sensitivity was recorded when a hotspot was simulated on a coax cable in a laboratory analysis (see relative change calculations in Appendix C).

The key point with this diagnostic method will be to have a reliable resistive impedance baseline registered in electric utility operating systems. Far away deviations from this baseline are potential alarms for faults. Multi-physics models for thermal anomalies like the one developed in this thesis work, together with economic perspective are used to find optimized maintenance and

replacement cycles of underground power cables. The result of such optimization brings about effective cost maintenance of underground power cables, minimizes power outages, and improve system reliability.

The resistive impedance measurements of a coax at 7.5475 MHz using a NanoVNA revealed interesting findings related to the detection of mechanical faults in cables. The sensitivity of impedance measurements to cable damage was evident, with intentional modifications causing measurable impedance changes. This sensitivity, particularly at the specified frequency, underscores the reliability of impedance analysis in identifying and characterizing cable mechanical faults. Even though impedance slightly and steadily increased when the cable under test was mechanically damaged, the depth of the notch mattered. Deeper cuts into the conductor revealed a 3.8% increase in resistive impedance compared to a 0.8% increase when a portion of the outer sheath was damaged. From the laboratory scale study and results on this damage model, these values are not far from the baseline line which was 50 Ω. Therefore, although resistive impedance spectroscopy is sensitive to mechanical damages in power cables, it may not be a suitable diagnostic method for such faults except in the case of deep cuts in the cable.

Analysis of water-trees-induced-faults reported a similar impedance trend to that of mechanical faults. The healthy cable test sample had an impedance of 50.1 Ω and after replication of conditions for the formation of water trees, impedance was recorded to be 50.6 Ω. Bearing in mind that water trees develop over long periods, early detection of these faults using resistive impedance spectroscopy may not be an ideal option. Due to experimental constraints, it was not possible to quantify the degree of water trees created, hence a more realistic analysis is not possible at the time of submission of the thesis work.

In conclusion, while resistive impedance may not be a suitable early diagnostic method for water trees and mechanical damage, the results from the impedance-temperature study for thermal

anomaly detection in underground power cables has potential contribution for fault diagnostic in distribution and transmission lines.

5.1 Thesis contributions

- A first step in exploring the feasibility of resistive impedance spectroscopy as an anomaly detection technique was carried out in this thesis work. A physics-based model based on temperature distribution and impedance spectrometry was developed and experimentally validated. Mechanical damage and water trees were experimentally assessed as well. An advanced integrated version of these models and experimental results can be used by energy distribution and transmission engineers to detect anomalies in underground cable network systems.
- The findings of the thesis work can further assist in decision making for optimal inspection and replacement intervals. Condition monitoring of cables helps to analyze and classify cable failures and their urgency. Available information on cables' health allows utility regulators to plan for maintenance, manage maintenance costs and downtime.
- Also, robust diagnostic techniques like the one in this study can help reduce the number of sudden power outages and mitigate impacts of power outages in our society.
- In the presence of faulty cables in the network, current load is sometimes redistributed. This is done by reducing the load on damaged cables and increasing it on healthy cables, rather than complete replacement of cables. The findings in this study can help determine which cables are healthy and which are damaged.
- Finally, the thesis work further contributes to existing knowledge in literature.

5.2 Future direction and recommendations

As future work, resistive impedance baselines and how much deviation is considered normal and abnormal will be investigated. For an experimental analysis, data will be collected over longer

periods and the study will be extended to other damage models such as PDs. This will broaden, solidify, and continue to verify the findings in this work. Additionally, it is planned to place the developed model and impedance findings in conditions corresponding to typical underground cable operation conditions. Some potential technological advancements offer promising avenues to facilitate the extraction and analysis of cable data before and after faults. These same technologies can be used to implement resistive impedance spectroscopy as a diagnostic technique for thermal anomalies in real operating cables.

Integrating thermal models with electrical analysis, harnessing AI, and enhancing sensor technologies can contribute to a more comprehensive and accurate understanding of cable impedance behavior, enabling proactive fault detection and improving the overall reliability of underground power cable systems. Some recommendations include:

- **Power line communication (PLC) and modems (PLMs):** Developing more advanced grid sensors can provide accurate and high-resolution data along the cable's length and in time cable's health conditions. PLC coupled with PLMs is an evolving technology for grid diagnostics which more electrical utility companies should explore. These "wired wireless" communication channels or modems use a carrier-frequency technique to transfer data over low voltage power lines. PLC is beneficial in that it is trivial to install, it does not require new wiring and it provides high data rates [82]. PLMs can be used to measure, record, and extract resistive impedance of the line for fault analysis.
- **Artificial intelligence:** The application of machine learning and artificial intelligence to fault identification and thermal damage specifically, can help automate anomaly detection that might be challenging using other identification techniques. AI approaches are more efficient and accurate.

  A machine learning solution where anomaly detection algorithms were layered on top of power line modems, forming an emulator for condition monitoring has been recently

proposed in [57]. Semi-supervised anomaly detection was used to train an emulated power distribution network (having modems located at different nodes) with normal data only and thermally damaged scenarios. This was a successful and efficient approach as a damaged cable with high sensitivity and specificity was detected amongst several other damages and severities.

- **Sensor fusion and data analytics:** Combining data from multiple sensors and using data analytics techniques to gain more insights into cable health could be another option to achieve more robust fault detection in underground power cables. Analyzing cable network temperatures with resistive impedance data will be an efficient and practical diagnostic technique for thermal anomalies in remote power cables.
- **Innovative cable fault location systems:** The STX40 by Megger stands out as an innovative cable fault location system, offering electric utilities a powerful and robust diagnostic tool. This fully automated, portable, and weatherproof equipment excels in identifying, pre-locating, and determining fault conditions specifically in extruded low voltage and medium voltage XLPE, EPR, and paper-insulated lead-covered (PILC) cables. Distinguishing between low and high impedance faults reveals unique characteristics, each with its own limitations in fault location methods. The STX40 mitigates these limitations with its seven built-in fault locating methods, including insulation resistance testing, radar-time domain reflectometry, sheath testing, and sheath fault pinpointing. In addition, fully automated systems like the STX40 will reduce personnel training and time requirements. With existing diagnostic limitations across the cable fault diagnostic field, such a comprehensive toolbox will be essential for addressing diverse fault scenarios involving multiple fault types.

In conclusion, the integration of physics of failure principles and non-invasive monitoring techniques not only demonstrates promising potential but stands as a pivotal avenue for elevating the reliability of underground electrical power distribution systems. This comprehensive

approach allows for the proactive identification of potential issues, offering a robust foundation for the implementation of condition-based maintenance. By embracing these cutting-edge methodologies, we pave the way for a more resilient and efficient underground power distribution infrastructure, minimizing downtime, reducing operational risks, and ultimately ensuring a more sustainable and reliable energy delivery system for the future.

References

[1] R. E. Brown, *Electric Power Distribution Reliability*, 2nd ed. Boca Raton, FL, USA: CRC Press, 2017. doi: 10.1201/9780849375682.

[2] "2022 Long-term Reliability Assessment by NERC," North American Electric Reliability Corporation (NERC), 2022. Accessed: July 26, 2022. [Online]. Available: https://www.nerc.com/pa/RAPA/ra/Reliability%20Assessments%20DL/NERC_LTRA_2022.pdf

[3] J. Murphy and J. FitzGerald, "Deadly winter storm knocks out power to 1.5 m," Dec. 23, 2022. Accessed: Oct. 20, 2023. [Online]. Available: Winter storm live updates: Power outages hit 1.5m across US and Canada - BBC News

[4] SafeGlo, "Are blackouts increasing in Canada?" Accessed: Oct. 20, 2023. [Online]. Available: Are Blackouts & Power Outages Increasing in Canada? (safeglo.ca)

[5] Y. Wu, T. Fan, and T. Huang, "Electric Power Distribution System Reliability Evaluation Considering the Impact of Weather on Component Failure and Pre-Arranged Maintenance," *IEEE Access*, vol. 8, pp. 87800–87809, 2020, doi: 10.1109/ACCESS.2020.2993087.

[6] "Ausgrid regulation." Accessed: Oct. 20, 2023. [Online]. Available: ausgrid.com.au/-/media/Documents/Regulation/

[7] J. R. Parent, T. H. Meyer, J. C. Volin, R. T. Fahey, and C. Witharana, "An analysis of enhanced tree trimming effectiveness on reducing power outages," *Journal of environmental management*, vol. 241, pp. 397–406, 2019.

[8] J. A. Casey, M. Fukurai, D. Hernández, S. Balsari, and M. V. Kiang, "Power Outages and Community Health: a Narrative Review," *Curr Envir Health Rpt*, vol. 7, no. 4, pp. 371–383, Dec. 2020, doi: 10.1007/s40572-020-00295-0.

[9] E. Rosales-Asensio, M. de Simón-Martín, D. Borge-Diez, J. J. Blanes-Peiró, and A. Colmenar-Santos, "Microgrids with energy storage systems as a means to increase power resilience: An application to office buildings," *Energy*, vol. 172, pp. 1005–1015, Feb. 2019.

[10] S. Mukherjee, R. Nateghi, and M. Hastak, "Data on major power outage events in the continental US," *Data in brief*, vol. 19, pp. 2079–2083, 2018.

[11] "2016 Cost of Data Center Outages." Ponemon Institute ,2016. Accessed: Jul. 27, 2023. [Online]. Available: https://www.ponemon.org/research/ponemon-library/security/2016-cost-of-data-center-outages.html

[12] S. Matthewman and H. Byrd, "Blackouts: a sociology of electrical power failure," Dept. sociology. Auckland Uni., & Lincoln Uni., 2014.

[13] G. J. Rubin and M. B. Rogers, "Behavioural and psychological responses of the public during a major power outage: A literature review," *International Journal of Disaster Risk Reduction*, vol. 38, p. 101226, Aug. 2019, doi: 10.1016/j.ijdrr.2019.101226.

[14] L. Boukezzi, Y. Saadi, and A. Boubakeur, "The radial distribution of temperature in XLPE cable: An analysis with the Finite Volume Numerical Method (FVM)," in *2010 Annual Report Conference on Electrical Insulation and Dielectic Phenomena*, West Lafayette, IN: IEEE, Oct. 2010, pp. 1–4. doi: 10.1109/CEIDP.2010.5723951.

[15] G. J. Anders, *Rating of electric power cables: ampacity computations for transmission, distribution, and industrial applications*. Piscataway, NJ, USA: IEEE Piscataway, 1997.

[16] S. Govindarajan, A. Morales, J. A. Ardila-Rey, and N. Purushothaman, "A review on partial discharge diagnosis in cables: Theory, techniques, and trends," *Measurement*, vol. 216, p. 112882, Jul. 2023, doi: 10.1016/j.measurement.2023.112882.

[17] J. Densley, "Ageing mechanisms and diagnostics for power cables - an overview," *IEEE Electr. Insul. Mag.*, vol. 17, no. 1, pp. 14–22, Jan. 2001, doi: 10.1109/57.901613.

[18] J. D. Cutnell, D. E. Kranbuehl, E. M. Turner, and W. E. Vaughan, "Dielectric Permittivity Measurements at Centimeter Wavelengths," *Review of Scientific Instruments*, vol. 40, no. 7, pp. 908–915, Jul. 1969, doi: 10.1063/1.1684102.

[19] V. F. Lvovich, *Impedance Spectroscopy: Applications to Electrochemical and Dielectric Phenomena*. Hoboken, NJ, USA: John Wiley & Sons, Inc., 2012. doi: 10.1002/9781118164075.

[20] Y. Ohki, T. Yamada, and N. Hirai, "Diagnosis of cable aging by broadband impedance spectroscopy," in *2011 Annual Report Conference on Electrical Insulation and Dielectric Phenomena*, Cancun, Mexico: IEEE, Oct. 2011, pp. 24–27. doi: 10.1109/CEIDP.2011.6232587.

[21] D. Rogovin, R. Lofaro, "Evaluation of the Broadband Impedance Spectroscopy Prognostic/Diagnostic Technique for Electric Cables Used in Nuclear Power Plants." Boeing

Company, Brookhaven National Lab., CA & NY, USA. [Online]. Available: https://www.nrc.gov/reading-rm/doc-collections/nuregs/contract/cr6904/cr6904.pdf

[22] Z. Zhou, D. Zhang, J. He, and M. Li, "Local degradation diagnosis for cable insulation based on broadband impedance spectroscopy," *IEEE Trans. Dielect. Electr. Insul.*, vol. 22, no. 4, pp. 2097–2107, Aug. 2015, doi: 10.1109/TDEI.2015.004799.

[23] M. Li *et al.*, "Feasibility Study on Online Diagnosis of Aging and Deterioration of Medium Voltage (MV) Three-Core Cable Based on Impedance Spectroscopy," *IEEE Access*, 2023, doi: 10.1109/ACCESS.2023.3265955.

[24] Y. Wang, J. Zhang, C. Yao, and H. Zhao, "A mathematical method for local defects and faults identification of 10 kV three-core cable based on input impedance spectrum," *IET Science Measure & Tech*, vol. 16, no. 8, pp. 467–478, Oct. 2022, doi: 10.1049/smt2.12119.

[25] S. H. Lee, J. B. Park, and Y. H. Choi, "Measurement of load impedance in power cables using wavelet-transform-based time–frequency domain reflectometry," *Meas. Sci. Technol.*, vol. 24, no. 9, p. 095008, Sep. 2013, doi: 10.1088/0957-0233/24/9/095008.

[26] B. Rasool, A. Rasool, and I. Khan, "Impedance Characterization of Power Line Communication Networks," *Arab J Sci Eng*, vol. 39, no. 8, pp. 6255–6267, Aug. 2014, doi: 10.1007/s13369-014-1235-z.

[27] E.-A. Sánchez-Moctezuma, L.-J. Santander-Hernández, F. Álvarez-Mendoza, and C. Angeles-Camacho, "Real-Time Analysis of the Impedance–Temperature Relationship in Electric Distribution Lines Using PMUs," *Energies*, vol. 14, no. 6, p. 1661, Mar. 2021, doi: 10.3390/en14061661.

[28] E. Barsoukov and J. R. Macdonald, *Impedance spectroscopy: theory, experiment, and applications*. Hoboken, NJ, USA: John Wiley & Sons, 2018.

[29] J. L. Lauletta, Y. Sozer, and J. A. De Abreu-Garcia, "A novel sensing device for underground cable condition assessment," in *2015 IEEE Electrical Insulation Conference (EIC)*, Seattle, WA, USA: IEEE, Aug. 2015, pp. 523–528. doi: 10.1109/ICACACT.2014.7223561.

[30] M. G. Granger, Y. Sozer, J. A. De Abreu Garcia, R. J. Veillette, A. Ibrahem, and A. R. Boynuegri, "A non-intrusive system for measuring underground power utility cable impedance," in *2016 IEEE Power and Energy Society General Meeting (PESGM)*, Boston, MA, USA: IEEE, Jul. 2016, pp. 1–5. doi: 10.1109/PESGM.2016.7741978.

[31] D. Righini and A. M. Tonello, “Non-Intrusive Network Impedance Estimation with State-of-the-Art PLC Modems,” in *2020 IEEE International Symposium on Power Line Communications and its Applications (ISPLC)*, Malaga, Spain: IEEE, May 2020, pp. 1–6. doi: 10.1109/ISPLC48789.2020.9115400.

[32] T. S. Pang, P. L. So, K. Y. See, and A. Kamarul, “Modeling and Analysis of Common-Mode Current Propagation in Broadband Power-Line Communication Networks,” *IEEE Trans. Power Delivery*, vol. 23, no. 1, pp. 171–179, Jan. 2008, doi: 10.1109/TPWRD.2007.911015.

[33] L. Forstel and L. Lampe, “Grid diagnostics: Monitoring cable aging using power line transmission,” in *2017 IEEE International Symposium on Power Line Communications and its Applications (ISPLC)*, Madrid, Spain: IEEE, 2017, pp. 1–6. doi: 10.1109/ISPLC.2017.7897106.

[34] M. Ahmed and W. L. Soo, “Power line carrier (PLC) based communication system for distribution automation system,” in *2008 IEEE 2nd International Power and Energy Conference*, Johor Bahru, Malaysia: IEEE, Dec. 2008, pp. 1638–1643. doi: 10.1109/PECON.2008.4762742.

[35] M. O. Ahmed and L. Lampe, “Power Line Communications for Low-Voltage Power Grid Tomography,” *IEEE Trans. Commun.*, vol. 61, no. 12, pp. 5163–5175, Dec. 2013, doi: 10.1109/TCOMM.2013.111613.130238.

[36] Y. Huo, G. Prasad, L. Atanackovic, L. Lampe, and V. C. M. Leung, “Grid surveillance and diagnostics using power line communications,” in *2018 IEEE International Symposium on Power Line Communications and its Applications (ISPLC)*, Manchester: IEEE, Apr. 2018, pp. 1–6. doi: 10.1109/ISPLC.2018.8360200.

[37] Q.-A. Huang, R. Hui, B. Wang, and J. Zhang, “A review of AC impedance modeling and validation in SOFC diagnosis,” *Electrochimica Acta*, vol. 52, no. 28, pp. 8144–8164, 2007, doi: https://doi.org/10.1016/j.electacta.2007.05.071.

[38] Y. Ning, D. Wang, Y. Li, and H. Zhang, “Location of Faulty Section and Faults in Hybrid Multi-Terminal Lines Based on Traveling Wave Methods,” *Energies*, vol. 11, no. 5, p. 1105, May 2018, doi: 10.3390/en11051105.

[39] A. Borghetti, M. Bosetti, M. Di Silvestro, C. A. Nucci, and M. Paolone, “Continuous-Wavelet Transform for Fault Location in Distribution Power Networks: Definition of Mother Wavelets Inferred From Fault Originated Transients,” *IEEE Trans. Power Syst.*, vol. 23, no. 2, pp. 380–388, May 2008, doi: 10.1109/TPWRS.2008.919249.

[40] S. Das, S. Santoso, A. Gaikwad, and M. Patel, “Impedance-based fault location in transmission networks: theory and application,” *IEEE Access*, vol. 2, pp. 537–557, 2014, doi: 10.1109/ACCESS.2014.2323353.

[41] A. Yadav and A. Swetapadma, “Enhancing the performance of transmission line directional relaying, fault classification and fault location schemes using fuzzy inference system,” *IET Generation, Transmission & Distribution*, vol. 9, no. 6, pp. 580–591, 2015.

[42] Zhiling Long, N. H. Younan, and T. O. Bialek, “Underground power cable fault detection using complex wavelet analysis,” in *2012 International Conference on High Voltage Engineering and Application*, Shanghai, China: IEEE, Sep. 2012, pp. 59–62. doi: 10.1109/ICHVE.2012.6357058.

[43] A. H. A. Bakar, M. S. Ali, C. Tan, H. Mokhlis, H. Arof, and H. A. Illias, “High impedance fault location in 11kV underground distribution systems using wavelet transforms,” *International Journal of Electrical Power & Energy Systems*, vol. 55, pp. 723–730, 2014, doi: https://doi.org/10.1016/j.ijepes.2013.10.003.

[44] A. Sundaram, “Distribution fault location: field data and analysis,” *EPRI (1012438)*, 2006.

[45] N. Hirai, T. Yamada, and Y. Ohki, “Comparison of broadband impedance spectroscopy and time domain reflectometry for locating cable degradation,” in *2012 IEEE International Conference on Condition Monitoring and Diagnosis*, Bali, Indonesia: IEEE, Sep. 2012, pp. 229–232. doi: 10.1109/CMD.2012.6416417.

[46] H. Orton, “History of underground power cables,” *IEEE Electr. Insul. Mag.*, vol. 29, no. 4, pp. 52–57, Jul. 2013, doi: 10.1109/MEI.2013.6545260.

[47] I. A. Metwally, A. H. Al-Badi, and A. S. Al Farsi, “Factors influencing ampacity and temperature of underground power cables,” *Electr Eng*, vol. 95, no. 4, pp. 383–392, Dec. 2013, doi: 10.1007/s00202-012-0271-5.

[48] J. I. Aizpurua *et al.*, “A Diagnostics Framework for Underground Power Cables Lifetime Estimation Under Uncertainty,” *IEEE Trans. Power Delivery*, vol. 36, no. 4, pp. 2014–2024, Aug. 2021, doi: 10.1109/TPWRD.2020.3017951.

[49] A. Sturchio, G. Fioriti, V. Salusest, L. Calcara, and M. Pompili, “Thermal behavior of distribution MV underground cables,” in *2015 AEIT International Annual Conference (AEIT)*, Naples, Italy: IEEE, Oct. 2015, pp. 1–5. doi: 10.1109/AEIT.2015.7415247.

[50] M. Rerak and P. Ocłoń, “Thermal analysis of underground power cable system,” *J. Therm. Sci.*, vol. 26, no. 5, pp. 465–471, Oct. 2017, doi: 10.1007/s11630-017-0963-2.

[51] M. S. Al-Saud, M. A. El-Kady, and R. D. Findlay, “A new approach to underground cable performance assessment,” *Electric Power Systems Research*, vol. 78, no. 5, pp. 907–918, 2008, doi: https://doi.org/10.1016/j.epsr.2007.06.010.

[52] L. Mariut, E. Helerea, G. Lungoci, and S. Abagiu, “Thermal analysis of underground power cables-A monitoring procedure,” in *2012 International Conference on Applied and Theoretical Electricity (ICATE)*, Craiova, Romania: IEEE, Oct. 2012, pp. 1–6. doi: 10.1109/ICATE.2012.6403398.

[53] G. Petrović, M. Cvetković, T. Garma, and T. Kilić, “An approach to thermal modeling of power cables installed in ducts,” *Electric Power Systems Research*, vol. 214, p. 108916, Jan. 2023, doi: 10.1016/j.epsr.2022.108916.

[54] L. Exizidis, I. Papagiannopoulos, V. Chatziathanasiou, G. D. Mey, and B. Więcek, “Evaluation of a buried power cable’s thermal behavior using phase diagrams and calculation of the phase difference between temperature and power,” *Applied Thermal Engineering*, vol. 70, no. 1, pp. 770–775, 2014, doi: https://doi.org/10.1016/j.applthermaleng.2014.05.101.

[55] C. Verschaffel-Drefke, M. Schedel, C. Balzer, V. Hinrichsen, and I. Sass, “Heat Dissipation in Variable Underground Power Cable Beddings: Experiences from a Real Scale Field Experiment,” *Energies*, vol. 14, no. 21, p. 7189, Nov. 2021, doi: 10.3390/en14217189.

[56] L. Boukezzi and A. Boubakeur, “Effect of Thermal Aging on the Electrical Characteristics of XLPE for HV Cables,” *Trans. Electr. Electron. Mater.*, vol. 19, no. 5, pp. 344–351, Oct. 2018, doi: 10.1007/s42341-018-0043-7.

[57] M. Yeganejou, T. Ryan, M. Reshadi, S. Dick, and M. G. Lipsett, “Condition Monitoring of Underground Power Cables Via Power-Line Modems and Anomaly Detection,” *IEEE Trans. Power Delivery*, pp. 1–10, 2023, doi: 10.1109/TPWRD.2023.3322380.

[58] L. Kaimal and R. Kulkarni, “Understanding Partial Discharges and Its Role in Condition Monitoring of Insulators,” in *Proceedings of Third International Conference on Communication, Computing and Electronics Systems*, vol. 844, V. Bindhu, J. M. R. S. Tavares, and K.-L. Du, Eds., in Lecture Notes in Electrical Engineering, vol. 844., Singapore: Springer Singapore, 2022, pp. 209–226. doi: 10.1007/978-981-16-8862-1_15.

[59] J. Perkel and J. C. Hernandez-Mejia, “Medium voltage cable system partial discharge,” *Georgia Tech NEETRAC, Cable Diagnostic Focused Initiative (CDFI)*, vol. 7, 2016. Accessed: Aug 08, 2022 [Online]. Available: https://www.neetrac.gatech.edu/publications/CDFI/7-MV-Partial-Discharge-39_with-Copyright.pdf

[60] M. R. Hussain, S. S. Refaat, and H. Abu-Rub, “Overview and Partial Discharge Analysis of Power Transformers: A Literature Review,” *IEEE Access*, vol. 9, pp. 64587–64605, 2021, doi: 10.1109/ACCESS.2021.3075288.

[61] S. Famakin and C. Kim, “Modeling for Underground Cable Water Tree Growth Dynamics,” *JPEE*, vol. 07, no. 12, pp. 51–65, 2019, doi: 10.4236/jpee.2019.712004.

[62] M. Acedo, I. Radu, F. Frutos, J. C. Filippini, and P. Notingher, “Water treeing in underground power cables: modelling of the trees and calculation of the electric field perturbation,” *Journal of Electrostatics*, vol. 53, no. 4, pp. 267–294, Oct. 2001, doi: 10.1016/S0304-3886(01)00164-4.

[63] S. Nakamura, T. Ozaki, N. Ito, and J. Kawai, “Change of dielectric property with water-treed region,” *IEEE Trans. Dielect. Electr. Insul.*, vol. 9, no. 3, pp. 329–334, Jun. 2002, doi: 10.1109/TDEI.2002.1007694.

[64] X. Zhu, Y. Yin, J. Wu, and X. Wang, “Study on Aging Characteristics of XLPE Cable Insulation Based on Quantum Chemical Calculation,” *IEEE Trans. Dielect. Electr. Insul.*, vol. 27, no. 6, pp. 1942–1950, Dec. 2020, doi: 10.1109/TDEI.2020.009025.

[65] Y. Ohki, N. Hirai, and Y. Tanaka, “Improvement of electrical insulation performance of silicone rubber cables due to exposure to heat and radiation,” *J of Applied Polymer Sci*, vol. 140, no. 43, p. e54595, Nov. 2023, doi: 10.1002/app.54595.

[66] B. X. Du and J. Li, “Electrical and mechanical ageing behaviors of used heat-shrinkable insulation tubes,” *IEEE Trans. Dielect. Electr. Insul.*, vol. 21, no. 4, pp. 1875–1881, Aug. 2014, doi: 10.1109/TDEI.2014.104324.

[67] K. Son *et al.*, “Signal Integrity Analysis of High-Speed Channel considering Thermal Distribution,” in *2021 IEEE 30th Conference on Electrical Performance of Electronic Packaging and Systems (EPEPS)*, Austin, TX, USA: IEEE, Oct. 2021, pp. 1–3. doi: 10.1109/EPEPS51341.2021.9609215.

[68] X. Hua, L. Wang, and Y. Zhang, “Analysis and Diagnosis of Shielded Cable Faults Based on Finite-Element Method and Time-Reversal Time-Frequency Domain Reflectometry,” *IEEE Trans. Ind. Electron.*, vol. 69, no. 4, pp. 4205–4214, Apr. 2022, doi: 10.1109/TIE.2021.3071685.

[69] M. Karahan and O. Kalenderli, “Coupled Electrical and Thermal Analysis of Power Cables Using Finite Element Method,” in *Heat Transfer - Engineering Applications*, V. Vikhrenko, Ed., Turkey: InTech, 2011. doi: 10.5772/27350.

[70] G. D. Raithby and K. G. T. Hollands, “A General Method of Obtaining Approximate Solutions to Laminar and Turbulent Free Convection Problems,” in *Advances in Heat Transfer*, vol. 11, Elsevier, 1975, pp. 265–315. doi: 10.1016/S0065-2717(08)70076-5.

[71] A. Cywiński and K. Chwastek, “A Multiphysics Analysis of Coupled Electromagnetic-Thermal Phenomena in Cable Lines,” *Energies*, vol. 14, no. 7, p. 2008, Apr. 2021, doi: 10.3390/en14072008.

[72] P. Ocłoń, J. Pobędza, P. Walczak, P. Cisek, and A. Vallati, “Experimental Validation of a Heat Transfer Model in Underground Power Cable Systems,” *Energies*, vol. 13, no. 7, p. 1747, Apr. 2020, doi: 10.3390/en13071747.

[73] V. Chatziathanasiou, P. Chatzipanagiotou, I. Papagiannopoulos, G. D. Mey, and B. Więcek, “Dynamic thermal analysis of underground medium power cables using thermal impedance, time constant distribution and structure function,” *Applied Thermal Engineering*, vol. 60, no. 1, pp. 256–260, 2013, doi: https://doi.org/10.1016/j.applthermaleng.2013.07.009.

[74] A. A. Al-Dulaimi, M. T. Guneser, and A. A. Hameed, “Thermal Modeling for Underground Cable Under the Effect of Thermal Resistivity and Burial Depth Using Finite Element Method,” in *Innovations in Smart Cities Applications Volume 5*, vol. 393, M. Ben Ahmed, A. A. Boudhir, İ. R. Karaş, V. Jain, and S. Mellouli, Eds., in Lecture Notes in Networks and Systems, vol. 393. , Cham: Springer International Publishing, 2022, pp. 339–352. doi: 10.1007/978-3-030-94191-8_27.

[75] E. J. Lundquist, J. R. Nagel, S. Wu, B. Jones, and C. Furse, “Advanced Forward Methods for Complex Wire Fault Modeling,” *IEEE Sensors J.*, vol. 13, no. 4, pp. 1172–1179, Apr. 2013, doi: 10.1109/JSEN.2012.2227996.

[76] M. A. Elhirbawy, T. T. Nguyen, L. Jennings, and W. W. L. Keerthipala, “Calculation of electromagnetic fields established by power transmission line using finite difference

techniques," in *IEEE CCECE2002. Canadian Conference on Electrical and Computer Engineering. Conference Proceedings (Cat. No.02CH37373)*, Winnipeg, Man., Canada: IEEE, 2002, pp. 311–316. doi: 10.1109/CCECE.2002.1015240.

[77] R. de L. Vollaro, L. Fontana, and A. Vallati, "Thermal analysis of underground electrical power cables buried in non-homogeneous soils," *Applied Thermal Engineering*, vol. 31, no. 5, pp. 772–778, 2011, doi: https://doi.org/10.1016/j.applthermaleng.2010.10.024.

[78] D. I. Doukas, T. A. Papadopoulos, A. I. Chrysochos, D. P. Labridis, and G. K. Papagiannis, "Multiphysics Modeling for Transient Analysis of Gas-Insulated Lines," *IEEE Trans. Power Delivery*, vol. 33, no. 6, pp. 2786–2793, Dec. 2018, doi: 10.1109/TPWRD.2018.2820022.

[79] O. Chávez, F. Godínez, F. Méndez, and A. Aguilar, "Prediction of temperature profiles and ampacity for a monometallic conductor considering the skin effect and temperature-dependent resistivity," *Applied Thermal Engineering*, vol. 109, pp. 401–412, Oct. 2016, doi: 10.1016/j.applthermaleng.2016.08.044.

[80] L. Gonzalez and V. Dmitriev, "Electrothermal analysis of modified OPGW cables using Multiphysics Model," in *2015 SBMO/IEEE MTT-S International Microwave and Optoelectronics Conference (IMOC)*, Porto de Galinhas, Brazil: IEEE, Nov. 2015, pp. 1–5. doi: 10.1109/IMOC.2015.7369208.

[81] T. Szczegielniak, D. Kusiak, and P. Jabłoński, "Thermal Analysis of the Medium Voltage Cable," *Energies*, vol. 14, no. 14, p. 4164, Jul. 2021, doi: 10.3390/en14144164.

[82] C. Vlachou and S. Henri, *A practical guide to power-line communication*. Cambridge, UK: Cambridge University Press, 2022. [Online]. Available: https://doi.org/10.1017/9781108890823

Appendix A: Python code - Steady-state radial temperature distribution in an XLPE cable

```
import numpy as np

class FourLayerSolution:
    def
__init__(self,rad_cond,rad_ins,rad_sh,rad_jac,k_cond,k_ins,k_sh,k_jac,T_amb,resistance_cond,current,
area_cond,alpha_jac):
        self.rad_cond = rad_cond
        self.rad_ins = rad_ins
        self.rad_sh = rad_sh
        self.rad_jac = rad_jac
        self.k_cond = k_cond
        self.k_ins = k_ins
        self.k_sh = k_sh
        self.k_jac = k_jac
        self.T_amb = T_amb
        self.resistance_cond = resistance_cond
        self.current = current
        self.area_cond = area_cond
        self.alpha_jac = alpha_jac
        self.heat_flux_cond = ((self.current)**2)*self.resistance_cond/self.area_cond
        self.heat_flux_sh = 0

    def evaluate_coefficients(self):

        self.E = (-(self.heat_flux_cond/(2*self.k_sh))*(self.rad_cond**2)) +
((self.heat_flux_sh/(2*self.k_sh))*(self.rad_ins**2))
        self.G = (-(self.heat_flux_sh/(2*self.k_jac))*(self.rad_sh**2)) +
(-(self.heat_flux_cond/(2*self.k_jac))*(self.rad_cond**2))+
((self.heat_flux_sh/(2*self.k_jac))*(self.rad_ins**2))

        self.H = self.T_amb - ((self.k_jac/self.alpha_jac)*(self.G/self.rad_jac)) -
(self.G*np.log(self.rad_jac))

        self.F = ((self.heat_flux_sh/(4*self.k_sh))*(self.rad_sh**2)) - (self.E *
np.log(self.rad_sh)) + (self.G * np.log(self.rad_sh)) + self.H


        self.C  = (-(self.heat_flux_cond/(2*self.k_ins))*(self.rad_cond**2))

        self.D = (-(self.heat_flux_sh/(4*self.k_sh))*(self.rad_ins**2)) + (self.E *
np.log(self.rad_ins)) - (self.C * np.log(self.rad_ins)) + self.F
        self.A = 0
        self.B = ((self.heat_flux_cond/(4*self.k_cond))*(self.rad_cond**2)) +
(self.C*np.log(self.rad_cond)) + self.D

    def get_temperature_cond(self,r_cond):
            self.evaluate_coefficients()
            T_cond = (self.A* np.log(r_cond))  -
((self.heat_flux_cond*(r_cond**2))/(4*self.k_cond)) + self.B
            return T_cond

    def get_temperature_ins(self,r_ins):
            self.evaluate_coefficients()
            T_ins = self.C* np.log(r_ins) + self.D
            return T_ins

    def get_temperature_sh(self,r_sh):
            self.evaluate_coefficients()
            T_sh = self.E*np.log(r_sh)  - ((self.heat_flux_sh*(r_sh**2))/(4*self.k_sh)) + self.F
            return T_sh

    def get_temperature_jac(self,r_jac):
            self.evaluate_coefficients()
            T_jac = self.G*np.log(r_jac) + self.H
            return T_jac
```

```
from four_layer_solution import *
import numpy as np
from matplotlib import pyplot as plt


# Define the parameters
rad_cond = 10.25/1000
rad_cond_ins = 15.01/1000
rad_cond_ins_sh = 15.70/1000
rad_cond_ins_sh_jac = 17.90/1000

rad_ins = rad_cond_ins - rad_cond
rad_sh = rad_cond_ins_sh - rad_cond_ins
rad_jac = rad_cond_ins_sh_jac - rad_cond_ins_sh

k_cond = 400
k_ins = 0.29
k_sh = 400
k_jac = 0.1

T_amb = 20
alpha_jac = 10
resistance_cond = 0.0601
area_cond = np.pi*(rad_cond**2)
# area_cond =3.93e-4
current = 10

four_layer =
FourLayerSolution(rad_cond,rad_cond_ins,rad_cond_ins_sh,rad_cond_ins_sh_jac,k_cond,k_ins,k_sh,k_jac,T_amb,\

                                resistance_cond,current,area_cond,alpha_jac)
eval_points_cond = np.linspace(1e-20,rad_cond,10)
eval_points_ins = np.linspace(rad_cond,rad_cond_ins,10)
eval_points_sh = np.linspace(rad_cond_ins,rad_cond_ins_sh,10)
eval_points_jac = np.linspace(rad_cond_ins_sh,rad_cond_ins_sh_jac,10)


T_cond = four_layer.get_temperature_cond(eval_points_cond)
T_ins = four_layer.get_temperature_ins(eval_points_ins)
T_sh = four_layer.get_temperature_sh(eval_points_sh)
T_jac = four_layer.get_temperature_jac(eval_points_jac)

#plot the temperature distribution
plt.plot(eval_points_cond,T_cond,label='Conductor')
plt.plot(eval_points_ins,T_ins,label='Insulation')
plt.plot(eval_points_sh,T_sh,label='Sheath')
plt.plot(eval_points_jac,T_jac,label='Jacket')

# # save the temperature distribution for visualization
# np.savetxt('T_cond.txt',T_cond)
# np.savetxt('T_ins.txt',T_ins)
# np.savetxt('T_sh.txt',T_sh)
# np.savetxt('T_jac.txt',T_jac)

# np.savetxt('eval_points_cond.txt',eval_points_cond)
# np.savetxt('eval_points_ins.txt',eval_points_ins)
# np.savetxt('eval_points_sh.txt',eval_points_sh)
# np.savetxt('eval_points_jac.txt',eval_points_jac)

# generate the resistance distribution for the conductor
R_ref = 5.75e-05
alpha_ref = 3.93e-3

R_cond = R_ref*(1+alpha_ref*(T_cond-20))

# plt.plot(eval_points_cond,R_cond,label='Resistance')

plt.plot(T_cond,R_cond,label='Resistance')
np.savetxt('R_cond.txt',R_cond)
```

Appendix B: MATLAB code - Transient radial heat conduction in an XLPE Cable

```
global therm_cond;
global spec_heat;
global rho;       % global density

global l2_LBC;
global l2_RBC;
global l3_LBC;
global l3_RBC;
global l4_LBC;
global l4_RBC;



therm_cond = [400, 0.29, 400, 0.1];       % Thermal conductivity (W/(m*°C))
spec_heat = [385, 1739.13, 385, 965.91];  % Specific heat capacity (J/
(kg*°C))
rho = [8700, 1380, 8700, 1760];           % Density (kg/m^3)

R_init = [0.0601,2.78*10^21,0.061,9.93*10^19]; % ref. resistance in ohm/
kilometers
alpha = [0.00393,0,0,0];

T_ref = 20;        % temperature reference in °C

num_layers = 4;
layer_names= {'Conductor', 'Insulation','Sheath','Jacket'};
layer_thickness = [0.90, 3.40, 0.70, 2.20];   % Thickness of each layer (mm)


diam = [20.5, 30.1, 31.4,35.8];     % in mm
rad = [10.25, 15.01 ,15.7, 17.9];    %in mm

r_l2 = rad(2) - rad(1);
r_l3 = rad(3) - rad(2);
r_l4 = rad(4) - rad(3);
n_disc = 25;

x_l1 = linspace(0,rad(1)/1000,n_disc);           % conversion to meters
x_l2 = linspace(rad(1)/1000,rad(2)/1000,n_disc);
x_l3 = linspace(rad(2)/1000,rad(3)/1000,n_disc);
x_l4 = linspace(rad(3)/1000,rad(4)/1000,n_disc);

t_l1_init = 20*ones(1,n_disc);                   %this is temperature
t_l2_init = 20*ones(1,n_disc);
t_l3_init = 20*ones(1,n_disc);
t_l4_init = 20*ones(1,n_disc);

t_init = 0;                       % time
t_fin = 3600;
n_pnts = 600;
t_delta = (t_fin - t_init)/n_pnts;
t_act = linspace(t_init,t_fin,n_pnts);
```



```
t_l1_sol = zeros(n_pnts,n_disc);
t_l1_sol(1,:) = t_l1_init;        % representing the first point as initial
cond.
t_l2_sol = zeros(n_pnts,n_disc);
t_l2_sol(1,:) = t_l2_init;
t_l3_sol = zeros(n_pnts,n_disc);
t_l3_sol(1,:) = t_l3_init;
t_l4_sol = zeros(n_pnts,n_disc);
t_l4_sol(1,:) = t_l4_init;

Z_l1_sol = zeros(n_pnts,n_disc);
Z_l1_sol(1,:) = R_init(1)*(1*ones(1,n_disc) +alpha(1)*(t_l1_sol(1,:) -
T_ref));     % representing the first point as initial c.


m = 1;
for i=1:n_pnts-1

    t = linspace((i-1)*t_delta,i*t_delta,50);


    sol_l1 = pdepe_mod(m,@heatcyl,@heatic,@heatbc,x_l1,t,[],t_l1_sol(i,:));
    t_l1_sol(i+1,:) = sol_l1(end,:);

    global l2_LBC;
    l2_LBC = t_l1_sol(i+1,end);
    global l2_RBC;
    l2_RBC = t_l3_sol(i,1);
    sol_l2 = pdepe_mod(m,@heatcart_l2,@heatcartic,@heatcartbc_l2,x_l2,t,
[],t_l2_sol(i,:));

    t_l2_sol(i+1,:) = sol_l2(end,:);

    global l3_LBC;
    l3_LBC = t_l2_sol(i+1,end);
    global l3_RBC;
    l3_RBC = t_l4_sol(i,1);
    sol_l3 = pdepe_mod(m,@heatcart_l3,@heatcartic,@heatcartbc_l3,x_l3,t,
[],t_l3_sol(i,:));

    t_l3_sol(i+1,:) = sol_l3(end,:);


    global l4_LBC;
    l4_LBC = t_l3_sol(i+1,end);
    global l4_RBC;
    l4_RBC = 125;

    global t_j;
    t_j = t_l4_sol(i,end);
    sol_l4 = pdepe_mod(m,@heatcart_l4,@heatcartic,@heatcartbc_l4,x_l4,t,
[],t_l4_sol(i,:));
```

```
    t_l4_sol(i+1,:) = sol_l4(end,:);

    Z_l1_sol(i+1,:) = R_init(1)*(1*ones(1,n_disc) + alpha(1)*(t_l1_sol(i+1,:)
- T_ref));

end

t_all = [t_l1_sol t_l2_sol t_l3_sol t_l3_sol];
figure(1)
u = t_l1_sol(:,:,1);
surf(x_l1,t_act,u)
xlabel('x')
ylabel('t')
zlabel('T(x,t)')
% view([150 25])

figure(2)
u = t_l2_sol(:,:,1);
surf(x_l2,t_act,u)
xlabel('x')
ylabel('t')
zlabel('T(x,t)')
% view([150 25])

figure(3)
u = t_l3_sol(:,:,1);
surf(x_l3,t_act,u)
xlabel('x')
ylabel('t')
zlabel('T(x,t)')
% view([150 25])

figure(4)
u = t_l4_sol(:,:,1);
surf(x_l4,t_act,u)
xlabel('x')
ylabel('t')
zlabel('T(x,t)')
% view([150 25])


%%plot the impedance

figure(5)
u = Z_l1_sol(:,:,1);
surf(t_l1_sol,t_act,u)
xlabel('T(x,u)')
ylabel('t')
zlabel('Z(x,t)')
% view([150 25])

%plot()

% pde for the remaining three layers
```



```
%pde for layer 2 "Insulation'
function [c,f,s] = heatcart_l2(x,t,u,dudx)
global therm_cond;
global spec_heat;
global rho;
c = spec_heat(2)*rho(2);  %thermal capacity*density
f = dudx;
s=0;
end

%pde for layer 3 "sheath
function [c,f,s] = heatcart_l3(x,t,u,dudx)
global therm_cond;
global spec_heat;
global rho;
c = spec_heat(3)*rho(3);  %thermal capacity*density
f = dudx;
s=0;
end

%pde for layer 4 "jacket"
function [c,f,s] = heatcart_l4(x,t,u,dudx)
global therm_cond;
global spec_heat;
global rho;
c = spec_heat(4)*rho(4);  %thermal capacity*density
f = dudx;
s=0;
end



% define the boundary conditions for all the layers
%BC for the second layer
function [pL,qL,pR,qR] = heatcartbc_l2(xL,uL,xR,uR,t)
global l2_LBC;
global l2_RBC;
pL = uL - l2_LBC;
qL = 0;
pR = uR - l2_RBC;
qR = 0;
end

%BC for the third layer
function [pL,qL,pR,qR] = heatcartbc_l3(xL,uL,xR,uR,t)
global l3_LBC;
global l3_RBC;
pL = uL - l3_LBC;
qL = 0;
pR = uR - l3_RBC;
qR = 0;
end
```

```
% BC for the fourth layer
function [pL,qL,pR,qR] = heatcartbc_l4(xL,uL,xR,uR,t)
global l4_LBC;
global l4_RBC;
global t_j;
h=10;
pL = uL - l4_LBC;
qL = 0;
t_amb = 20;
pR = h*(t_j-t_amb);
k= 0.1;
qR = k;
end
```

Appendix C: Relative change computations

Relative changes for impedance-temperature experiment

Range of impedance in healthy state:

Impedance range = max impedance – min impedance = 91.6 – 75.87 = 15.73 Ω

Percentage change in impedance due to hotspot

Percentage change = $\left(\frac{Impedance\ with\ hotspot - Average\ healthy\ state\ impedance}{average\ healthy\ state\ impedance}\right) * 100$

$$\left(\frac{97.4 - \frac{75.87+91.6}{2}}{\frac{75.87+91.6}{2}}\right) * 100 \ = 23.79\%$$

Relative changes for mechanical damage experiment

Sheath peeled off:

Percentage change = $\left(\frac{Impedance\ with\ sheath\ peeled\ off - Healthy\ state\ impedance}{Healthy\ state\ impedance}\right) * 100$

$$\left(\frac{50.6-50.2}{50.2}\right) * 100 = 0.8\%$$

Insulation peeled off:

Percentage change = $\left(\frac{Impedance\ with\ insulation\ peeled\ off - Healthy\ state\ impedance}{Healthy\ state\ impedance}\right) * 100$

$$\left(\frac{51.6-50.2}{50.2}\right) * 100 = 2.79.8\%$$

Notch in conductor:

Percentage change = $\left(\frac{Impedance\ with\ notch - Healthy\ state\ impedance}{Healthy\ state\ impedance}\right) * 100$

$$\left(\frac{52.1-50.2}{50.2}\right) * 100 = 3.79\%$$